Microbiological and metagenomic insights into the biogeochemical weathering of Fe(II)-silicates and pyrite by chemolithotrophic bacteria

By

Stephanie A. Napieralski

A dissertation submitted in partial fulfilment of

the requirements for the degree of

Doctor of Philosophy

(Geoscience)

at the

UNIVERSITY OF WISCONSIN-MADISON

2020

Date of final oral examination: 12/19/2019

The dissertation is approved by the following members of the Final Oral Committee:

Eric E. Roden, Professor, Geoscience
Clark M. Johnson, Professor, Geoscience
Matthew Ginder-Vogel, Associate Professor, Civil and Environmental Engineering
Katherine D. McMahon, Professor, Bacteriology
Eric S. Boyd, Associate Professor, Microbiology and Immunology, Montana State University

To my parents, Raymond and Debra Napieralski, thank you for loving and supporting me unconditionally. Without you, none of this would have been possible.

Acknowledgements

I first and foremost need to sincerely thank my advisor Professor Eric Roden. It has been an absolute pleasure to work with Eric and I am extremely grateful to have had the opportunity to work under the advisement of not only a tremendous scientist but also a kind, supportive and respectful man. Eric's support and guidance was of paramount importance in my development as a scientist, from the early stages of my PhD where he took the time to guide me through the development of my dissertation research to the final stages where I was given the leeway to operate semi-autonomously knowing he would be more than happy to assist as needed. I look forward to continuing to work alongside Eric as I transition from his student to his colleague. I will count him as a not only a mentor, but a genuine friend for years to come. Thank you, Eric, for being you, and for all the coffee, leftovers and wonderful baked goods.

I also need to acknowledge my committee members, Professors Clark Johnson, Matt Ginder-Vogel, Trina McMahon and Eric Boyd for their guidance and support over the course of my studies here at UW-Madison. Thank you all for your valuable feedback and input as I progressed through my graduate career.

Completion of my PhD would not have been possible without the assistance from a variety of interdisciplinary collaborators. Thank you to my collaborators at Pennsylvania State University, especially Professor Susan Brantley for the helpful discussions and feedback which served not only to develop the ideas for my PhD research, but also challenge me to think about my data in ways that I would otherwise have neglected. To the rest of the Penn State group, including Virginia Marcon, Brandon Forsythe and Scott Hynek, thank you for your assistance with my field work, from logistical planning to execution. Thank you to Dr. Heather Buss, who's

expertise was indispensable when designing and executing my experiments on silicate weathering. Thank you to the mineralogy group here at UW-Madison including Dr. Huifang Xu, Seungyeol Lee and Yihag Fang for your assistance in collect, analyzing and interpreting TEM data which an invaluable component of my dissertation. Additional thanks are due to Aurélien Moy and Bil Schneider for patiently helping with my SEM imaging.

My research would not have been possible without funding from the NASA Astrobiology Institute and The University of Wisconsin Microbiome Initiative. My education was further supported by the UW-Madison Department of Geoscience and the Ken and Linda Ciriacks Distinguished Graduate Student Fellowship.

To the Geomicrobiology Lab group, past and present, including Nathan Fortney, Shaomei He, Jackie Mejia, Noah Stern, Lisa Haas and Allison Hartman, thank you. To Nathan and Shaomei in particular, thank you for being patient and helpful while I learned the bioinformatic ropes from you. More than anything, thank you Nathan for being a friend and sympathetic ear during those times when that's all I needed. I also need to acknowledge the many undergraduate students who assisted me with my laboratory work including Chris Setzke, Evan Handowski, Sabrina Krepel and Margaret Klein.

To my fellow graduate students, thank you for providing a welcoming and supportive community throughout my graduate studies. I have had the pleasure of meeting and interacting with some of the most bright and talented individuals one can imagine including Sarah Bremmer Thiru Reddy, Bre Hashman, Nick Levitt, Adam Denny Ben Linzmeier, Mike Johnson, Lesley Parker, Beatriz Cosenza and Colby Schwaderer. Thank you all for your inspiration, support and friendship. Graduate school is as challenging as it is rewarding, and I almost certainly could not have made it through without the friends I have made during my time at UW. A very special

thank you is due to the best friend anyone could imagine, Rachelle Turnier. Thank you for everything Rachelle, you truly are a gem.

Lastly, but not by any means least, I need to express my sincerest gratitude to my family their unconditional love and support. To my parents, Raymond and Debra, thank you for always being there for me. To my grandparent, Melvin and Beverly Wood, thank you for everything you've done for me over the course of my education. There will never be any quarters more valuable than those I cannot bear to spend. To my sibling, Amber, Nicholas and Enjoli thank you and your families for giving me joy and the privilege of being Aunt Stephanie. All my love to all of you.

Table of Contents

Abstract

Earth's Critical Zone is defined as the thin layer of the terrestrial surface ranging from the top of the vegetative canopy to the depths of actively circulating groundwater. At the base of the Critical Zone, fresh rock, through complex set of physical, chemical and potentially biological reactions, is transformed to regolith, releasing a study flux of solutes essential for the maintenance of Earth's biosphere. The near surface weathering of minerals by microorganisms has been extensively studied, usually through the lens of heterotrophic metabolisms and plant-microbe-mineral interactions in the rhizosphere where acidolysis and chelation have been shown to drive mineral dissolution. However, weathering is also a redox titration between fresh, reduced rock and an oxidizing atmosphere and the oxidation of Fe(II) is often rate limiting with respect to mineral weathering. Reduced Fe(II)-bearing minerals thus potentially represent a vast reservoir of chemical energy that can potentially fuel the metabolism of chemolithotrophic microorganisms, i.e. organisms which obtain energy for growth from inorganic, or "lithospheric" compounds. The activity of chemolithotrophic microorganisms in turn has the potential to mediate the reactions shaping the base of the Critical Zone. Combining microbiological, metagenomic and geochemical based approaches, I utilized the NSF Critical Zone Observatory Network to investigate the potential role of chemolithotrophic microorganisms in the weathering of bedrock of two differing lithologies. The Rio Icacos watershed of the Luquillo Critical Zone Observatory (LCZO) in Puerto Rico in underlain by the Rio Blanco Quartz Diorite containing the Fe(II)-silicate minerals biotite and hornblende. Susquehanna Shale Hills Critical Zone Observatory (SSHCZO), located in Central Pennsylvania, is underlain by the Rose Hills Shale, a grey shale containing the Fe-sulfide mineral pyrite (FeS_2). Laboratory enrichment culturing utilizing solid phase Fe(II)-minerals demonstrate that the presence of a live inocula obtained

from the *in-situ* weathering fronts of both LCZO and SSHCZO dramatically enhances the rate of oxidation of Fe(II)-silicates and FeS_2, respectively. The enhanced oxidation of Fe(II)-silicates was directly linked to the growth of chemolithotrophic Fe(II)-oxidizing bacteria (FeOB), with an observed enrichment in extracellular electron transfer (EET) genes know to be involved in Fe(II)-oxidation. In contrast, the enhanced oxidation of FeS_2 is best explained by the activity of chemolithotrophic sulfur oxidizing bacteria (SOB) and a novel potential mechanism for SOB interaction with extracellular FeS_2 is proposed. Finally, I assessed the enrichment culture results in the context of relevant geological constraints. While I conclude that FeOB are likely catabolic with regard to *in situ* Fe(II)-silicate oxidation at LCZO, the subsurface oxidation of pyrite within the nanoporous shale at SSHCZO almost certainly proceeds abiotically. Nevertheless, this work provides valuable insight into the potential pathways and mechanisms by which both chemolithotrophic FeOB and SOB may interact with insoluble Fe(II)-bearing mineral phases, thus providing a foundation for future studies to further unravel the complex reactions involved in the transformation of rock to regolith.

Introduction

The Earth's Critical Zone is defined as the thin layer of the terrestrial surface, ranging from the top of the vegetative canopy to the unaltered bedrock. At the base of the Critical Zone, rock is subjected to a variety biogeochemical process that work to alter both its physical structure and chemical composition, converting rock to regolith in the process known as weathering. Weathering of rock is a modulator of Earth's habitably, from regulating the concentration of CO_2 and O_2 in the atmosphere (Berner, 2006) to the release bioessential solutes otherwise stored in insoluble mineral reservoirs. The role of biota in mineral weathering has long been recognized and is extensively described (Banfield et al., 1999; Barker et al., 1998; Uroz et al., 2009). Microbially accelerated weathering is most often attributed to the activity of heterotrophic microorganisms (Hutchens et al., 2003) for purposes of nutrient acquisition (Calvaruso et al., 2006). It is important to note, however, that the rate limiting step in the weathering of Fe-bearing minerals is often the oxidation of Fe(II) (Hering and Stumm, 1990). Thus what many of the above-mentioned mechanisms of microbially mediated weathering fail to address is the potential for metabolic energy generation coupled to the oxidative weathering of Fe(II)-minerals (Bach and Edwards, 2003; Shock, 2009).

While there has been increasing interest in the role of chemolithotrophic microorganisms in the alteration of the basaltic oceanic crust (Edwards et al., 2004), studies investigating the role chemolithotrophic Fe(II)-oxidizing bacteria (FeOB) in terrestrial weathering are lacking. It has been demonstrated that structural Fe(II) in the mineral biotite is capable of sustaining FeOB growth *in vitro* (Shelobolina et al., 2012). This model, whereby FeOB directly utilize insoluble mineral bound Fe(II) as a source of metabolic energy, necessitates the involvement of redox-active outer membrane proteins to transfer electrons from a source exterior to the cell to the cell

interior for energy generation. This phenomenon is known as extracellular electron transfer (EET), and although first discovered in heterotrophic Fe(III)-reducing organisms such as *Shewanella* and *Geobacter* (Shi et al., 2007), analogous systems have now been recognized to operate in FeOB (Beckwith et al., 2015; He et al., 2017; He et al., 2016; Liu et al., 2012). In addition to EET being implicated in the chemolithotrophic oxidation of Fe(II)-silicates, it has also been proposed to be an important phenomenon in microbially catalyzed oxidation of the Fe-sulfide mineral pyrite at circumneutral pH (Percak-Dennett et al., 2017). Percak-Dennett and colleagues (2017) proposed a model in which chemolithotrophic Fe(II) oxidization at the mineral surface mediates oxidation of reduced sulfur in pyrite. The work described in the following three chapters of my dissertation combines microbiological, metagenomic and geochemical based approaches to address the central hypothesis that chemolithotrophic microorganisms, including FeOB can accelerate the oxidative weathering of Fe(II)-silicates and pyrite in natural weathering environments.

In Chapter 1, I investigate the potential for FeOB to accelerate the oxidation of the Fe(II)-bearing silicate minerals biotite and hornblende contained in the Rio Blanco Quartz Diorite underlying the Rio Icacos Watershed at Luquillo Critical Zone Observatory (LCZO) in Puerto Rico. Previous studies on subsurface weathering of the Rio Blanco Quartz Diorite have suggested the weathering flux of Fe(II)-minerals across the rindlet-saprolite interface is capable of supporting a chemolithotrophic microbial community at depth (Buss et al., 2005); however, experimental evidence to support the theoretical calculations was lacking. Utilizing a natural inoculum obtained from the subsurface rindlet-saprolite interface, quartz diorite oxidizing enrichment cultures were established and geochemically monitored to document Fe(II) oxidation activity over a ca. 2.4 year period. Metagenomic analysis was performed on both *in situ* regolith

and a diorite oxidizing enrichment culture to determine the metabolic potential of microorganisms putatively involved in Fe(II) oxidation, including searching for EET pathways. Scanning and transmission electron microscopy with energy dispersive spectroscopy was used to assess mineralogical transformations. Finally, artificial weathering studies were performed on microbially oxidized diorites to assess the degree to which prior oxidation might affect the efficiency of proton promoted mineral dissolution.

Chapter 2 builds upon previous work by Percak-Dennett and colleagues (2017) to investigate the potential role of chemolithotrophic microorganisms in the *in situ* subsurface oxidative weathering of FeS_2 at Susquehanna Shale Hills Critical Zone Observatory in Pennsylvania. The oxidative weathering of pyrite at SSHCZO occurs as the deepest reaction front in a nanoporous, though fractured grey shale unit of the Rose Hill Formation (Brantley et al., 2013). Previously proposed mechanisms for the circumneutral pH oxidation of FeS_2 by either chemolithotrophic FeOB or SOB were framed within these geological constraints. *In situ* mineral deployments were used as a source of inoculum to establish FeS_2 oxidizing enrichment cultures. 16S rRNA gene sequencing, shotgun metagenomic and geochemical analyses were used to determine potential metabolic pathways involved in the enhanced oxidation of FeS_2 and to interpret the potential role of chemolithotrophy in the *in situ* oxidative weathering of FeS_2 at SSHCZO. As the previously proposed mechanisms (Percak-Dennett et al., 2017) were insufficient to explain the observed genomic and geochemical trends, bioinformatic analyses were performed to uncover and propose a new mechanisms by which SOB interact directly with extracellular FeS_2 to accelerate its oxidation.

Chapter 3 builds on the knowledge obtained in Chapter 1 to assesses the hypothesis that the FeOB-driven redox associated mineralogical transformations of the Rio Blanco Quartz

Diorite renders the Fe(II)-mineral components more susceptible to heterotrophically driven modes of mineral dissolution. An outcrop of the Rio Blanco Quartz Diorite, visibly colonized by plants and thus containing abundant organic matter, was chosen to investigate the potential for *in situ* interactions between the well-established modes of heterotrophically enhancing weathering silicate minerals and the chemolithotrophic activity of FeOB. Diorite-oxidizing enrichment cultures were established using material obtained from the outcrop rindlet zone. After 615 days of incubation under imposed chemolithotrophic conditions, microbially oxidized and unoxidized abiotic control diorite were reseeded with inocula and provided with 1.0 mM glucose to establish heterotrophic incubations. Resultant geochemical and metagenomic data was integrated to develop a model for potential microbial weathering interactions *in situ*.

References

Bach, W., Edwards, K.J., 2003. Iron and sulfide oxidation within the basaltic ocean crust: implications for chemolithoautotrophic microbial biomass production. Geochim Cosmochim Acta, 67(20): 3871-3887.

Banfield, J.F., Barker, W.W., Welch, S.A., Taunton, A., 1999. Biological impact on mineral dissolution: application of the lichen model to understanding mineral weathering in the rhizosphere. Proc Natl Acad Sci U S A, 96(7): 3404-3411.

Barker, W.W., Welch, S.A., Chu, S., Banfield, J.F., 1998. Experimental observations of the effects of bacteria on aluminosilicate weathering. American Mineralogist, 83: 1551-1563.

Beckwith, C.R. et al., 2015. Characterization of MtoD from Sideroxydans lithotrophicus: a cytochrome c electron shuttle used in lithoautotrophic growth. Front Microbiol, 6: 332.

Berner, R.A., 2006. GEOCARBSULF: A combined model for Phanerozoic atmospheric O2 and CO2. Geochimica et Cosmochimica Acta, 70(23): 5653-5664.

Brantley, S.L., Holleran, M.E., Jin, L., Bazilevskaya, E., 2013. Probing deep weathering in the Shale Hills Critical Zone Observatory, Pennsylvania (USA): the hypothesis of nested chemical reaction fronts in the subsurface. Earth Surface Processes and Landforms, 38(11): 1280-1298.

Buss, H.L. et al., 2005. The coupling of biological iron cycling and mineral weathering during saprolite formation, Luquillo Mountains, Puerto Rico. Geobiology, 3: 247-260.

Calvaruso, C., Turpault, M.P., Frey-Klett, P., 2006. Root-associated bacteria contribute to mineral weathering and to mineral nutrition in trees: a budgeting analysis. Appl Environ Microbiol, 72(2): 1258-66.

Edwards, K.J., Bach, W., McCollom, T.M., Rogers, D.R., 2004. Neutrophilic Iron-Oxidizing Bacteria in the Ocean: Their Habitats, Diversity, and Roles in Mineral Deposition, Rock

Alteration, and Biomass Production in the Deep-Sea. Geomicrobiology Journal, 21(6): 393-404.

He, S., Barco, R.A., Emerson, D., Roden, E.E., 2017. Comparative Genomic Analysis of Neutrophilic Iron(II) Oxidizer Genomes for Candidate Genes in Extracellular Electron Transfer. Front Microbiol, 8: 1584.

He, S., Tominski, C., Kappler, A., Behrens, S., Roden, E.E., 2016. Metagenomic Analyses of the Autotrophic Fe(II)-Oxidizing, Nitrate-Reducing Enrichment Culture KS. Appl Environ Microbiol, 82(9): 2656-2668.

Hering, J.G., Stumm, W., 1990. Oxidative and reductive dissolution of minerals. Reviews in Mineralogy and Geochemistry, 23(1): 427-465.

Hutchens, E., Valsami-Jones, E., McEldowney, S., Gaze, W., McLean, J., 2003. The role of heterotrophic bacteria in feldspar dissolution – an experimental approach. Mineralogical Magazine, 67(6): 1157-1170.

Liu, J. et al., 2012. Identification and Characterization of MtoA: A Decaheme c-Type Cytochrome of the Neutrophilic Fe(II)-Oxidizing Bacterium Sideroxydans lithotrophicus ES-1. Front Microbiol, 3: 37.

Percak-Dennett, E. et al., 2017. Microbial acceleration of aerobic pyrite oxidation at circumneutral pH. Geobiology, 15(5): 690-703.

Shelobolina, E. et al., 2012. Microbial lithotrophic oxidation of structural Fe(II) in biotite. Appl Environ Microbiol, 78(16): 5746-52.

Shi, L., Squier, T.C., Zachara, J.M., Fredrickson, J.K., 2007. Respiration of metal (hydr)oxides by Shewanella and Geobacter: a key role for multihaem c-type cytochromes. Mol Microbiol, 65(1): 12-20.

Shock, E.L., 2009. Minerals as energy sources for microorganisms. Economic Geology, 104(8): 1235-1248.

Uroz, S., Calvaruso, C., Turpault, M.P., Frey-Klett, P., 2009. Mineral weathering by bacteria: ecology, actors and mechanisms. Trends Microbiol, 17(8): 378-87.

Chapter 1

Microbial chemolithotrophy mediates oxidative weathering of granitic bedrock

Stephanie A. Napieralski[1*], Heather L. Buss[2], Susan L. Brantley[3], Seungyeol Lee[1], Huifang Xu[1] and Eric E. Roden[1*]

[1]Department of Geoscience, NASA Astrobiology Institute, University of Wisconsin-Madison, Madison WI 53706. [2]School of Earth Sciences, University of Bristol, Bristol BS8 1RJ, UK. [3]Earth and Environmental Systems Institute, and the Department of Geosciences, Pennsylvania State University, University Park PA 16802.

*Corresponding author e-mail: snapieralski@wisc.edu; eroden@geology.wisc.edu

Keywords: Weathering, Chemolithotrophy, Critical Zone

Napieralski, S. A., Buss, H. L., Brantley, S. L., Lee, S., Xu, H., and Roden, E.E., 2019, Microbial chemolithotrophy mediates oxidative weathering of granitic bedrock: PNAS 116(52):26394-26401.

Abstract

The flux of solutes from the chemical weathering of the continental crust supplies a steady supply of essential nutrients necessary for the maintenance of Earth's biosphere. Promotion of weathering by microorganisms is a well-documented phenomenon and is most often attributed to heterotrophic microbial metabolism for the purposes of nutrient acquisition. Here we demonstrate the role of chemolithotrophic ferrous iron [Fe(II)]-oxidizing bacteria in biogeochemical weathering of subsurface Fe(II)-silicate minerals at the Luquillo Critical Zone Observatory in Puerto Rico. Under chemolithotrophic growth conditions, mineral-derived Fe(II) in the Rio Blanco Quartz Diorite served as the primary energy source for microbial growth. An enrichment in homologs to gene clusters involved in extracellular electron transfer was associated with dramatically accelerated rates of mineral oxidation and ATP generation relative to sterile diorite suspensions. Transmission electron microscopy and energy dispersive spectroscopy revealed the accumulation of nanoparticulate Fe-oxyhydroxides on mineral surfaces only under biotic conditions. Microbially-oxidized quartz diorite showed greater susceptibility to proton promoted dissolution, which has important implications for weathering reactions *in situ*. Collectively our results suggest that chemolithotrophic Fe(II)-oxidizing bacteria are likely contributors in the transformation of rock to regolith.

Significance

We utilized the Luquillo Critical Zone Observatory (LCZO) in Puerto Rico to test the hypothesis that mineral-derived Fe(II) within the granitic bedrock at LCZO is capable of supporting microbial Fe(II)-based chemolithotrophy, and that the resultant redox-driven mineralogical transformations contribute to bedrock weathering. While this hypothesis had been previously postulated based on theoretical calculations of Fe(II) loss and potential chemolithotrophic Fe(II)-oxidizing bacterial growth across the bedrock-saprolite interface, to date it has not been verified experimentally. Our study definitively demonstrates the ability of chemolithotrophic Fe(II)-oxidizing bacteria to accelerate oxidative transformation of Fe(II)-silicate minerals. In addition, our work presents new insight into the complex microbial community interactions which must be considered when assessing the role of microorganisms in bedrock weathering.

Introduction

The role of microorganisms in the weathering of minerals has long been recognized (1). More recent interest in the role of Fe(II)-oxidizing bacteria (FeOB) has been driven by the recognition that Fe(II)-bearing mineral phases, such as Fe(II)-silicates and pyrite, represent a potential wealth of energy to fuel chemolithotrophic metabolisms, both terrestrially (2) and on other rocky planetary bodies such as Mars (3). Thus far the best attempts to characterize the activity of FeOB and their relationship to Fe(II)-silicate weathering come from studies on the subaqueous alteration of the basaltic oceanic crust where it has been demonstrated that FeOB colonize highly reactive basaltic glasses and form thick microbial mats near hydrothermal vent features (4-6). However, controversy remains as to the ability of these marine microorganisms to directly utilize solid phase Fe(II) to fuel their metabolisms (7, 8), and it has been suggested that

dissolved Fe(II) released is the major energy source for biomass formation in the vicinity of hydrothermal vents (9).

Compared to the extensive studies targeting oceanic systems, investigations into the role of FeOB in continental weathering are more limited. The potential role of FeOB in Fe-silicate weathering has been postulated, the supposition being that redox driven crystallographic changes should be sufficient to lead to mineral dissolution (10). Although it has been established that structural Fe(II) in biotite is capable of supporting FeOB growth *in vitro* (11), efforts to more fully characterize the role of bacteria in terrestrial weathering processes (10, 12, 13) and to link FeOB activity to weathering of volcanic rocks (14) have yielded no definitive evidence for the involvement of FeOB *in situ*. Nevertheless, multiple lines of circumstantial evidence have been presented for the potential involvement of FeOB in the weathering of the Rio Blanco Quartz Diorite underlying the Rio Icacos watershed of the Luquillo Critical Zone Observatory, Luquillo PR (15-17). The Rio Blanco Quartz Diorite is primarily composed of plagioclase feldspar and quartz with lesser amounts of the Fe(II)-bearing silicate phases biotite (~10 wt%) and hornblende (~7 wt%). It is estimated to have one of the highest weathering fluxes known for a granitic material (18). The regolith developed from the Rio Blanco Quartz Diorite consists of a 1-meter thick soil overlying an oxidized saprolite zone comprised primarily of quartz, altered biotite, secondary kaolinite, and goethite with a variable depth of 2 m to perhaps 30 m (18, 19). The interface of partially altered, fractured rocky material between individual unaltered bedrock corestones and overlying saprolite is termed the “rindlet zone” (20). Here diffusion of oxygen into the crystalline rock is thought to cause oxidation of biotite, producing strain that ultimately causes the bedrock to fracture and weather spheroidally, exhibiting a concentric, onion skin-like profile commonly observed during weathering of some granites (21) (see Figure 1 inset). Further

oxidative weathering of biotite occurs within the rindlet zone and the complete depletion of hornblende occurs across a narrow, c.a. 7 cm band of rindlets before the rindlet-saprolite interface (22). Within this zone, an increase in cell density has been previously reported, consistent with theoretical calculations suggesting that the gradient of Fe(II) generated by weathering across this zone is capable of supporting a robust community of lithotrophic FeOB at depth (15). Accordingly, we observed an increase in microbial biomass as determined by ATP content of the regolith (Figure 1) relative to the overlying saprolite, indicating the presence of an actively metabolizing microbial community coincident with a sharp gradient in solid-phase Fe(II) at the rindlet saprolite interface. Within this biogeochemical framework, we sought to test the hypothesis (15) that mineral-derived Fe(II) is capable of supporting chemolithotrophic cellular growth coupled to Fe(II) oxidation. In addition, electron microscopic analysis and simulated weathering experiments explored how microbial redox driven mineralogical transformations may contribute to the previously documented (15, 18, 20-22) weathering systematics of the Rio Blanco Quartz Diorite.

Results and Discussion

Chemolithotrophic Fe(II)-oxidizing enrichment cultures

Ground (<45 μm) Rio Blanco Quartz Diorite was incubated over a period of ca. 2.4 years (864 days) under imposed chemolithotrophic conditions with natural inocula from 3 separate rindlet-saprolite interface samples (Cores A, B and C). Significant oxidation was observed in the presence of a live inocula compared to sterile abiotic controls. The ratio of Fe(II) to Fe(tot) in dilute HCl extracts of solid phase material declined over time from 76.3 to 43.1% (Figure 2a) in the most extreme example of microbial oxidation. This change in the dilute HCl extractable Fe pool corresponds to the oxidation of ca. 0.6% of the total Fe(II) content of the quartz diorite.

Given that no significant oxidation occurred under abiotic conditions, our results demonstrate that microbial acceleration of Fe(II)-silicate oxidation was essentially infinite on the time scale of this experiment. ATP abundance, indicating the generation of metabolic energy, was up to an order of magnitude higher in cultures containing diorite compared to cultures provided with pure (Fe(II)-free) quartz sand (Figure 2b,c). Both the quartz sand and the quartz diorite had no detectable (<0.005%) particulate organic carbon (POC) content, suggesting ATP generation was not primarily linked to the oxidation of trace POC in mineral substrates. ATP has been demonstrated to correlate directly with biomass carbon (23, 24). Thus, using a conversion of 10 μmol ATP g^{-1} biomass C (25) and assuming that the pool of dilute HCl-extractable Fe(II) represents Fe(II) available for microbial oxidation (11), microbial growth yields in μmol biomass C μmol^{-1} Fe(II) oxidized were estimated. Biomass yields over the first 172 days (to peak ATP production) from individual reactors inoculated with material from Cores A and B were between 0.013 and 0.020 μmol of biomass C μmol^{-1} Fe(II) oxidized (Calculations in SI Appendix Table S1), consistent with previously reported growth yields for neutrophilic chemolithotrophic FeOB in opposing gradient media (26). Growth yields from reactors inoculated with material from Core C were more variable between replicates and higher than would be predicted for Fe(II) oxidation alone. As the extent of oxidation in C reactors was lower than observed for A and B reactors with comparable ATP production, this observation is best explained by input from alternative metabolisms in Core C reactors. However, taken together, these results suggest that the oxidation of mineral-derived Fe(II) in the quartz diorite was the primary source of metabolic energy generation and resultant microbial growth in the majority of reactors. After initial growth, spurred by the availability of fresh mineral surfaces, ATP generation declined across all reactors

while Fe(II) continues to be oxidized, suggesting the establishment of a maintenance condition, whereby individual cells are still metabolizing without actively increasing in biomass.

Shotgun metagenomic analysis revealed that the microbial community in the quartz diorite-oxidizing enrichment culture was dramatically simplified compared to the *in-situ* rindlet-saprolite sample (SI Appendix Figure S1). The enrichment culture metagenome was dominated by organisms belonging to the Betaproteobacteria, including the genera *Cupriavidus* and *Burkholderia* and the order Neisseriales (Figure SI Appendix S2). Such organisms have been previously shown by 16S rRNA gene amplicon sequencing surveys to be abundant in weathering systems (10, 27) and the ability of *C. necator* to grow by oxidation of Fe-phyllosilicate minerals has been demonstrated (28). Taxonomically, the Neisseriales sp. in enrichments appears to be closely related to the lithotrophic, Fe(II)-oxidizing, nitrate reducing organism *Pseudogulbenkiania* sp. strain 2002 , which is capable of nitrate-dependent growth on solid phase Fe(II) (29). In addition to these dominant organisms having taxonomic affinity to previously described FeOB, seven metagenome assembled genomes (MAGs) obtained from the coassembled metagenomes contain homologs to the known Fe(II) oxidation pathway of the acidophilic FeOB *Acidithiobacillus ferroxidans* (Figure 3). In *A. ferroxidans* the outer membrane bound c-type cytochrome Cyc2 is the iron oxidase (30, 31). As is the case with the oxidation of soluble Fe(II) by *A. ferroxidans*, the oxidation of mineral bound Fe(II) would necessarily be performed extracellularly (11) with subsequent transport of electrons to the intracellular components of the electron transport chain via a periplasmic electron carrier. This process, termed extracellular electron transfer (EET), was originally recognized in dissimilatory Fe(III)-reducing organisms (32) but has subsequently been shown to be utilized by FeOB (33, 34). Homologs to the Cyc2-type EET system have been found to be present in a broad range of FeOB

genomes, including those of aerobic neutrophilic FeOB (33, 35) and recently validated via meta-omics (36). Organisms of the genera *Ralstonia* and *Rhodopseudomonas* which are known to harbor FeOB (37, 38) were among the top 10 genera in the enrichment culture based on read classification, (Figure SI Appendix S2) however, no MAGs containing EET pathways of these genera were obtained. Additionally, while ectomycorrhizal fungi have been noted to oxidatively weather structural Fe(II) in biotite (39), fungal associated sequences were not detected in the raw reads for either metagenome or the coassembled metagenome, likely due to the extremely low organic carbon content at the bedrock-saprolite interface (15) and the chemolithotrophic culturing conditions in our experiments.

Many chemolithotrophic organisms are capable of growing autotrophically, most commonly by the use of the ubiquitous enzyme Ribulose-1,5-bisphosphate carboxylase (RuBisCO), which serves as the entry point for inorganic carbon into the Calvin Cycle. Of the MAGs that contained putative EET pathways, three also contained the complete RuBisCo system, including two *Cupriavidus* MAGs (Figure 3), which supports the idea that these organisms can grow chemolithoautotrophically. Notably, there are multiple MAGs with putative EET pathways that do not contain RuBisCo, including a *Xanthomonadaceae*, most closely related to the soil bacterium *Dyella japonica.* Though not described as Fe(II) oxidizers, a homolog to Cyc2 gene was also found in the non-autotrophic *D. japonica A8* (40). While chemolithoheterotrophy is a less common metabolic strategy than chemolithoautotrophy and remains to be validated in *Dyella* sp., the potential for Fe(II) chemolithoheterotrophy cannot be discounted. Mapping of the metagenomic reads from individual samples back to each MAG from the co-assembled metagenome reveals that the putative chemolithotrophs became enriched in the diorite-oxidizing cultures relative to the *in-situ* sample (Figure 3).

Mineralogical and geochemical effects of FeOB activity

Potential mineralogical changes associated with FeOB activity in the enrichment cultures were assessed via field emission scanning electron microscopy (FE-SEM) and transmission electron microscopy (TEM) with selected area electron diffraction (SAED). Inspection of whole biotite grains revealed a roughening of grain edges after incubation with live inocula that was not observed after abiotic incubation over the same time period. Significant alteration of the basal plane of biotite was observed (Figure 4). Etch pits, noted to be formed by siderophore promoted dissolution (41) were not observed on hornblende surfaces. However, microbially oxidized hornblende surfaces displayed other subtle differences in morphology suggestive of surface alteration (Figure 5). Upon further inspection via bright field TEM nanosized particles were found along the basal plane of microbially-oxidized biotite and the edges of the surface steps of hornblende (Figure 6). Initial time zero samples from inoculated cultures displayed clean biotite and hornblende crystal surfaces (Figure 6). The lack of these features in the inoculated samples at time zero, as well as their absence after 864 days of abiotic incubation (SI Appendix Figures S3,S4), implies that the nano-particles were generated over the course of the experiment by microbial oxidation and not acquired when the weathered inocula were added to the fresh diorite. TEM-EDS spectra demonstrate that the nano-particles are Fe-oxyhydroxides, as indicated by Fe enrichment on the microbially oxidized surfaces compared to clean surfaces (Figure 6). The iron oxyhydroxides were around 3-5 nm, similar in size to common examples of ferrihydrite (42), suggesting the precipitation of ferrihydrite on the surface of Fe-bearing minerals was triggered by microbial oxidation.

In addition to the accumulation of nano-size Fe-oxyhydroxides, small but significant differences were observed in the total amount of silicon (Si) released from the diorite in the

biotic vs. abiotic reactors. Although the aqueous concentration of Si was indistinguishable between these treatments (Figure 7), the biotic reactors showed a 13-40% increase (relative to abiotic controls and time zero samples) in the amount of Si that was released via extraction with NaOH to raise the pH and desorb any Si that may have been associated with Fe-oxyhydroxides (43). As a result, there was a significant (two-tailed $p=0.0398$) increase in total Si release accompanying the microbial oxidation.

No significant differences in the aqueous concentrations of major cations (Mg, Ca, K, Na) were observed between microbially-oxidized and abiotic or time zero controls. This observation is in contrast to numerous studies on microbially-mediated weathering which have demonstrated enhanced release of major rock-forming cations during incubation under heterotrophic conditions (44-46). While initially surprising, it is important to consider the mechanistic differences in mineral dissolution under chemolithotrophic versus heterotrophic conditions. It is well known that heterotrophically driven dissolution involves acidolysis and chelation by organic ligands (10). In the absence of respiratory CO_2 generation or low molecular weight organic acids produced as either a byproduct of heterotrophic metabolism or extracellular secretion for nutrient acquisition and/or biofilm formation, one would not expect acidolysis or chelation to be the dominant weathering mechanism under the chemolithotrophic, circumneutral pH conditions of our experiments. It has been noted that microscale pH gradients within microbial biofilms on colonized silicate minerals can be lowered as much as 1.1 pH units compared to bulk pH (47). Epifluorescence microscopy demonstrated preferential cellular association with solid mineral phases (SI Appendix Figure S5), where cells appeared as sparse, singular entities along mineral edges (SI Appendix Figure S6). Similarly diffuse, monolayered biofilms have previously been observed under the carbon limited colonization of basaltic glasses

(8). As such, localized biofilm acidolysis is also likely to be insignificant (46). Low molecular weight organic acids generated from the partial oxidation of glucose, in addition to siderophores, also act as effective chelators. Chelation has been noted to be an important driver of silicate dissolution at near neutral pH (48) with several studies noting the effect of siderophores in enhancing solubilization of cations during silicate mineral dissolution (41, 49, 50). Given that siderophores are produced specifically for Fe(III) acquisition as a micronutrient under Fe(III)-stress (51), their activity would not be expected to produce the oxidative weathering trend observed in this study. While it is not possible to totally rule out the activity of siderophores in this experiment, the data are not consistent with chelation as a primary driver of oxidative weathering under our experimental conditions. Rather, our data collectively point to direct enzymatic oxidation of mineral-derived Fe(II) by chemolithotrophic iron oxidizers for metabolic energy generation. This model is consistent with previously reported models of *in situ* weathering where biological cycling of Fe in the deep saprolite has been inferred based on isotopic measurements (52) and both heterotrophic and lithotrophic microorganisms have been detected at the rindlet-saprolite interface (16, 17). Fe and Mn precipitates previously observed in the outer rindlets, interpreted to result from downward infiltration Fe and Mn rich fluids (53), could instead be the result of mobilization and reprecipitation of iron by local oxidative weathering by FeOB in the outer rindlet zone where these organisms are expected to be of importance.

Enhanced weatherability of microbially-oxidized diorite

Under the imposed chemolithotrophic conditions and considering the proposed mechanism of a direct enzymatic attack on mineral-derived Fe(II) at circumneutral pH, it follows that complete stoichiometric dissolution of the Fe(II)-silicate mineral would not immediately

occur and would not be evident over the relatively short time period of this experiment. Rather, Fe(III) may be partially expulsed from the crystal lattices to compensate for the charge imbalance created by oxidation, which would likely result in decreased structural integrity of the mineral as previous studies have shown (11). This mechanism is consistent with the accumulation of nano-sized Fe-oxyhydroxides on biotite and hornblende surfaces (Figure 6). It is well noted that crystallographic defects and dislocations are sites of preferential weathering in minerals such as hornblende (54). Thus, it may be envisioned that microbially-oxidized minerals would be more susceptible to other modes of chemical weathering, including proton promoted dissolution owing to the inherent disruption of the mineral structure. To address this hypothesis, a portion of the microbially-oxidized quartz diorite was extracted for 24 hours in 10 mM HNO_3, followed by analysis of major cation concentrations in the dilute acid extract measured by ICP-OES. HNO_3-extractable Ca and Mg were significantly (two-tailed $p=0.0120$ and 0.0470, respectively) elevated in microbially-oxidized quartz diorites relative to the unoxidized controls (Figure 7). Major sources of these two cations in the Rio Blanco Quartz diorite include hornblende, biotite and plagioclase (Na,Ca-feldspar). In the case of biotite, which would be the dominant source of K in addition to a source of Mg, HNO_3-extractable K was significantly ($p=0.0010$) lower in biotic reactors than in abiotic controls. It has been shown that the extractability of K from biotite is related to the oxidation state of the octahedral iron with higher K retention correlating to increased oxidation of structural Fe(II) (55-57). It has also been observed that oxidized biotites in natural weathering systems can retain significant portions of their K (58). Although K does become depleted (relative to the bedrock) within and above the rindlet-saprolite interface (22), this depletion is attributed to continual removal by fluid flow within micro-cracks in the rindlet interiors that form during quartz diorite weathering. Because

such fluid flow was absent in our incubation experiments, the repression of K release upon acid extraction observed here is best explained by enhanced retention linked to a decrease in structural Fe(II) in biotite within the closed reaction system. While it is likely that some dissolution of plagioclase contributed to the observed aqueous chemistry, the lack of Fe in its mineral structure makes it generally unresponsive to the activity of FeOB. As such, any dissolution of the relatively sodic plagioclase (compared to other rock constituents) upon acid treatment would be expected to be comparable between oxidized and unoxidized diorites. The lack of significant difference (two-tailed $p=0.1429$) in acid-extractable Na concentrations between unoxidized control and microbially oxidized diorites is consistent with this idea and suggests that the difference in acid-extractable Ca, Mg and K between control and oxidized diorites was linked to reduced structural integrity of ferromagnesian minerals as a result of prior FeOB activity.

Conclusions

This study demonstrates that chemolithotrophic FeOB inhabiting the rindlet-saprolite interface of the Rio Blanco Quartz Diorite are capable of growing on mineral-derived Fe(II) as their primary source of metabolic energy, utilizing genomically encoded extracellular electron transfer pathways. The enrichment of these organisms under imposed chemolithotrophic conditions points to their potential to be involved in the subsurface weathering of the Rio Blanco Quartz Diorite. In contrast to the ground quartz diorite used in this experiment, the slow diffusion of oxygen into low porosity fresh bedrock is posited to be necessary for the initial fracturing that forms the rindlet zone (53) and therefore likely modulates weathering over geologic time scales. However, once porosity is sufficient to allow advective transport of fluids and microbial colonization along cracks and fractures, in light of the results of this study, it

seems likely that that FeOB play an important role in the overall weathering regime of the Rio Blanco Quartz Diorite, particularly within the saprolite-adjacent part of the rindlet zone where rapid depletion of mineral-bound Fe(II) is observed. The fact that microbially-oxidized quartz diorites were more susceptible to proton promoted dissolution also has important implications for the effectiveness of acidolysis and/or chelation weathering processes associated with heterotrophic microbial metabolism. While the focus of the study was exclusive to the role of FeOB in Fe(II)-silicate weathering and care must be taken when extrapolating laboratory studies to events in natural systems, our findings point clearly to the need for further investigation into the interplay between chemolithotrophically and heterotrophically driven silicate mineral weathering.

Methods

Field Sampling. In June of 2016 three cores (A, B and C) were taken from saprolite atop Guaba Ridge at Luquillo Critical Zone Observatory by hand auger to the depth of refusal (i.e., into the outer rindlet zone) which varied from 248 cm (Core B) to 785 cm (Core A), with Core C being of intermediate depth (627 cm) reflecting the topology of the bedrock beneath Guaba Ridge. All cores were taken within close proximity to a previously established lysimeter field, (18, 59) and care was taken to avoid repeat sampling of sites previously cored. Samples were collected aseptically at approximately 40-50 cm intervals for Core A as previously described (15). Cores B and Core C were sampled intermittently. Material collected was shipped overnight to UW-Madison on blue ice packs and portions were either refrigerated at 4 °C for live culturing or frozen at -80°C upon arrival for DNA extraction. 0.5 g aliquots of each sample were placed in 20 mM EDTA and frozen at -80°C for ATP analysis.

Chemolithotrophic Enrichment Culturing. Solid phase mineral-oxidizing enrichment cultures were established using whole rock Rio Blanco Quartz Diorite obtained from a road cut exposure. Mineral stoichiometries and abundances were determined previously by White et al. (1998); bulk elemental abundances (aqua regia digestion, ICP-OES analysis, ALS Geochemistry, Reno, NV) are provided in SI Appendix Table 2. Following collection, external weathered surfaces were removed using a rock saw. Large pieces of quartz diorite were fragmented using a jaw crusher to obtain suitable sized fractions for further pulverization using a shatter box. Shattered quartz diorite was sieved to <45 μm. Luquillo artificial groundwater (L-AGW) was prepared to a final mM solution concentration of 0.06 $MgCl_2 \cdot 6H_2O$, 0.04 KH_2PO_4, 0.05 $NaNO_3$, 0.1 $NaHCO_3$, 0.03 $Ca(NO_3)_2 \cdot 4H_2O$ and 0.01 Na_2SO_4. All glassware was combusted overnight at 550°C to minimize carbon contamination. In an anaerobic chamber, 5.0 g of pulverized quartz diorite or pure quartz sand (Acros Chemicals, 140-381 μm) was placed in a 120 mL bottle and 50 mL anoxic L-AGW was added. Bottles were crimp sealed with a rubber stopper and autoclaved. After sterilization, the headspace was flushed with sterile air to render the cultures aerobic. Duplicate reactors of each mineral treatment (quartz diorite or quartz) were inoculated with ca. 1.0 g of material from one of the three (A, B, C) samples obtained from the rindlet-saprolite interface, stoppered and incubated in the dark. Duplicate abiotic controls for each treatment were aerated and left uninoculated. 5.0% (volume) CO_2 was added to the headspace of each bottle as a carbon source for autotrophic growth. The pH of reactors after equilibration with CO_2 and mineral phases was circumneutral (6.7-7) in all reactors. Samples were taken immediately following inoculation and after 14, 28, 56, 84, 129, 172, 397 and 864 days.

Analytical Techniques. ATP: 0.5 mL of mineral suspension was placed into cold 20 mM ETDA and vortexed and immediately frozen at stored -80°C prior to ATP biomass

determination. At the time of analysis samples for ATP were thawed, vortexed once more and centrifuged. ATP content of the supernatant was determined via luminescence using BacTiter-Glo™, (Promega, Madison WI) with calibration to a standard curve prepared in 20 mM EDTA. **Solid-phase Fe(II):** The ratio of Fe(II) to total Fe released by 0.5 M HCl extraction was determined on *in situ* core samples and the solids from 1.0 mL of enrichment culture subsamples. The solids were extracted for 24 hours in 5 mL of 0.5 M HCl on an orbital shaker. For natural samples, 0.5 g regolith was added directly to acid for 24-hour extraction. Fe(II) of each extract was determined by the standard Ferrozine assay (60) and the measurement was repeated after the addition of hydroxylamine-HCl for determination of Fe(total) with Fe(III) determined by difference. **Particulate Organic Carbon:** Particulate organic matter of the Rio Blanco Quartz Diorite and Fe(II)-free quartz sand was determined via high temperature combustion using a Flash EA 1112 Flash Combustion Analyzer. **Cations:** Major cation concentrations (Ca, K, Mg, Na, Si) in the aqueous phase of the cultures were determined using inductively coupled plasma optical emission spectroscopy (ICP-OES) using a Varian Vista-MPX ICP-OES. The aqueous phase from duplicate reactors was pooled, filtered through a 0.22 µm filter and diluted 1:5 in Milli-Q water. Samples were run unacidified to avoid precipitation of silicon, with standards prepared for an appropriate calibration curve also in Milli-Q water. **Silica:** At the termination of the experiment, any sorption of Si to biogenic Fe-(oxy)hydroxides was assessed by high pH desorption. 1.0 mL of culture was aseptically removed and centrifuged to pellet the solids. The supernatant was removed and an equal volume of 10 mM NaOH was added to the remaining solids. The slurry was agitated for 24 hours and the supernatant was recovered by centrifugation. Si content was determined spectrophotometrically using the heteropoly blue assay. Following verification of consistency between ICP-OES and heteropoly blue Si determination, total Si

release at 864 days was calculated as the sum of aqueous Si and sorbed Si. **Epifluorescence microscopy:** Subsamples of live inoculated and abiotic control cultures were taken at 196 days for epifluorescence microscopy. Whole culture solution was immediately stained with 4′,6-diamidino-2-phenylindole (DAPI) (ThermoFisher Scientific) following manufacturer's protocols and imaged on a Nikon E600 compound phase contrast epifluorescence microscope.

Proton Promoted Dissolution Determination. The susceptibility of oxidized and unoxidized quartz diorites to proton promoted dissolution was assessed as previously described (61) for mineral acid dissolution to avoid ambiguity regarding the potential dual role of organic acids as chelators. After 864 days, 1.0 mL of culture from each inocula and the abiotic control were pelleted via centrifugation to recover the solid phase. The supernatant was removed and an equal volume of 10 mM HNO_3 was added and the slurry was agitated for 24 hours on an orbital shaker. The aqueous phase was collected via centrifugation and passed through a 0.22 µm filter. Individual samples where diluted 1:5 in HNO_3 for ICP-OES analysis. Cation concentrations (Ca, K, Mg, Na) were determined by calibration to a standard curve prepared in 10 mM HNO_3. To assess any differences that may have arisen as a consequence of the inclusion of natural weathered material as inocula at time zero, all samples were compared to the initial conditions (time zero) for their respective inocula (A, B or C), or fresh diorite in the case of the abiotic control.

Mineralogical Analysis. Samples were prepared for field emission scanning electron microscopy (FE-SEM) by dropping whole, undiluted liquid culture suspensions of time zero, a microbially oxidized sample inoculated with core A material (the same sample for which the metagenome was obtained) and an abiotically incubated control onto carbon tape affixed to a stub mount. Samples were air dried and carbon coated prior to imaging. Images were acquired

using a Cameca SXFiveFE with an accelerating voltage of 15 kV. Transmission electron microscopy (TEM) samples were prepared for the same samples as FE-SEM by dropping suspensions of crushed samples onto lacy‑carbon-coated 200-mesh Cu grids. TEM imaging and selected-area electron diffraction (SAED) analysis were carried out using a Philips CM200-UT microscope operated at 200 kV in the Materials Science Center at the University of Wisconsin-Madison. The chemical composition was obtained using TEM-EDS system equipped with a Li-drifted Si detector (Oxford instruments Link ISIS). An electron beam diameter of ~50 nm was used for collecting X-ray EDS spectra.

DNA Extraction, Sequencing and Metagenomic Analysis. DNA was extracted from *in situ* core samples and enrichment culture subsamples via the SDS-based extraction method adapted from Zhou, Bruns, & Tiedje (62). Reagent volumes were appropriately scaled to accommodate 0.5 g extractions, and 2 volumes of ethanol was used for DNA precipitation at -20°C. Crude DNA was resuspended in 50 µL 10 mM Tris (pH 8). Multiple extractions were performed until a sufficient mass of DNA for metagenomic sequencing was reached. Replicate extracts were cleaned and pooled using Zymo Clean and Concentrator-5 (Zymo Research, Irvine CA). Enrichment culture DNA from the 129 day sample was obtained via pelleting 2.0 mL culture and extraction of solids using the same method as above.

DNA was submitted to University of Wisconsin-Madison Biotechnology Center for metagenomic library preparation and 2x250 paired end sequencing on the Illumina HiSeq 2500 Rapid platform. Raw reads were quality trimmed to remove low quality sequences. Taxonomy of individual reads was estimated using Kraken (63) and the standard Kraken database. Reads from individual metagenomic libraries were concatenated and co-assembled using IDBA-UD (64) utilizing the high-performance computing cluster in the Center for High Throughput Computing

(CHTC) at University of Wisconsin-Madison. Assembled contigs were clustered into phylogenetic bins using MetaBAT v2.12.1 (65). The bin set was evaluated for completion and contamination using CheckM (66). Consensus taxonomy of individual bins was determined using single copy housekeeping genes identified in CheckM and MegaBLAST (67) alignment of individual contigs to the Nation Center for Biotechnology nucleotide database using metaWRAP (68). Blobology (69) was used to visualize and compare the microbial community compositions. Quantification of the abundance of each bin across samples was performed within the bin quantification module of metaWRAP. Individual bins were reassembled producing a final set of metagenome assembled genomes (MAGs) deemed to be of high quality if greater than 70% complete and less than 10% redundant. MAGs were screened for putative extracellular electron pathways as previously described (35). Sequencing data generated in this experiment have been deposited in the Sequence Read Archive (SRA) of the GenBank database under the accession numbers SRR8611926 and SRR8611927, the diorite-oxidizing enrichment culture and *in situ* sample, respectively.

Data Analysis. Unpaired t-tests were used in statistical comparison between unoxidized (time zero and control) and microbially oxidized (A, B, C) using GraphPad Prism version 7.05 (www.graphpad.com). Two tailed p-values are reported.

Acknowledgements

We thank the NSF Luquillo Critical Zone Observatory (LCZO) for access to facilities and assistance with field work. This work was supported by the NASA Astrobiology Institute and a University of Wisconsin Microbiome Initiative award to EER. SLB and HLB acknowledge support from the LCZO (NSF EAR-0722476 and EAR-1331841).

References

1. J. F. Banfield, W. W. Barker, S. A. Welch, A. Taunton, Biological impact on mineral dissolution: application of the lichen model to understanding mineral weathering in the rhizosphere. *Proc Natl Acad Sci U S A* **96**, 3404-3411 (1999).
2. W. Bach, K. J. Edwards, Iron and sulfide oxidation within the basaltic ocean crust: implications for chemolithoautotrophic microbial biomass production. *Geochim Cosmochim Acta* **67**, 3871-3887 (2003).
3. B. M. Jakosky, E. L. Shock, The biological potential of Mars, the early Earth, and Europa. *J Geophys Res Planets* **103**, 19359-19364 (1998).
4. K. J. Edwards *et al.*, Ultra-diffuse hydrothermal venting supports Fe-oxidizing bacteria and massive umber deposition at 5000 m off Hawaii. *ISME J* **5**, 1748-1758 (2011).
5. C. M. Santelli *et al.*, Abundance and diversity of microbial life in ocean crust. *Nature* **453**, 653-656 (2008).
6. L. A. Sudek *et al.*, Submarine Basaltic Glass Colonization by the Heterotrophic Fe(II)-Oxidizing and Siderophore-Producing Deep-Sea Bacterium Pseudomonas stutzeri VS-10: The Potential Role of Basalt in Enhancing Growth. *Front Microbiol* **8**, 363 (2017).
7. M. Y. Xiong, E. S. Shelobolina, E. E. Roden, Potential for microbial oxidation of ferrous iron in basaltic glass. *Astrobiology* **15**, 331-340 (2015).
8. B. Bailey, A. Templeton, H. Staudigel, B. M. Tebo, Utilization of Substrate Components during Basaltic Glass Colonization by Pseudomonas and Shewanella Isolates. *Geomicrobiol J* **26**, 648-656 (2009).
9. A. S. Templeton *et al.*, A seafloor microbial biome hosted within incipient ferromanganese crusts. *Nature Geoscience* **2**, 872-876 (2009).
10. S. Uroz, C. Calvaruso, M. P. Turpault, P. Frey-Klett, Mineral weathering by bacteria: ecology, actors and mechanisms. *Trends Microbiol* **17**, 378-387 (2009).
11. E. Shelobolina *et al.*, Microbial lithotrophic oxidation of structural Fe(II) in biotite. *Appl Environ Microbiol* **78**, 5746-5752 (2012).
12. S. Uroz *et al.*, Functional assays and metagenomic analyses reveals differences between the microbial communities inhabiting the soil horizons of a Norway spruce plantation. *PLoS One* **8**, e55929 (2013).
13. B. Wild *et al.*, In-situ dissolution rates of silicate minerals and associated bacterial communities in the critical zone (Strengbach catchment, France). *Geochim Cosmochim Acta* **249**, 95-120 (2019).
14. C. S. Cockell, Life in the lithosphere, kinetics and the prospects for life elsewhere. *Philos Trans A Math Phys Eng Sci* **369**, 516-537 (2011).
15. H. L. Buss *et al.*, The coupling of biological iron cycling and mineral weathering during saprolite formation, Luquillo Mountains, Puerto Rico. *Geobiology* **3**, 247-260 (2005).
16. S. J. Hall *et al.*, Drivers and patterns of iron redox cycling from surface to bedrock in a deep tropical forest soil: a new conceptual model. *Biogeochemistry* **130**, 177-190 (2016).
17. M. L. Minyard *et al.*, Bacterial Associations with Weathering Minerals at the Regolith-Bedrock Interface, Luquillo Experimental Forest, Puerto Rico. *Geomicrobiol J* **29**, 792-803 (2012).
18. A. F. White *et al.*, Chemical weathering in a tropical watershed, Luquillo Mountains, Puerto Rico: I. Long-term versus short-term weathering fluxes. *Geochim Cosmochim Acta* **62**, 209-226 (1998).

19. J. Orlando *et al.*, Architecture of the deep critical zone in the Río Icacos watershed (Luquillo Critical Zone Observatory, Puerto Rico) inferred from drilling and ground penetrating radar (GPR). *Earth Surface Processes and Landforms* **41**, 1826-1840 (2016).
20. B. F. Turner, R. F. Stallard, S. L. Brantley, Investigation of in situ weathering of quartz diorite bedrock in the Rio Icacos basin, Luquillo Experimental Forest, Puerto Rico. *Chemical Geology* **202**, 313-341 (2003).
21. R. Fletcher, H. Buss, S. Brantley, A spheroidal weathering model coupling porewater chemistry to soil thicknesses during steady-state denudation. *Earth Planet Sci Lett* **244**, 444-457 (2006).
22. H. L. Buss, P. B. Sak, S. M. Webb, S. L. Brantley, Weathering of the Rio Blanco quartz diorite, Luquillo Mountains, Puerto Rico: Coupling oxidation, dissolution, and fracturing. *Geochim Cosmochim Acta* **72**, 4488-4507 (2008).
23. D. L. Balkwill *et al.*, Equivalence of microbial biomass measures based on membrane lipid and cell wall components, adenosine triphosphate, and direct counts in subsurface aquifer sediments. *Microbial Ecology* **16**, 73-84 (1988).
24. D. S. Jenkinson, S. A. Davidson, D. S. Powlson, Adenosine triphosphate and microbial biomass in soil. *Soil Biol Biochem* **11**, 521-527 (1979).
25. M. Contin, A. Todd, P. C. Brookes, The ATP concentration in the soil microbial biomass. *Soil Biol Biochem* **33**, 701-704 (2001).
26. D. Sobolev, E. Roden, Characterization of a neutrophilic, chemolithoautotrophic Fe(II)-oxidizing β-Proteobacterium from freshwater wetland sediments. *Geomicrobiol J* **21**, 1-10 (2004).
27. C. Lepleux *et al.*, Correlation of the abundance of betaproteobacteria on mineral surfaces with mineral weathering in forest soils. *Appl Environ Microbiol* **78**, 7114-7119 (2012).
28. E. Shelobolina *et al.*, Isolation of phyllosilicate-iron redox cycling microorganisms from an illite-smectite rich hydromorphic soil. *Front Microbiol* **3**, 134 (2012).
29. K. A. Weber, F. W. Picardal, E. E. Roden, Microbially catalyzed nitrate-dependent oxidation of biogenic solid-phase Fe(II) compounds. *Environ Sci Technol* **35**, 1644-1650 (2001).
30. C. Appia-Ayme, N. Guiliani, J. Ratouchniak, V. Bonnefoy, Characterization of an operon encoding two c-type cytochromes an aa3-type cytochrome oxidase, and rusticyanin in Acidithiobcillus ferrooxidans ATCC 33020. *Appl Environ Microbiol* **65**, 4781-4787 (1999).
31. C. Castelle *et al.*, A new iron-oxidizing/O2-reducing supercomplex spanning both inner and outer membranes, isolated from the extreme acidophile Acidithiobacillus ferrooxidans. *J Biol Chem* **283**, 25803-25811 (2008).
32. D. R. Lovley, D. E. Holmes, K. P. Nevin, "Dissimilatory Fe(III) and Mn(IV) Reduction" in Advances in Microbial Physiology. (2004), vol. 49, pp. 219-286.
33. R. A. Barco *et al.*, New Insight into Microbial Iron Oxidation as Revealed by the Proteomic Profile of an Obligate Iron-Oxidizing Chemolithoautotroph. *Appl Environ Microbiol* **81**, 5927-5937 (2015).
34. J. Liu *et al.*, Identification and Characterization of MtoA: A Decaheme c-Type Cytochrome of the Neutrophilic Fe(II)-Oxidizing Bacterium Sideroxydans lithotrophicus ES-1. *Front Microbiol* **3**, 37 (2012).

35. S. He, R. A. Barco, D. Emerson, E. E. Roden, Comparative Genomic Analysis of Neutrophilic Iron(II) Oxidizer Genomes for Candidate Genes in Extracellular Electron Transfer. *Front Microbiol* **8**, 1584 (2017).
36. S. M. McAllister *et al.*, Validating the Cyc2 neutrophilic Fe oxidation pathway using meta-omics of Zetaproteobacteria iron mats at marine hydrothermal vents. bioRxiv:10.1101/722066 (2019).
37. E. D. Swanner, R. M. Nell, A. S. Templeton, Ralstonia species mediate Fe-oxidation in circumneutral, metal-rich subsurface fluids of Henderson mine, CO. *Chemical Geology* **284**, 339-350 (2011).
38. Y. Jiao, A. Kappler, L. R. Croal, D. K. Newman, Isolation and characterization of a genetically tractable photoautotrophic Fe(II)-oxidizing bacterium, Rhodopseudomonas palustris strain TIE-1. *Appl Environ Microbiol* **71**, 4487-4496 (2005).
39. S. Bonneville, A. W. Bray, L. G. Benning, Structural Fe(II) Oxidation in Biotite by an Ectomycorrhizal Fungi Drives Mechanical Forcing. *Environ Sci Technol* **50**, 5589-5596 (2016).
40. J. W. Chen, K. G. Chan, Genome sequence of Dyella japonica strain A8, a quorum-quenching bacterium that degrades N-acylhomoserine lactones, isolated from Malaysian tropical soil. *J Bacteriol* **194**, 6331 (2012).
41. H. L. Buss, A. Lüttge, S. L. Brantley, Etch pit formation on iron silicate surfaces during siderophore-promoted dissolution. *Chem Geol* **240**, 326-342 (2007).
42. U. Schwertmann, R. M. Taylor, "Iron Oxides" in Minerals in Soil Environments. (Soil Science Society of America, Madison, WI, 1989), 10.2136/sssabookser1.2ed.c8, pp. 379-437.
43. L. Sigg, W. Stumm, The interaction of anions and weak acids with the hydrous goethite (α-FeOOH) surface. *Colloids and Surfaces* **2**, 101-117 (1981).
44. L. Wu, A. D. Jacobson, M. Hausner, Characterization of elemental release during microbe–granite interactions at T=28°C. *Geochim Cosmochim Acta* **72**, 1076-1095 (2008).
45. B. Frey *et al.*, Weathering-associated bacteria from the Damma glacier forefield: physiological capabilities and impact on granite dissolution. *Appl Environ Microbiol* **76**, 4788-4796 (2010).
46. W. W. Barker, S. A. Welch, S. Chu, J. F. Banfield, Experimental observations of the effects of bacteria on aluminosilicate weathering. *American Mineralogist* **83**, 1551-1563 (1998).
47. L. J. Liermann *et al.*, Microenvironments of pH in biofilms grown on dissolving silicate surfaces. *Chem Geol* **171**, 1-16 (2000).
48. P. Vandevivere, S. A. Welch, W. J. Ullman, D. L. Kirchman, Enhanced dissolution of silicate minerals by bacteria at near-neutral pH. *Microb Ecol* **27**, 241-251 (1994).
49. B. E. Kalinowski *et al.*, X-ray photoelectron evidence for bacteria-enhanced dissolution of hornblende. *Geochim Cosmochim Acta* **64**, 1331-1343 (2000).
50. L. J. Liermann, B. E. Kalinowski, S. L. Brantley, J. G. Ferry, Role of bacterial siderophores in dissolution of hornblende. *Geochim Cosmochim Acta* **64**, 587-602 (2000).
51. J. B. Neilands, Siderophores: structure and function of microbial iron transport compounds. *J Biol Chem* **270**, 26723-26726 (1995).

52. H. L. Buss, R. Mathur, A. F. White, S. L. Brantley, Phosphorus and iron cycling in deep saprolite, Luquillo Mountains, Puerto Rico. *Chem Geol* **269**, 52-61 (2010).
53. A. K. Navarre-Sitchler *et al.*, Porosity and surface area evolution during weathering of two igneous rocks. *Geochim Cosmochim Acta* **109**, 400-413 (2013).
54. R. A. Berner, E. L. Sjoberg, M. A. Velbel, M. D. Krom, Dissolution of pyroxenes and amphiboles during weathering. *Science* **207**, 1205-1206 (1980).
55. I. Barshad, F. M. Kishk, Oxidation of ferrous iron in vermiculite and biotite alters fixation and replaceability of potassium. *Science* **162**, 1401-1402 (1968).
56. R. J. Gilkes, R. C. Young, J. P. Quirk, Artificial weathering of oxidized biotite: I. potassium removal by sodium chloride and sodium tetraphenylboron solutions. *Soil Sci Soc Am J* **37**, 25-28 (1973).
57. R. J. Gilkes, R. C. Young, J. P. Quirk, Artificial weathering of oxidized biotite: II. rates of dissolution in 0.1, 0.01, 0.001M HCl. *Soil Sci Soc Am J* **37**, 29-33 (1973).
58. G. Y. Jeong, H. B. Kim, Mineralogy, chemistry, and formation of oxidized biotite in the weathering profile of granitic rocks. *Am Mineral* **88**, 352-364 (2003).
59. S. F. Murphy *et al.*, Chemical weathering in a tropical watershed, Luquillo Mountains, Puerto Rico: II. Rate and mechanism of biotite weathering. *Geochim Cosmochim Acta* **62**, 227-243 (1998).
60. L. L. Stookey, Ferrozine-A new spectrophotometric reagent for iron. *Anal Chem* **42**, 778-781 (1970).
61. C. Balland, A. Poszwa, C. Leyval, C. Mustin, Dissolution rates of phyllosilicates as a function of bacterial metabolic diversity. *Geochim Cosmochim Acta* **74**, 5478-5493 (2010).
62. J. Zhou, M. A. Bruns, J. M. Tiedje, DNA recovery from soils of diverse composition. *Appl Environ Microbiol* **62**, 316-322 (1996).
63. D. E. Wood, S. L. Salzberg, Kraken: ultrafast metagenomic sequence classification using exact alignments. *Genome Biology* **15** (2014).
64. Y. Peng, H. C. Leung, S. M. Yiu, F. Y. Chin, IDBA-UD: a de novo assembler for single-cell and metagenomic sequencing data with highly uneven depth. *Bioinformatics* **28**, 1420-1428 (2012).
65. D. D. Kang, J. Froula, R. Egan, Z. Wang, MetaBAT, an efficient tool for accurately reconstructing single genomes from complex microbial communities. *PeerJ* **3**, e1165 (2015).
66. D. H. Parks *et al.*, CheckM: assessing the quality of microbial genomes recovered from isolates, single cells, and metagenomes. *Genome Res* **25**, 1043-1055 (2015).
67. S. F. Altschup *et al.*, Basic Local Alignment Search Tool. *J Mol Biol* **215**, 403-410 (1990).
68. G. V. Uritskiy, J. DiRuggiero, J. Taylor, MetaWRAP-a flexible pipeline for genome-resolved metagenomic data analysis. *Microbiome* **6**, 158 (2018).
69. S. Kumar *et al.*, Blobology: exploring raw genome data for contaminants, symbionts and parasites using taxon-annotated GC-coverage plots. *Front Genet* **4**, 237 (2013).

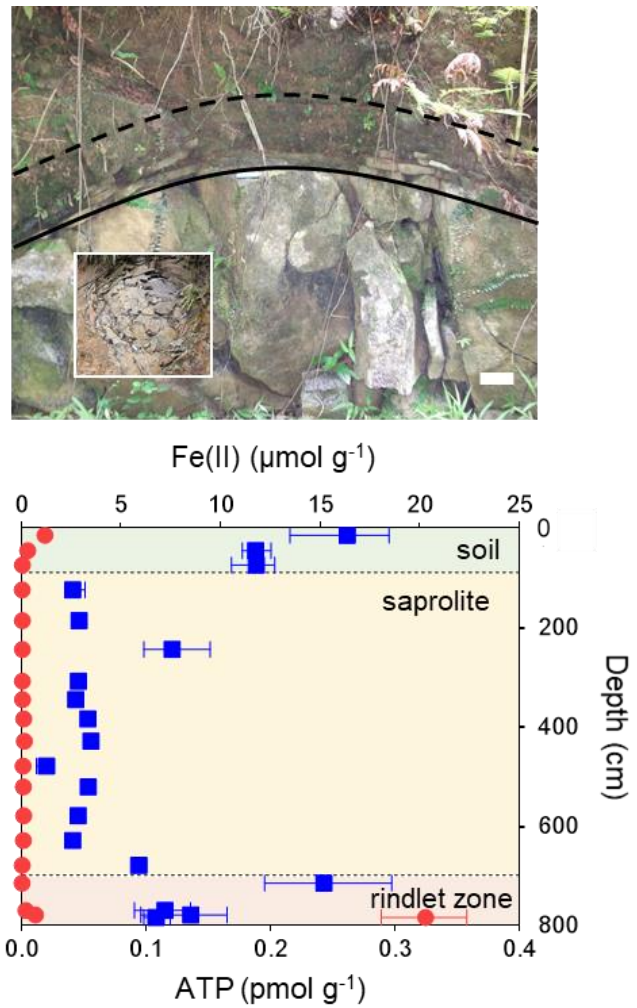

Figure 1 Top: Roadcut exposure of the Rio Blanco Quartz Diorite, used for illustrative purposes to conceptualize the subsurface weathering system at Guaba Ridge within the Rio Icacos watershed of the Luquillo Critical Zone Observatory in Puerto Rico. The rindlet zone, approximately delineated between the solid line (bedrock-rindlet interface) and the dashed line (rindlet-saprolite interface), overlies the corestones of bedrock and is the zone of active weathering targeted in this study. Scale bar equals 10 cm. The inset at left shows a plan view of the rindlet zone exposed elsewhere. Bottom: Total 0.5 M HCl extractable Fe(II) (red circles) and ATP content (blue squares) of the actual subsurface regolith obtained by hand auger atop Guaba Ridge (Core A) including soil, saprolite and the outer rindlet zone which was partially penetrated with auger refusal occurring prior to reaching the bedrock-rindlet interface (note that the subsurface rindlet zone is substantially thicker than that revealed by the roadcut). Data points and error bars denote the mean and range of triplicate measurements.

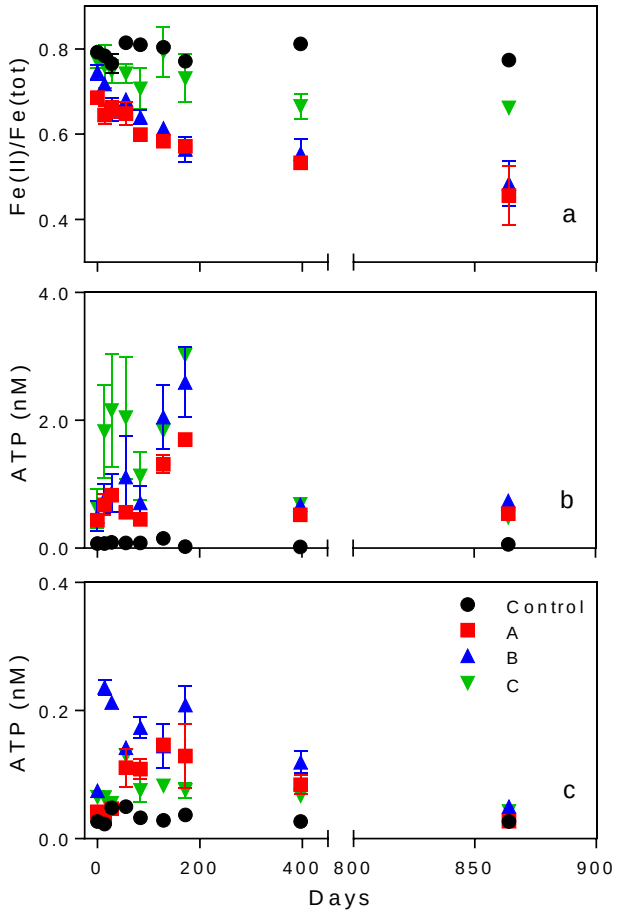

Figure 2 Molar ratio of Fe(II) to total Fe concentration [Fe(II)/Fe(tot)] in dilute HCl extracts of solid phase material in quartz diorite enrichment cultures containing three separate inocula from the rindlet-saprolite interface (A,B,C) compared to abiotic uninoculated controls. (a); ATP content of cultures containing quartz diorite (b) or quartz sand (c). Data points and error bars denote the mean and range of duplicate cultures.

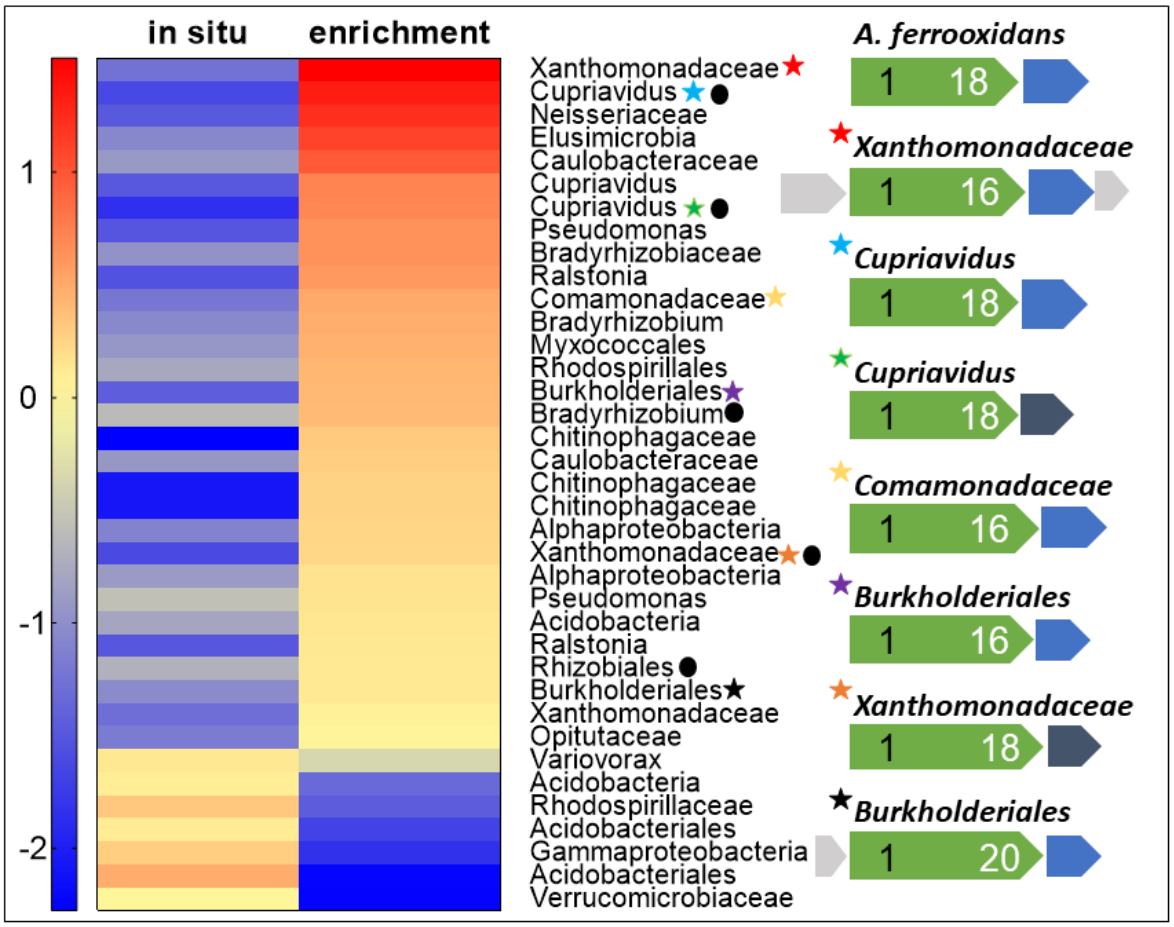

Figure 3 Heat map comparison of high-quality MAG abundance (log genomes per million reads) and taxonomy between the *in-situ* bedrock-saprolite interface sample (785cm depth) and quartz diorite-oxidizing enrichment culture from the same inocula. Stars indicate the presence of homologs to the model Cyc2 iron oxidation system of *Acidithiobacillus ferrooxidans*. Corresponding gene maps (indicated by star color) are shown for each Cyc2 homolog, compared to the model (top). Extracellular or outer membrane putative Cyc2 proteins (green) are scaled to the size of the protein with the number of N-terminal heme binding motifs indicated in black and C-terminal transmembrane domains in white. Periplasmic electron carriers including monoheme c-type cytochromes (blue) or high potential iron-sulfur proteins (dark grey) and hypothetical proteins (light grey) are also indicated. Presence of RuBisCo indicated by a circle.

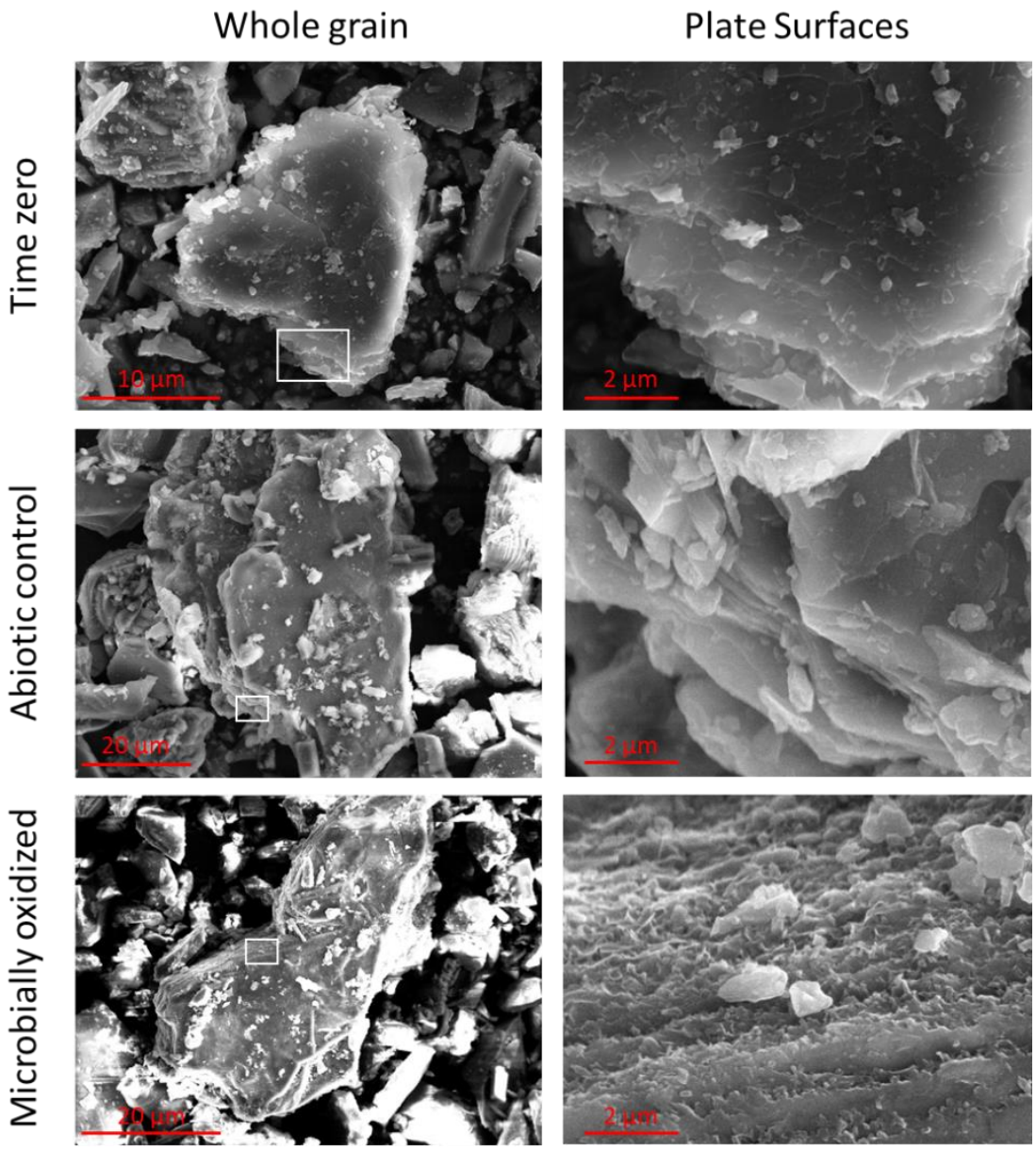

Figure 4 FE-SEM images of biotite at the whole grain scale (left) and basal plane (right). Note the differences in scale on whole grain images as individual grain sizes are variable. For consistency, basal plane images are at the same scale. The approximate area of the basal plane presented is outlined in white on the grain scale images. Note the ragged appearance of the basal plane observed after microbial incubation.

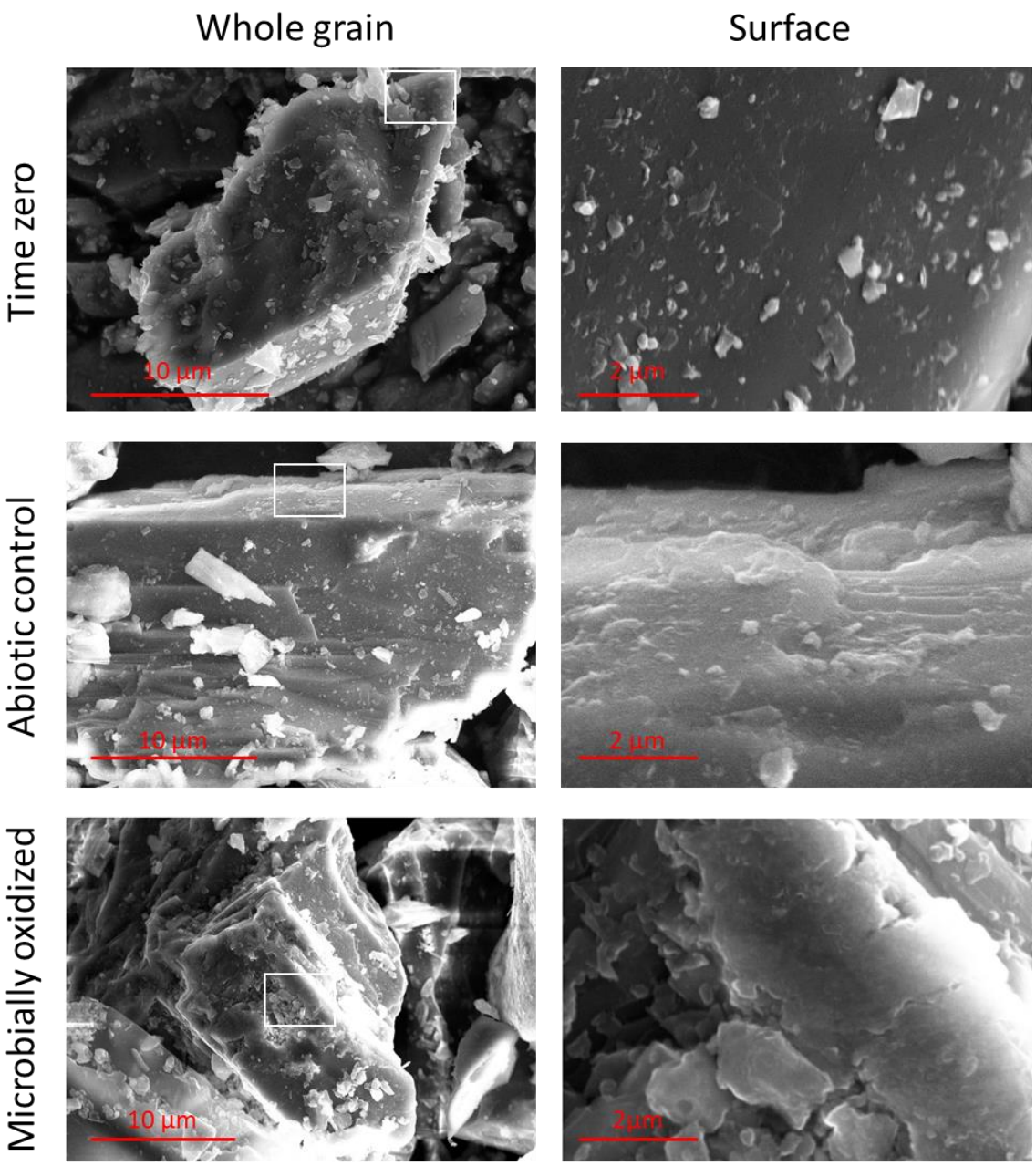

Figure 5 FE-SEM images of hornblende at the whole grain scale (left) and surface scale (right). Note the differences in scale on whole grain images as individual grain sizes are variable. For consistency, surface images are at the same scale. The approximate area of the hornblende surfaces is outlined in white on the grain scale image.

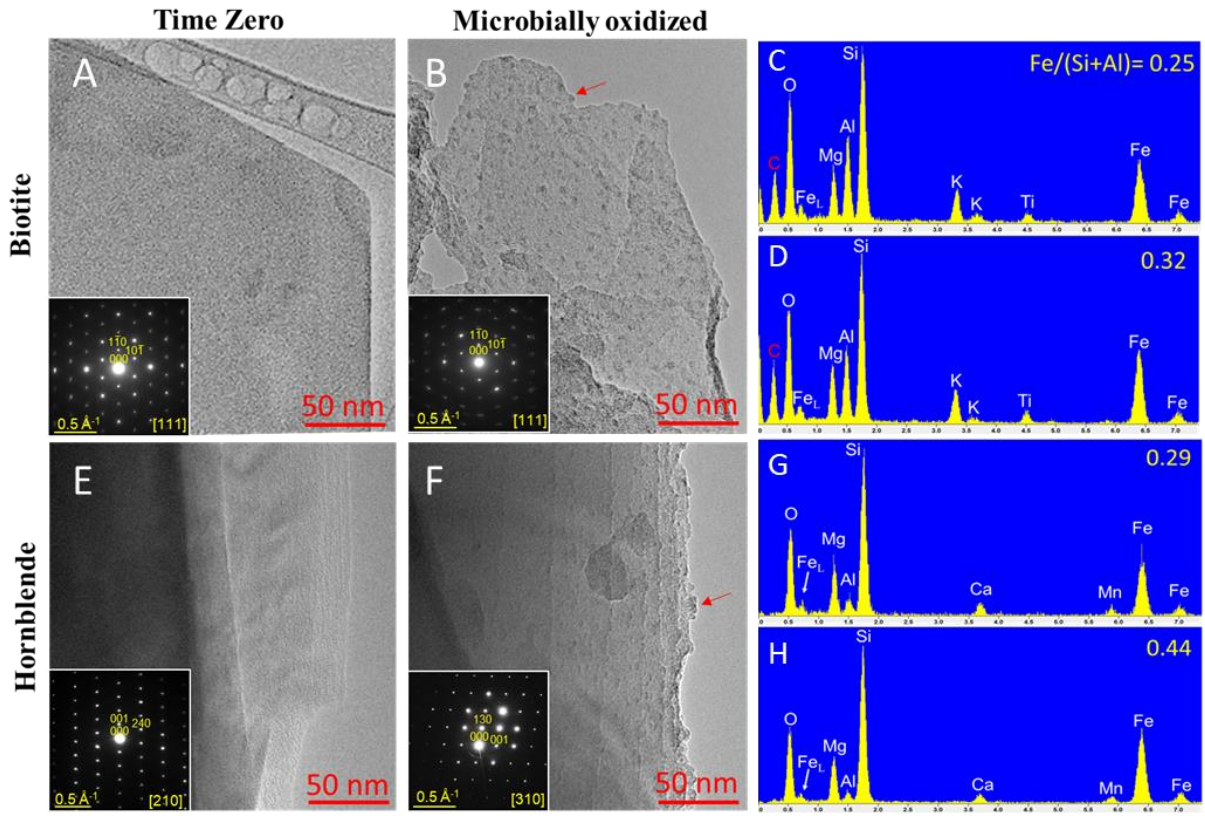

Figure 6 Bright field TEM images and SAED patterns (inset) showing widespread nano-sized Fe-oxyhydroxide particles (examples indicated by arrows) along the basal plane of microbially-oxidized biotite (B) and surface steps of hornblende (F), which were absent in unoxidized time zero samples (A and E). The size (ca. 3-5 nm) of the Fe-oxyhydroxides is consistent with ferrihydrite. X-ray TEM-EDS spectra confirm the enrichment of Fe (as indicated by the Fe/(Si+Al) atomic ratio) on both microbially oxidized biotite (D) and hornblende (H) compared to initial time zero surfaces (C and G).

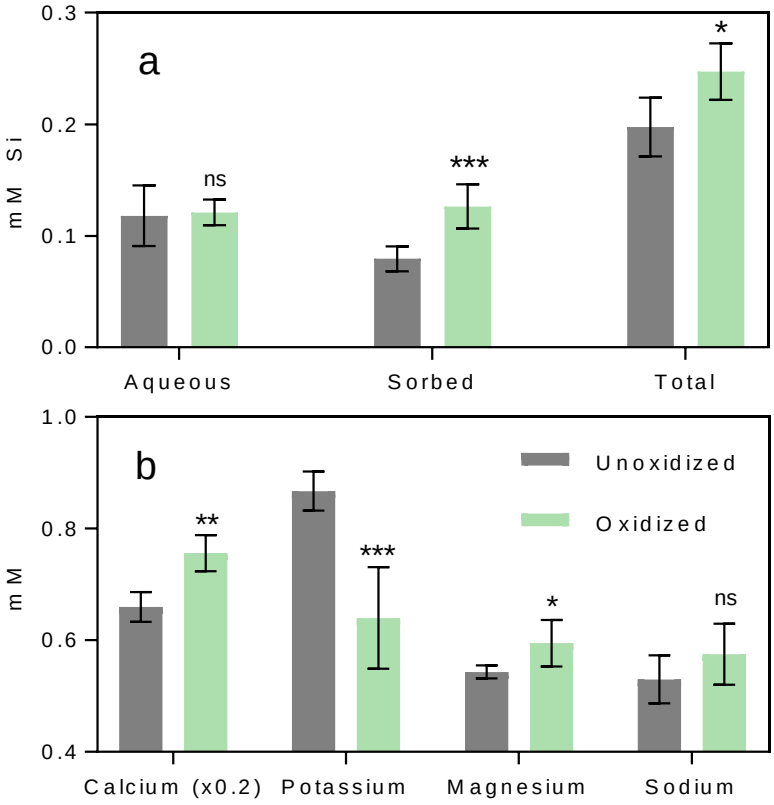

Figure 7 (a) Concentrations of aqueous, sorbed and total Si released from unoxidized (combined time zero and abiotic controls), and microbially-oxidized quartz diorite (A, B and C) after 864 days of incubation. (b) Concentrations of HNO_3-extractable cations released from unoxidized microbially-oxidized samples (A, B and C). For both panels, n=6 for microbially-oxidized samples (duplicate cultures from 3 inocula after 864 days), and n=10 for unoxidized (duplicate cultures from time zero for 3 inocula and abiotic control and the abiotic control after 864 days incubation). Two tailed p-values for unpaired t-test between unoxidized and microbially oxidized are indicated for $p<0.5$ by one star, $p<0.01$ by two stars, and $p<0.001$ by three stars.

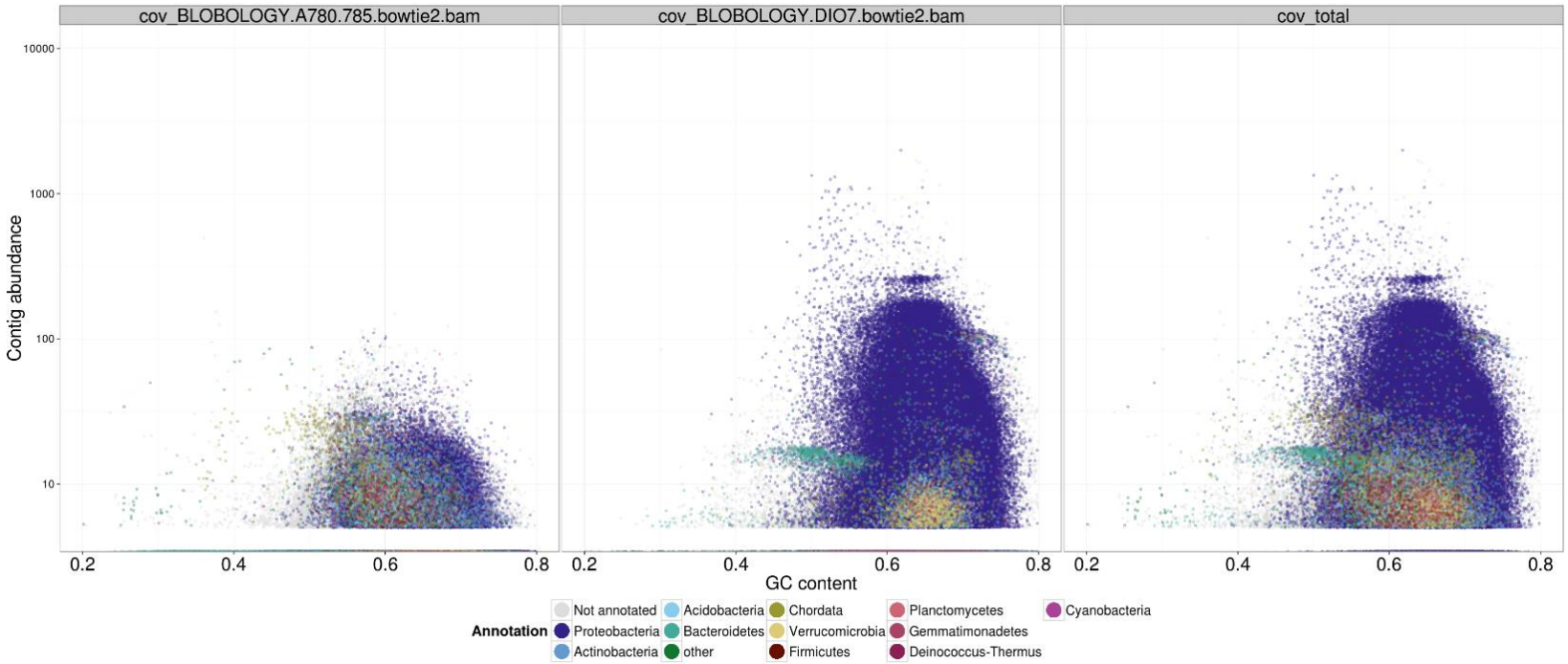

Fig. S1. GC versus contig abundance Blob plots of individual contigs (n= 584329) from the total coassembly (right) and the *in situ* metagenome (left) obtained from 7.85 m depth (Sample A) and a quartz diorite enrichment culture from the same inocula (center), colored by phylum level classification demonstrating a decrease in community complexity and enrichment in *Betaproteobacteria* in the enrichment culture.

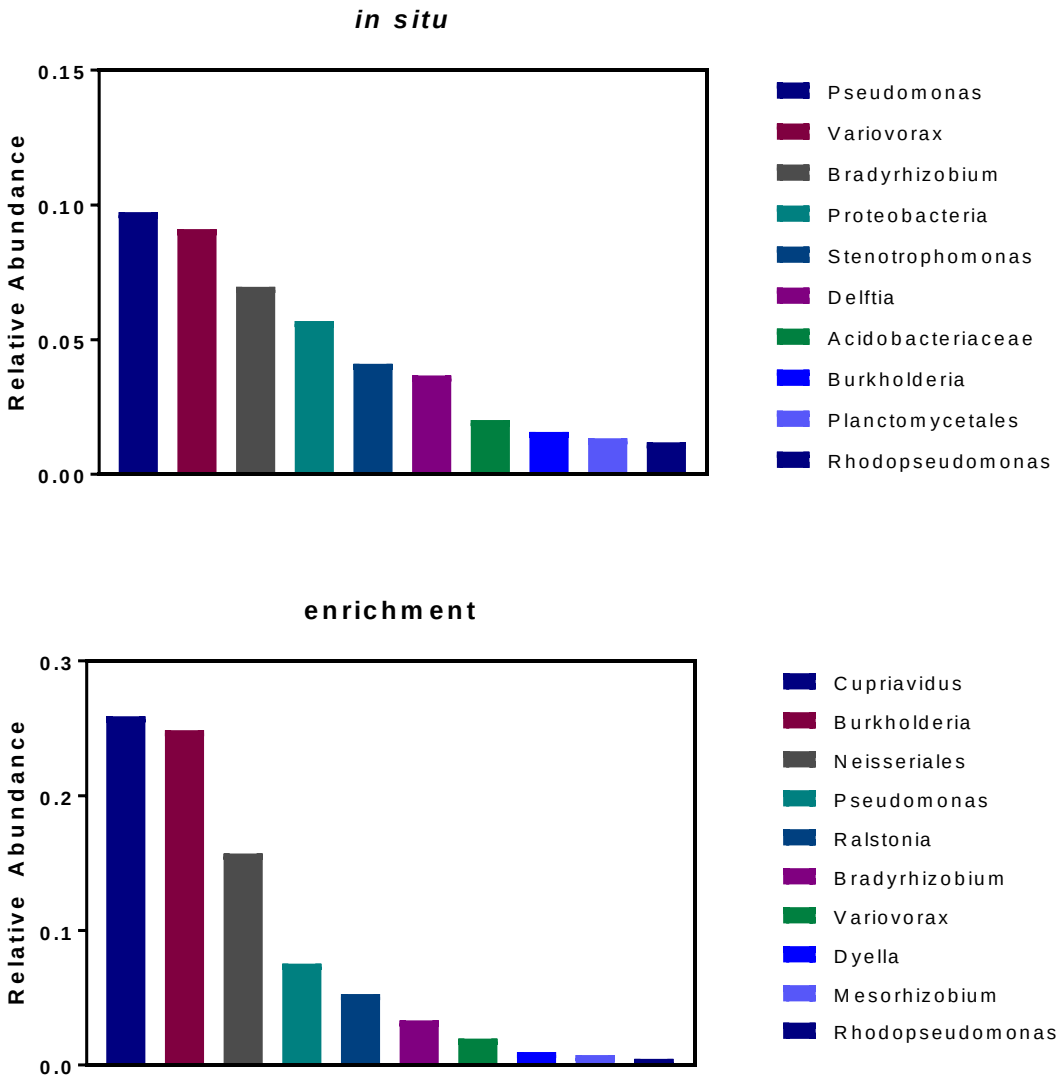

Fig. S2. Relative abundance of the 10 most abundant genera, or higher taxonomic classification if unable to achieve genera-level classification in the *in situ* (top) and enrichment culture (bottom) metagenomes based on taxonomic classification of individual reads.

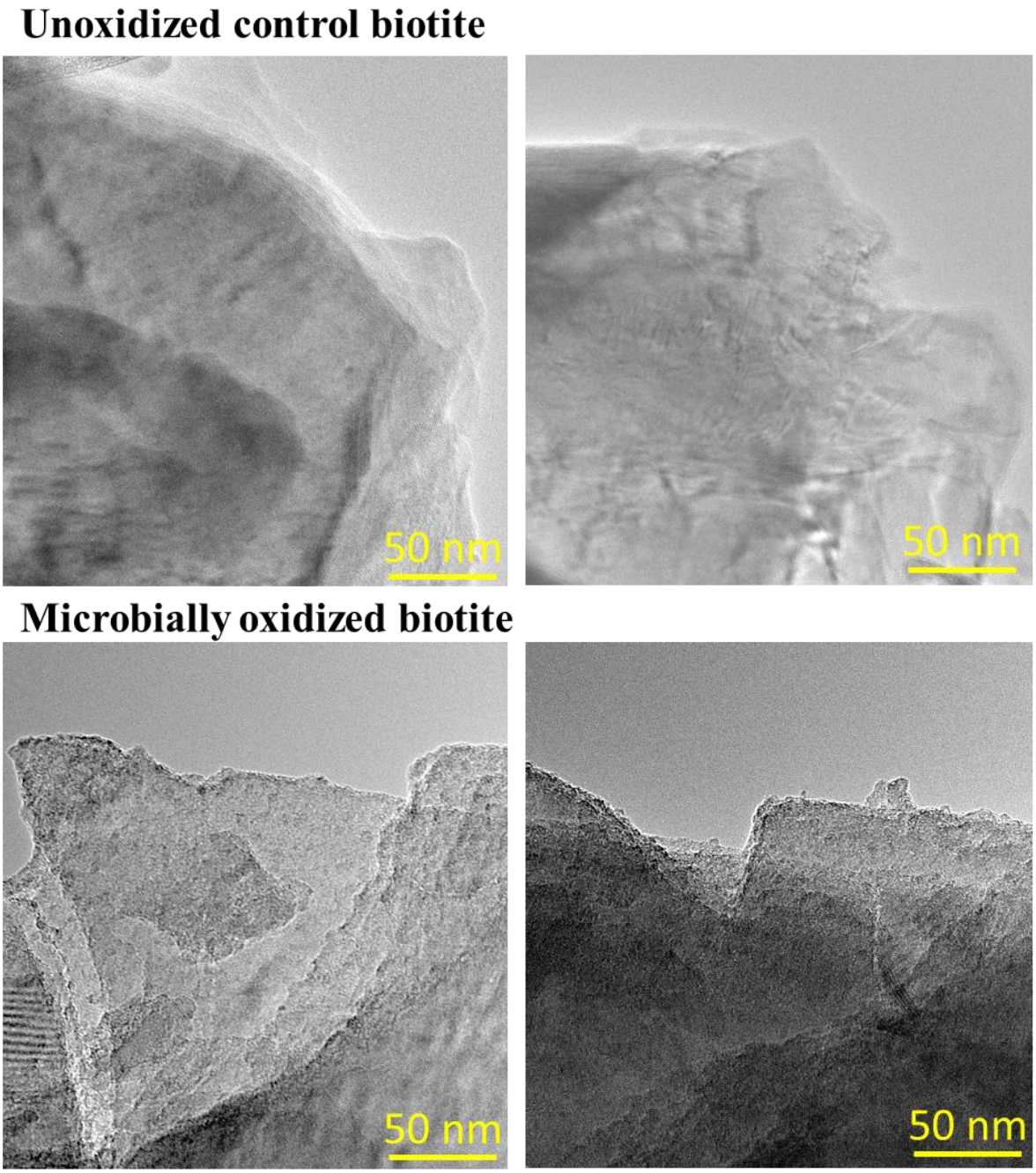

Fig. S3. Bright field TEM images comparing abiotic control (top) and microbially oxidized (bottom) biotite surfaces after 864 days incubation.

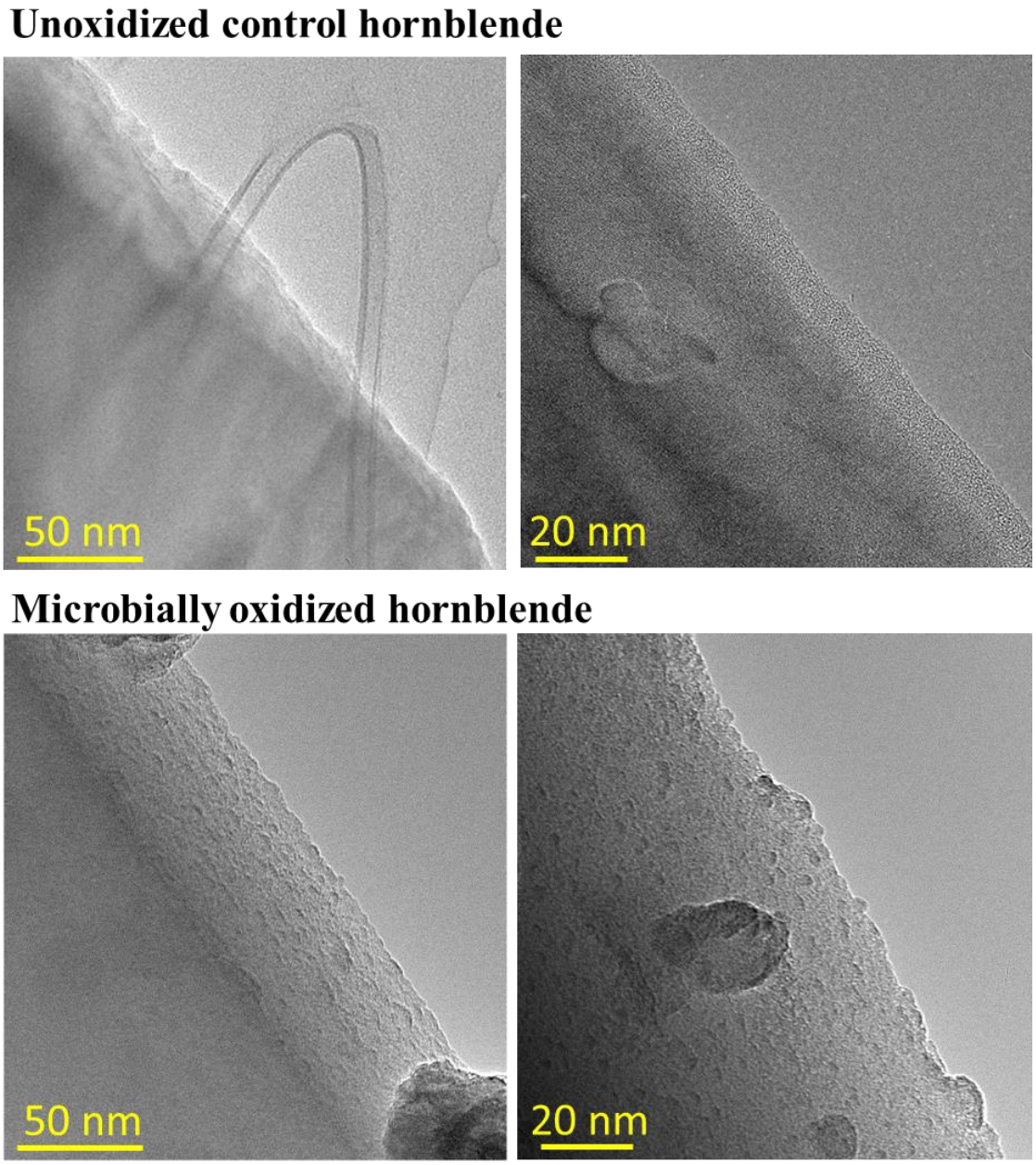

Fig. S4. Bright field TEM images comparing abiotic control (top) and microbially oxidized (bottom) hornblende surfaces after 864 days of incubation.

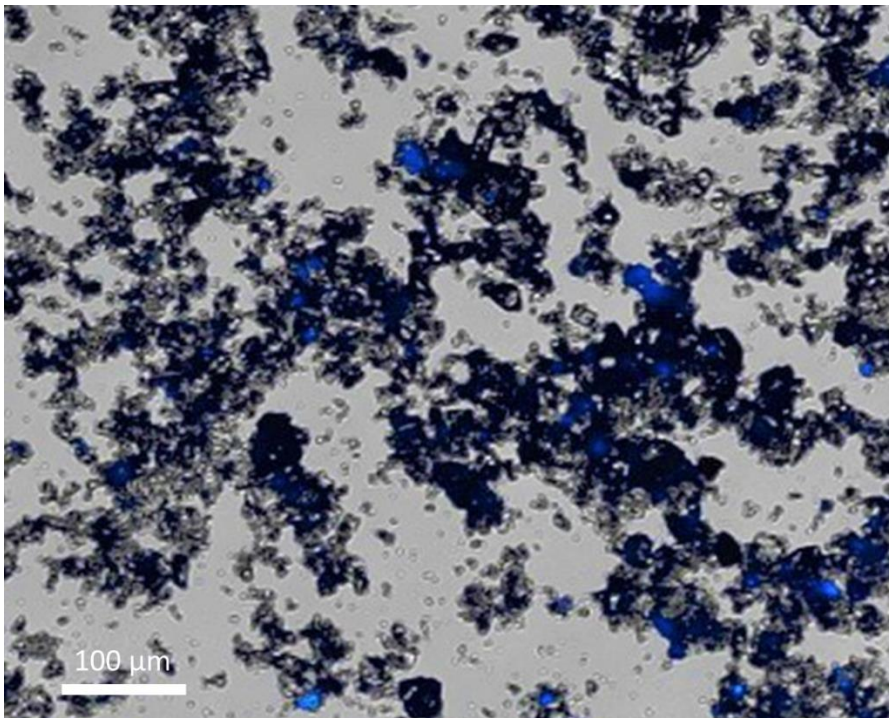

Fig. S5. Composite image (epifluorescence and light) of DAPI stained diorite oxidizing enrichment culture showing close association of cells (bright blue spots) with mineral grains.

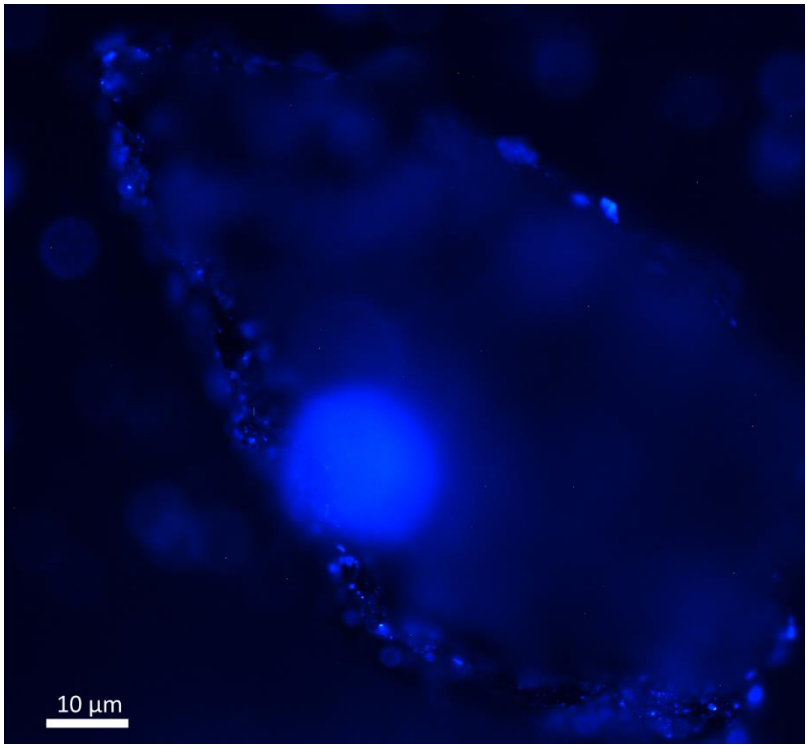

Fig. S6. Epifluorescence microscopy of a DAPI stained individual biotite grain obtained from enrichment culture revealing sparse microbial colonization of mineral edges.

Table S1 Calculated growth yields in µmol biomass C µmol^{-1} Fe(II) oxidized in individual reactors.

Sample	nM ATP	g C/L	µmol C/mL	Initial Fe(II) µmol/mL	Initial Fe(II)/Fe(tot)	Final Fe(II)/Fe(tot)	Δ Fe(II)/Fe(tot)	Fe(II) oxidized	yield
A1	1.646	0.00016	0.014	7.442	0.697	0.572	0.125	0.930	0.015
A2	1.751	0.00018	0.015	7.161	0.674	0.572	0.102	0.730	0.020
B1	3.142	0.00031	0.026	7.174	0.728	0.535	0.193	1.385	0.019
B2	2.045	0.00020	0.017	7.711	0.763	0.593	0.170	1.311	0.013
C1	3.033	0.00030	0.025	8.430	0.787	0.787	0.000	0.000	n/a
C2	3.007	0.00030	0.025	7.665	0.755	0.674	0.081	0.621	0.040

Table S2 Abundance of major elements in the Rio Blanco Quartz Diorite as determined by aqua regia digestion and ICP-OES analysis.

Element	**Abundance (wt %)**
Al	7.17
Ca	3.87
Fe	3.81
K	1.06
Mg	1.33
Na	2.04
Ti	0.304

Chapter 2

Microbial chemolithotrophic oxidation of pyrite in a subsurface shale weathering environment: geologic considerations and potential mechanisms

Stephanie A. Napieralski[1], Virginia Marcon[2], Yihang Fang[1], Susan L. Brantley[2], Huifang Xu[1] and Eric E. Roden[1]

[1]Department of Geoscience, University of Wisconsin-Madison, Madison WI 53706. [2]Earth and Environmental Systems Institute, and the Department of Geosciences, Pennsylvania State University, University Park PA 16802.

In preparation for submission to Geobiology

Abstract

Oxidative weathering of pyrite plays an important role in the biogeochemical cycling of Fe and S in terrestrial environments. The mechanism and occurrence of biologically accelerated pyrite oxidation under acidic conditions is well established, where microorganisms oxidize soluble ferrous iron that is otherwise stable at low pH. In contrast, much less is known about microbially-mediated pyrite oxidation at circumneutral pH. Recent work (Percak-Dennett et al., 2017) demonstrated the ability of aerobic chemolithotrophic microorganisms to accelerate pyrite oxidation at circumneutral pH and proposed two mechanistic models by which this phenomenon might occur. Here we assess the potential relevance of aerobic microbially-catalyzed circumneutral pH pyrite oxidation in relation to subsurface shale weathering at Susquehanna Shale Hills Critical Zone Observatory (SSHCZO) in Pennsylvania, USA. Specimen pyrite mixed with ground native shale was incubated in groundwater for three months at the inferred depth of the *in situ* pyrite oxidation front. The colonized materials were used as an inoculum for pyrite-oxidizing enrichment cultures in both buffered (10 mM Pipes) and unbuffered medium with and without ground native shale. Microbial activity accelerated the release of sulfate across all conditions tested, in some cases several-fold. 16S rRNA gene amplicon sequencing and shotgun metagenomic analysis revealed the dominance of a putative chemolithoautotrophic sulfur-oxidizing bacterium from the genus *Thiobacillus* in the enrichment cultures. Previously proposed models for aerobic microbial pyrite oxidation were assessed in terms of physical constraints, enrichment culture geochemistry, and metagenomic analysis. Although we conclude that subsurface pyrite oxidation at SSCHZO is largely abiotic in nature, this work nonetheless yields new insight into the potential pathways by which aerobic microorganisms can accelerate pyrite oxidation at circumneutral pH. Specifically, we propose the existence of a new “direct sulfur

interaction" pathway, whereby sulfhydrl-bearing outer membrane proteins mediate oxidation of pyrite surfaces through a persulfide intermediate, analogous to previously proposed mechanisms for direct microbial oxidation of elemental sulfur. The action of this and other direct microbial pyrite oxidation pathways have major implications for controls on pyrite weathering rates in circumneutral pH sedimentary environments where pore throat sizes permit widespread access of microorganisms to pyrite surfaces.

1 Introduction

Pyrite (FeS_2) is commonly observed in sedimentary rocks, e.g. shales, which comprise an estimated 25% of exposed continental rocks (Amiotte Suchet et al., 2003). Pyrite is also present in anoxic soils and in both freshwater and marine sedimentary environments where conditions for formation and preservation environments are appropriate. As such, pyrite is the most abundant sulfide mineral in Earth's crust, and its formation and destruction plays a critical role in modern iron and sulfur cycles (Raiswell and Canfield, 2012), as well as in modulation of Earth's O_2 and CO_2 budgets over geologic time (Berner, 2006). The oxidative weathering of pyrite is rapid in near surface environments due to the high reactivity of pyrite in the presence of molecular oxygen. An extensive body of literature exists on the oxidation of pyrite in anthropogenically disturbed systems, including those impacted by mining activities. The rapid exposure of sulfide bearing rock to atmospheric oxygen results in the generation of large quantities of sulfuric acid, presenting significant environmental concerns including acid rock drainage and mobilization of toxic metals (Blowes et al., 2003). Under acidic conditions, soluble ferric iron acts as dominant oxidant for pyrite, owing to the solubility of Fe(III) at low pH and the rapid reaction of Fe^{3+} ions with pyrite (Moses et al., 1987). It is has long been recognized and is well established that microbial communities in acid mine drainage are key in mediating pyrite oxidation by virtue of their ability to aerobically oxidize Fe^{2+} ions released during pyrite oxidation back to Fe^{3+} (Baker and Banfield, 2003; Colmer and Hinkle, 1947). Chemolithotrophic iron and sulfur oxidizing acidophiles such as *Acidithiobacillus ferrooxydans* and *A. thiooxidans* can thus effectively accelerate the rate limiting step of pyrite oxidation by several orders of magnitude (Singer and Stumm, 1970).

Though a volumetrically large reservoir of pyrite resides in undisturbed sedimentary rock below ground, the mechanism oxidation of subsurface pyrite is not well understood, particularly with regard to the potential role of microbial activity in oxidation. In such subsurface environments, the pH has the potential to remain largely circumneutral due to the buffering capacity of carbonate and silicate minerals (Nicholson et al., 1988; Vear and Curtis, 1981). While there is a growing body of literature on the circumneutral chemolithotrophic microbial oxidation of pyrite coupled to denitrification (Bosch and Meckenstock, 2012; Haaijer et al., 2007; Jørgensen et al., 2009), fewer studies have examined aerobic oxidation of pyrite by neutrophilic chemolithotrophs. The growth of such organisms has been previously suggested in hydrothermal habitats (Edwards et al., 2003; Wirsen et al., 1993) and subglacial ecosystems (Boyd et al., 2014; Harrold et al., 2015). Only recently, however, has explicit evidence for microbially accelerated aerobic pyrite oxidation at neutral pH been presented (Percak-Dennett et al., 2017). Percak-Dennett and colleagues (2017) demonstrated sustained enhancement of sulfate release in the presence of a live, natural inoculum over multiple generations in cultures grown on synthetic framboidal pyrite. Based upon genomic and geochemical evidence, the authors proposed two potential mechanisms whereby chemolithotrophic microorganisms could accelerate pyrite oxidation. The first mechanism, termed the “sorbed Fe redox cycling model”, is based on the mechanism of abiotic oxidation of pyrite at circumneutral pH proposed by Moses and Herman (1991). Here the cyclic oxidation and reduction of a surface associated Fe phase coupled the successive transfer of pyrite-S electrons to O_2 results in the eventual liberation of sulfate. In this case, direct surface contact by a Fe(II)-oxidizing bacteria (FeOB) is the mechanism for microbial catalysis. An alternative, “polythionate intermediate model” was also proposed, in which case chemical reaction of O_2 with pyrite generates partially oxidized sulfur

species (e.g. thiosulfate) which are consumed by sulfur oxidizing bacteria (SOB) thereby accelerating the overall oxidation via a Le Chatelier effect. Notably, in the case of the polythionate intermediate model, direct cell-mineral contact is not necessarily required for oxidation of aqueous polythionates. The validity and potential environmental significance of these proposed mechanisms remains an open question, particularly in nanoporous sedimentary materials such as shale where pyrite is commonly hosted.

In the absence of rapid exhumation, either by anthropogenic activity (i.e. mining) or natural processes (e.g. glacial scouring), pyrite oxidation largely occurs at depth where circulation of oxidant charged meteoric water leads to the establishment of subsurface reaction fronts. The oxidation of pyrite often occurs as the deepest reaction front in pyrite bearing rocks (Bolton et al., 2006; Brantley et al., 2013; Littke et al., 1991). Recent work has further confirmed that under modern rates of erosion and atmospheric O_2 concentrations, the oxidation of pyrite in rocks largely occurs below that land surface (Gu et al., 2019). In their study of deep pyrite oxidation at Susquehanna Shale Hills Critical Zone Observatory (SSHCZO), Gu and colleagues (2019) determined that pyrite oxidation is likely to be transport limited, where diffusion of oxidant into the matrix limits the overall rate of oxidation. Although the nanoporosity of the deep, unweathered Rose Hills Shale at SSHCZO (Jin et al., 2011) is preclusive to direct microbial colonization of a large portion of the disseminated framboidal and euhedral pyrite, the protolith itself is fractured (Brantley et al., 2013). Pyrite oxidation was shown to largely occur within a length scale of centimeters from the fractures (Gu et al., 2019) where microorganism could, in theory, reside. Similarly, previous studies have suggested that microbial pyrite oxidation along fracture planes in receding shale cliffs could contribute to rock weakening (Cockell et al., 2011). SSHCZO provides an excellent opportunity to investigate the potential for

microbially mediated oxidative weathering of pyrite in shales, and to advance our understanding of microbially catalyzed oxidation of pyrite at circumneutral pH in general. By superimposing the relevant geologic constraints of a fractured subsurface shale on the potential mechanisms of microbially accelerated pyrite oxidation proposed by Percak-Dennett and colleagues (Fig. 1), we sought to further test these ideas and assess their potential relevance *in situ*. In order to allow for cultivation of potentially novel organisms involved in circumneutral pH pyrite oxidation, a supply of specimen pyrite was provided as a growth substrate. In doing so, rather than supplying thiosulfate directly, we were able to interrogate the relevance of the indirect polythionate intermediate model by replicating the likely source of the substrate *in situ*.

2 Materials and Methods

2.1 Site Description and Field Sampling

Located in Central Pennsylvania, SSHCZO is a small, forested catchment underlain by the Rose Hill formation with extensive geochemical and geomorphological data available (Brantley et al., 2013; Jin et al., 2014; Jin et al., 2010; Ma et al., 2013; Ma et al., 2011; Sullivan et al., 2016a; Sullivan et al., 2016b). Details relevant to this study are summarized here. The Rose Hill formation is a comprised primarily of a tightly folded Silurian age, organic poor grey shale. Primary mineralogy of the protolith has been previously established and is composed of illite (58 wt%), quartz (30 wt%) and chlorite (11 wt%) with trace Fe-oxides, pyrite and carbonate minerals (primarily ankerite) (Jin et al., 2010). Pyrite oxidation is hypothesized to occur along the deepest reaction front, ca. 22 m below land surface under the ridge crests. Sulfuric acid generation from the reaction of downward diffusing O_2 with pyrite reacts with other mineral phases, the first of which is likely to be the carbonate phases. The carbonate reaction thus closely overlies the pyrite reaction front and provides buffering capacity for pyrite oxidation (Brantley et al., 2013). Several

wells have been installed throughout the catchment, including well DC0 on the northern ridge, which was drilled prior to the establishment of the CZO. In August 2017 groundwater from well DC0 (28.65 m depth) was sampled for aqueous chemistry and microbial community analysis. Prior to sampling, DC0 was purged for 35 minutes. Approximately 2.0 L of groundwater was pumped through sterile 0.22 µM filters in duplicate for DNA extraction. Filters were promptly frozen and shipped to UW-Madison on dry ice and stored at -80°C until extraction. Measurements of temperature, conductivity, pH, E_h, dissolved oxygen, and cation concentrations were made as previously described (Sullivan et al., 2016a).

2.2 *In situ* Microcosms

In situ microcosms were prepared with specimen pyrite purchased from Ward's Scientific. Pyrite was hand ground with a mortar and pestle and sieved to 45 µm – 106 µm. Ground pyrite was cleaned via ultrasonication and dilute HNO_3 following previously established protocols (McKibben and Barnes, 1986) to remove fine dust and any oxidation rind. *In situ* microcosms were prepared in ca. 4-inch squares of 23 µm polyester mesh filter screening. Five g of > 106 µm fragments of Rose Hills Shale previously obtained from drill core and 5.0 g of pure quartz sand (Acros Chemicals, 140-381 µm) were added to each bag. For bags amended with pyrite, 1.0 g of pyrite was added. The bags were then tied closed with stainless steel jewelry wire and autoclaved. In the field the bags were secured with a stainless-steel carabiner to a stainless-steel wire, which was then was lowered down the well to the inferred depth of the pyrite oxidation front (ca. 28.6 m) and allowed to incubate *in situ* for 3 months. Upon removal, each bag was removed from the line and placed into a sterile Whirl-pack bag. Two bags from each treatment (with or without pyrite) were placed on dry ice for DNA extraction and two bags on blue ice for enrichment culturing. Samples were shipped overnight to the University of

Wisconsin and samples were placed at -80°C and 4°C prior to DNA extraction and culturing, respectively.

2.3 Enrichment Culturing

Enrichment cultures were established using solid mineral substrates to enrich for chemolithotrophic microorganisms. Varying mineralogical conditions were established using the previously prepared (see above) specimen pyrite (0.6 g) and/or 1.0g of fragmented and sieved (<106 µM) Rose Hills Shale previously obtained from drill core, along with 5 g of quartz sand. Mineral treatments were as follows: Sand only (S), sand with pyrite (S+Py), sand with shale (S+Sh), and sand with pyrite and shale (S+Py+Sh). Shale Hills artificial ground water (SH-AGW) pH 7.0 was prepared based on measured groundwater geochemistry in well DC0 (see Table S1), with final mM concentrations of 0.04 $CaCl_2 \cdot 2H_2O$, 0.035 $MgCl_2 \cdot 6H_20$, 0.01 KH_2PO_4, 0.1 $NaNO_3$, 0.002 $Na_2SiO_3 \cdot 9H_20$, 1.0 $NaHCO_3$, with or without 10 mM piperazine-N,N′-bis(2-ethanesulfonic acid) (PIPES) for buffered (B) and unbuffered (U) reactors, respectively. The minerals were suspended in 50 mL of SH-AGW in 120 mL culture bottles, bubbled with N_2 to prevent oxidation during sterilization, stoppered, and autoclaved. After sterilization, the headspace was flushed with sterile air and the cultures were inoculated with ca. 0.5 g of material from pyrite containing bags previously incubated *in situ* in well DC0. Abiotic controls were left uninoculated. All conditions (S-B, S-UB, S+Py-B, S+Py-UB, S+Sh-B, S+Sh-UB, S+Py+Sh-B, S+Py+Sh-UB) were performed in duplicate for live inoculated and uninoculated abiotic controls. Cultures were aseptically sampled at time zero and after 7, 14, 21, 35, 49, 63, 77, 91, 105, 126 and 167 days using a syringe and needle. Solids and aqueous phases were separated via centrifugation for the analyses described below.

2.4 Analytical Procedures

2.4.1 Aqueous geochemistry

Samples for aqueous SO_4^{2-} were diluted 1:5 for analysis by ion chromatography (IC, Dionex Model ICS-110). Total tetrathionate and thiosulfate were determined colorimetrically using the alkaline cyanolysis method described in (Nor and Tabatabai, 1975) scaled to accommodate a smaller volume of sample (1.0 mL). Aqueous phase samples were diluted 1:6 in 5 mM HNO_3 and filtered (0.22 µM) prior to determination of major cation (Ca, K, Mg, Na) concentrations via ICP-OES. Aqueous silicon was determined colorimetrically on 1:10 dilutions using the heteropoly blue method (Clesceri et al., 1998).

2.4.2 Solid-phase geochemistry

Mineral solids were extracted for 24 hours in 5.0 ml 0.5 M HCl on an orbital shaker. After extraction, the mixture was centrifuged and the concentration Fe(II) and Fe(total) in the extract was measure by the standard ferrozine assay (Stookey, 1970). For ATP analysis, 0.5 mL of whole culture (solid and aqueous) was placed into 0.25 ml of 20 mM ice cold EDTA, vortexed at maximum speed and immediately frozen at -80°C. For analysis, samples were thawed, vortexed again and centrifuged to recover the aqueous phase. ATP content was determined via luminescence using BacTiter-Glo (Promega, Madison WI) with calibration to a standard curve.

2.4.3 Microscopy

Whole culture aliquots from day 77 were stained using SYTO® Green and microbe-mineral interactions were examined using epifluorescene microscopy. For analysis of associated mineralogical changes, initial pyrite and mineral solids from the final time point (167 days) were dropped onto a carbon tape and carbon coated. Samples were imaged using a Hitachi S-3400 Scanning Electron Microscope (SEM) equipped with an electron dispersive spectroscopy (EDS) detector. Transmission electron microscopy (TEM) analysis was conducted at the Material

Science and Engineering Department in University of Wisconsin-Madison using a Tecnai T12 with a 120-kV acceleration voltage. TEM imaging and selected area electron diffraction data were collected by a 4k Gatan Ultrascan CCD. Pyrite grains were manually selected from the cultured materials, suspended in acetone and cleaved in agar mortar. The cleaved samples were then drop onto the carbon film 300 mesh copper grid. Composition were measure by the Thermo Scientific X-ray energy dispersive spectroscopy (EDS).

2.5 DNA Extraction, Sequencing and Analysis

2.5.1 DNA extraction

DNA was extracted from *in situ* bug bags and enrichment culture solidsfrom days 21, 77 and 167 according to previously described SDS-based extraction protocols (Zhou et al., 1996). Multiple aliquots of material from each *in situ* bag were extracted to obtain a sufficient mass of DNA for shotgun metagenomic sequencing. Replicate extracts were pooled and cleaned using Zymo Clean and Concentrator-5 (Zymo Research, Irvine Ca). Groundwater DNA was extracted from filters by slicing the filter into small pieces with a sterile razor, transferring the small pieces to a 2.0 mL screw-top microcentrifuge tube containing ca. 0.25 mL of 0.1mm zirconium beads. 0.5 mL of extraction buffer from Zhou, Bruns and Tiedje (1996) and 10 mg/mL of proteinase-K were added. Sample were incubated on a head block (37°C) with gentle agitation for 1 hour. 0.5 mL of phenol-chloroform-isoamyl alcohol (25:24:1) was then added to digest the filter and the tube was bead beat for 1 minute. DNA was the isolated following the standard phenol-chloroform-isoamyl alcohol (25:24:1) extraction and recovered via precipitation at -20°C in 2 volumes of ethanol.

2.5.2 16S rRNA gene amplicon sequencing and analysis

DNA was submitted to the University of Wisconsin-Madison Biotechnology Center (UWBC) for Illumina MiSeq 2x300 paired end sequencing of the V4 region of the 16 rRNA gene. Sequencing

data was processed using The Quantitative Insights into Microbial Ecology (QIIME) pipeline version 1.9.1 (Caporaso et al., 2010b). Raw reads were quality filtered to remove low quality and ambiguous sequences using default QIIME parameters prior to assembly of paired ends using fastq-join (Aronesty, 2013). Chimeric sequences were identified and discarded via de novo and reference-based detection using the usearch61 method (Edgar, 2010) and the SILVA ribosomal RNA database (Quast et al., 2013). Operational taxonomic units (OTUs) were identified by de novo clustering (0.97 threshold). Taxonomy was assigned to OTUs a via alignment against the SILVA database using PyNAST (Caporaso et al., 2010a).

2.5.3 Metagenomic assembly and annotation

Aliquots of DNA *in situ* mineral incubations and the final time point (167 days) of enrichment cultures were submitted to UWBC for metagenomic library preparation and 2x250 paired end sequencing on the Illumina HiSeq 2500 Rapid platform. A metagenomic library for a single pooled sample of groundwater DNA was sequencing using MiSeq 2x250. Raw metagenomic reads from all samples were quality filtered using the default parameters of Trim-Galore prior to concatenation and coassembly using MegaHit (Li et al., 2015). High quality metagenome assembled genomes (MAGs) were obtained from the coassembly using the Bin Refinement module within metaWRAP (Uritskiy et al., 2018) with initial binning output from MetaBAT2 (Kang et al., 2019), MaxBin2 (Wu et al., 2015) and CONCOCT (Alneberg et al., 2014). The quality and completion of individual MAGs as well as putative taxonomy was assessed by CheckM (Parks et al., 2015). Relative abundance of each MAG across each sample in the coassembly was determined using the Bin Quantification module of metaWRAP. Open reading frames were predicted using Prodigal (Hyatt et al., 2010) and functionally annotated using Prokka (Seemann, 2014). Extracellular electron transfer and sulfur oxidation pathways were

identified as previously described (He et al., 2017; Watanabe et al., 2019). Maximum likelihood phylogenetic trees in were constructed PhyML 3.0 (Guindon et al., 2010) with the LG substitution model (Le and Gascuel, 2008) for putative lithotroph MAGs using the concatenated alignments of conserved phylogenetic markers obtained from CheckM.

2.5.4 Searching for novel pathways for pyrite oxidation

The MAG (*Thiobacillus* related; see below) found to be most abundant across pyrite oxidizing enrichment culture metagenomes was further interrogated to uncover novel potential mechanisms for the oxidation of pyrite which may involve the extracellular metabolism of pyrite-S. The subcellular location of all MAG proteins was predicted using Cello (Yu et al., 2006). Proteins predicted to be outer membrane associated or extracellular were further examined for genomic proximity to known S-oxidation pathways. Potential homologs to the identified proteins of interest were found by a Blastp search (Altschul et al., 1990) of the NCBI database of non-redundant proteins. Homologous sequences were aligned using MUSCLE (Edgar, 2004) and conserved motifs visualized with WebLogo 3 (Crooks et al., 2004). Putative structures of proteins of interest were modelled using Phyre2 (Kelley et al., 2015).

3 Results

3.1 Groundwater Geochemistry and Microbial Community Composition

The geochemistry of groundwater at site DC0 and other locations at SSHCZO has been previously characterized (Sullivan et al., 2016). Samples for groundwater geochemistry and microbial community composition were also collected in this study at the time of *in situ* mineral deployment in August 2017. The chemistry of the groundwater collected during mineral deployment (Table S1) suggested that fluids from a mixture of redox conditions was obtained during sampling by peristaltic pump: the combination of low but measurable dissolved oxygen

(0.035 mM), substantial levels of dissolved iron (0.029 mM), and E_h of -180 mV is highly suggestive of redox disequilibrium. These results are not surprising given that (i) an oxidation-reduction front is known to exist at SSHCZO, based on prior aqueous and solid-phase geochemical distributions at various locations within the watershed (Sullivan et al., 2016; Brantley et al., 2013); and (ii) the well is screened to depth at DC0, such that mixing of fluids from different depths likely took place during peristaltic pump sampling. The minerals were deployed 1-2 m below the groundwater surface, and we thus assume that they were exposed to some dissolved O_2 during the 3-month incubation period. Nevertheless, the microbial community in the groundwater sample and the *in situ* incubated minerals (Tables S2 and S3, respectively) showed evidence of anaerobic heterotrophic taxa, notably Fe(III)-reducing *Geobacteraceae* as well as other anaerobic heterotrophic taxa (e.g. *Thermodesulfovibrionaceae*, *Clostridiaceae*, *Commononaceae*). The proliferation of Fe(III) reducers makes sense assuming Fe(II) oxidation (e.g. in the upper regions of the well) produces an ongoing supply of fresh Fe(III) oxides, which were visibly evident both on the mineral bags and in groundwater filters. In addition, the minerals were also colonized by microaerophilic, Fe(II)-oxidizing organisms from the genera *Gallionella* and *Crenothrix* (Emerson et al., 2010), which suggests that groundwater at DC0 supports the activity of both heterotrophic and chemolithotrophic microorganisms. For the purposes of this paper, the colonized minerals simply served an inoculum for pyrite-oxidizing enrichment cultures, and we make no attempt to explicitly link the organisms and activities that arose in those cultures to the microbial communities in the colonized minerals.

3.2 Enrichment Culture Geochemistry

3.2.1 pH

pH declined from ca. 7.0 to an average of 6.0 and 5.7 in the abiotic and live buffered sand+pyrite (S+Py-B) reactors, respectively (Fig. 2A). In the absence of buffer (S+Py-UB), pH declined rapidly from 7.8 to a final average values of 3.5 and 4.4 for abiotic and biotic sand plus pyrite reactors (Fig. 2B). pH remained with 0.5 units of the initial value in the buffered, shale-amended (S+Sh-B, S+Py+Sh-B) reactors, declining slightly to 7.1 in the live pyrite system (Fig. 2C). In the unbuffered shale-amended reactors, pH declined slightly in the presence of pyrite (S+Py+Sh-UB) and remained unchanged at 7.5-7.8 in its absence (S+Sh-UB) (Fig. 2D).

3.2.2 Sulfate

Sulfate generation was enhanced in the presence of a live inoculum relative to sterile controls under all conditions tested (Fig. 2E-H). Initial biotic rates of reaction (0-35 d) were 1.9-3.4-fold than abiotic rates in the four reaction systems, and total sulfate release over the 167-d incubation period was 1.2 to 4.7-fold higher in the biotic reactors (Table 1). Only small amounts of sulfate were generated from the oxidation of residual pyrite in the inoculum ("Live No Pyrite" in Fig. 2), indicating that most of the sulfate release in the pyrite-amended reactors came from oxidation of the added (ca. 200 mmol S L^{-1}) pyrite. The entire range of sulfate release values correspond to oxidation of 0.31-0.24 % of the added pyrite-S.

3.2.3 ATP

The ATP content of the live reactors was maximal at the start of the incubation and declined over time in all reactors (Fig. 2I-L); ATP was near to or below detection in the uninoculated controls. ATP levels were similar in the pyrite-containing and pyrite-free buffered reactors (Fig. 2I,K), which suggests that any cell growth associated with biologically-mediated pyrite oxidation in these reactors (Fig. 2E,G) was insufficient to keep up with biomass loss upon addition of the inoculum to the reactors. ATP levels were generally lower in the unbuffered pyrite-containing

vs. pyrite-free reactors (Fig. 2J,L). In the case of the shale-free systems (Fig. 2J), the rapid decline in ATP during the first few weeks of incubation can be explained by the precipitous drop in pH (Fig. 2B) that took place in conjunction with pyrite oxidation. The reason for the smaller but measurable difference in ATP between the pyrite-containing vs. pyrite-free shale-amended reactors (Fig. 2L) is unknown.

3.2.4 Polythionates

Polythionates (sum of thiosulfate and tetrathionate; see section 2.4.1) accumulated in the abiotic pyrite-containing reactors (Fig. 2M-P), but near or below detection in the pyrite-free reactors. Polythionates were consistently low in the live S+Py reactors (Fig. 2M-N) and consumed over time in the S+Sh+Py reactors (Fig. 2O-P). The onset of polythionate accumulation in the live unbuffered S+Py reactors (Fig. 2N) was associated with rapid decline in pH and ATP content (see above), signaling a shift from biotic+abiotic to abiotic-only pyrite oxidation.

3.2.5 Cations and silica

Accumulation of aqueous cations and silica were used an indicator of pyrite oxidation-driven dissolution of shale mineral phases, i.e. shale either present in the inoculum, or added separately (in addition to the inoculum) to the reactors. Ca release in particular was assumed to primarily signal the dissolution of carbonate phases (ankerite + calcite) abundant in the Rose Hill Shale (Brantley et al., 2013; Jin et al., 2010). Mg release was likely influenced by dissolution of both carbonate and silicate phases, whereas Si and K (not present in carbonate minerals) were assumed to be indicators of silicate dissolution. Ca release was stimulated dramatically by microbial activity in pyrite-amended reactors that did not receive additional shale (Fig. 2Q,R). Some of this increase could be attributed to biotic and/or abiotic oxidation of pyrite in the inoculum (see Fig. 2E,F), as there was a distinct increase (particularly in the buffered reactors) in

Ca in the inoculated pyrite-free reactors. Ca levels were higher across the board in the buffered shale-amended reactors (Fig. 2S), indicating dissolution of carbonate (i.e. by maintenance of near-neutral solution pH by the buffer) regardless of the presence of pyrite oxidation activity. Such dissolution thus masked the distinction between the effects of biotic vs. abiotic pyrite oxidation, although final Ca levels were maximal in the live pyrite-amended reactors. Ca release was stimulated in the live, unbuffered, pyrite-containing shale-amended reactors (Fig. 2T), although here again some of this increase could be attributed to oxidation of pyrite in the inoculum, as there was also a significant Ca increase in the pyrite-free controls. Mg and K showed patterns of release generally analogous to Ca (Fig. S1A-H), whereas net Si release occurred only in the shale-free reactors (Fig. S1I-L).

3.3 Microscopy and Mineralogical Alteration

Epifluorescence microscopic analysis from day 105 of the incubation demonstrated a close association of microbial cells with pyrite surfaces. Cells appeared to preferentially colonize pyrite surfaces, as minimal fluorescence was observed on quartz surfaces or in bulk solution (Fig. 3). Under SEM, initial pyrite surfaces were clean, smooth, and free of any oxide coatings; EDS showed an average weight percent of 52.2% S and 47.8% Fe (Supplemental Fig. 2). Significant alteration of the pyrite surfaces as well a depletion in solid-phase S (final average 36.8% S) was observed after 167 d of both biotic and abiotic incubation. Morphological differences in the altered pyrite surfaces were observed across culturing conditions. In the absence of shale, both buffered and unbuffered uninoculated control pyrite surfaces showed the presence of a lawn of porous, needle-like oxides with a morphology consistent with goethite. In live unbuffered S+Py reactors, pyrite surfaces were coated with a smoother, apparently amorphous Fe-oxide coating (Fig. 4) with only occasional goethite crystallites. TEM analysis

confirmed the presence of goethite on uninoculated control pyrite surfaces, and the presence of amorphous coatings on the biologically altered pyrite (Fig. S3). When shale was present, the extensive covering of goethite-like needles was not observed under any experimental condition. Rather, the surfaces appear to be covered in smooth, amorphous coatings, less porous than the needle-like lawn observed under abiotic conditions in the absence of shale (Fig. 5).

3.3 Microbial Communities in Enrichment Cultures

16S rRNA gene amplicon analysis of microbial communities in the pyrite-containing enrichment cultures revealed a predominance of organisms from the genus *Thiobacillus* (Fig. 6). In the absence of a pyrite, the most dominant genus was the *Pseudomonas*, a well-known heterotrophic taxon (Moore et al., 2006) that was previously shown to extensively colonize minerals incubated *in situ* in groundwater (Converse et al., 2015). However, *Thiobacillus* was also observed at high abundance in S-only and S+Sh reactors that displayed some release of sulfate, likely from oxidation of residual pyrite in the inoculum. The extent to which *Thiobacillus* dominated the S+Py and S+Py+Sh 16S rRNA gene amplicon libraries was variable across individual reactors and time, with the highest representation (92.7%) at day 77 in S+Py-B reactors. Contrasting trends in the temporal abundance of *Thiobacillus* were observed in unbuffered and buffered reactors, with a decrease in abundance over time in the unbuffered reactors.

3.4. Metagenomic Analysis of Putative Litho(auto)trophic Pathways

A total of 460 high-quality (>70% complete, <10% redundant) MAGs were obtained from the metagenomic coassembly of the colonized minerals, ground water, and enrichment cultures. Putative extracellular electron transfer (EET) pathways involved in Fe(II) oxidation were identified in 14 of the 460 MAGs. Homologs to the Cyc2-type iron oxidation pathway originally recognized in *A. ferrooxidans* (Appia-Ayme et al., 1999) were identified in five of the putative

FeOB MAGs. The outer membrane bound c-type monoheme cytochrome Cyc2 acts as a Fe(II) oxidase, transferring electrons to the inner membrane for energy generation via periplasmic electron carriers including Cyc1 (Castelle et al., 2008). Cyc2 type EET systems have subsequently been shown to be widely distributed in the genomes of neutrophilic FeOB (He et al., 2017), where its activity has been recently verified via meta-omics (McAllister et al., 2019) and implicated in the oxidative metabolism of solid phase Fe-minerals (Napieralski et al., 2019). The remaining nine FeOB MAGs contained homologs to the MtoABCD EET system (Emerson et al., 2013; Liu et al., 2012). The core proteins of this pathway include the decaheme c-type cytochrome MtoA which is inserted into the β-barrel porin MtoB, forming an outer membrane spanning electron conduit. Electrons are then delivered to the inner membrane cytochrome MtoC by the periplasmic cytochrome MtoD (He et al., 2017).

Of the 460 MAGs, 49 contained ORFs predicted encode genes for three essential proteins of the widely distributed sulfur oxidation pathway Sox, including the heterodimeric c-type cytochrome SoxAX, the SoxXY carrier complex, and the sulfate thiohydrolase SoxB (Friedrich et al., 2001). During the oxidation of thiosulfate, SoxAX oxidatively links a thiosulfate molecule to a cysteine residue of SoxY. The sulfane sulfur is then hydrolyzed to sulfate by SoxB (Friedrich et al., 2001; Watanabe et al., 2019). The hydrolysis of SoxYZ by SoxB leaves a cysteine-persulfide on SoxY. The sulfur dehydrogenase SoxCD, necessary for of oxidation of the sulfone sulfur carried by SoxXY was identified in 36 of the 49 MAGs containing SoxXYAB. In organisms lacking SoxCD, a reversely operating sirohaem dissimilatory sulfite reductase (DsrAB) is commonly employed (Dahl et al., 2005; Pott and Dahl, 1998). A complete reverse Dsr pathway (rDsrABCEFHJKLMNOPRS) was identified in seven of the MAGs containing SoxXYAB. Alternatively, a recently recognized heterodisulfide reductase pathway (Hdr)

pathway was identified (Koch and Dahl, 2018) in organisms lacking SoxCD and was identified in eight of the MAGs containing SoxXYAB. Both Dsr and Hdr pathways also require the presence of a membrane bound sulfite oxidation enzyme, SoeABC (Dahl et al., 2013). SoeABC is conserved in genomes of organisms employing Dsr and Hdr pathways (Watanabe et al., 2019), and accordingly present in all MAGs containing Dsr and Hdr based S-oxidation pathways.

Of the 63 MAGs that contained putative Fe or S oxidation pathways, a further 28 of them also contained a complete set of genes for inorganic carbon fixation via the Calvin Cycle, indicating an ability to grow chemolithoautotrophically. A summary of the distribution of chemolithoautotrophic pathways is provided in Fig. 7 with abundances reported across metagenomes in log genomes per million reads. The majority of the putative lithoautotrophs belong to the class β-protebacteria, with only four falling within the α-proteobacteria. Both FeOB and SOB were detected across all samples. In the groundwater metagenome (DC0-GWb), two chemolithoautotrophic MAGs are particularly abundant: a putative *Rhodocyclaceae* with both MtoABCD and the Sox-Hdr-Soe S-oxidation pathway, and a putative *Comamonadaceae* containing c-Sox which are the third and sixth most abundant MAGs found in the groundwater, respectively. Chemolithoautotrophic MAGs across *in situ* mineral-colonized metagenomes (DC0-1 through DC0-6) are also well represented, though the most abundant MAGs across these samples tend to be anaerobic Fe and S reducing taxa, particularly *Geobacter* and S-reducing *Nitrospiraceae* (Supplemental Table 4). The differential abundance of the putative lithoautotrophs indicates a strong enrichment for SOB in all pyrite-oxidizing enrichment culture metagenomes, for which a significant mass of DNA was available relative to both the groundwater and *in situ* microcosm metagenomes. Particularly abundant across all pyrite

amended cultures is MAG 449, which is tentatively identified as belonging to the genus *Thiobacillus* and contains the Sox-Hdr-Soe pathway for S-oxidation.

3.4.3 Identification of Potential Novel Pathways

As the most dominant MAG in pyrite oxidizing enrichments, MAG 449 was further interrogated to uncover potentially novel mechanisms for pyrite oxidation, including the potential for utilization of extracellular reduced sulfur. Of the 89 proteins predicted to be localized to the outer membrane (OM), two resided on the same contig as, and downstream from, the SoxXYZAB gene cluster (Fig. 8). The first of these (OM19) was identified as having homology to (i) β-barrel secretin, general secretion protein GspD, a central component of type II secretion system (T2SS), as well as (ii) the mannose-sensitive hemagglutinin (MSHA)-type pilus assembly protein MshL, a type IV secretion system (T4SS) secretin. The second OM associated protein (OM20), seven genes downstream from the putative GspD/MshL, was unannotated by Prokka. A Blastp search for potential homologs identified multiple hits to hypothetical proteins from known SOB, or MAGs from environmental samples where S-oxidation might be an important pathway (Supplemental Table 5). The nearest hit, at 73.5% ID at 99% query coverage was a hypothetical protein (WP_124704254.1) from the SOB *Sulfuriferula multivorans*. Alignment of the recovered homologs revealed a conserved proline-cysteine-proline (PCP) motif near the C-terminus of the protein (Fig. 9). Phyre2 prediction of protein structure identified Gsp pseudopilin GspG (20% ID, 98.2 confidence) and the Type IVa major pilin, PilA (25% ID, 96.4 confidence) as the most appropriate template. Other genes in the gene cluster include a putative AAA family ATPase, a homolog to the inner membrane platform GspF and several hypothetical proteins unannotated by Prokka. Arrangement of the gene cluster shares remarkable similarity to other T2SS, with the location of several of the small, annotated genes suggesting they may be type II pseudopilin or

type IV pilin subunits. Included in these putative pilin-like subunits is a small protein predicted to be extracellular, located 1 gene downstream from OM20. The best hit from a Blastp search of this protein was a type II secretion system protein (WP_124704253.1) also from *S. multivorans* with a 73.7% identity and 99% query coverage. Alignment of the putative homologs (Supplemental Table 6) again returned a conserved PCP as well as a conserved C residue at position 106 (Fig. 9).

4 Discussion

4.1 Enrichment Culture Geochemistry and Mineralogy

The enhanced generation of sulfate in presence of a live inoculum under all conditions tested (Fig. 2E-H) demonstrates the ability of microorganism from the SSHCZO subsurface to accelerate the oxidation of pyrite *in vitro.* Microbially-enhanced pyrite oxidation was accompanied by scavenging of polythionates which otherwise accumulated in abiotic reactors (Fig. 2M-P); mechanistic and biogeochemical implication of these results are discussed below. It is important to note that levels of polythionate accumulation in the abiotic reactors (≤ 0.097mM) were ca. 15-62 fold lower than net sulfate release (see Table S7, a result consistent with previous short-term studies of abiotic pyrite oxidation at circumneutral pH (Moses and Herman, 1987; 1991). The kinetics of the abiotic reaction of thiosulfate with dissolved oxygen are notoriously slow (Durham, 1974) and our own observations indicate a loss rate of less than 1% per day in sterile 0.1 mM thiosulfate solutions (data not shown). These findings suggest that rapid turnover of the polythionate pool through abiotic reaction with oxygen was not the major mechanism for sulfate release in the uninoculated reactors. As described below, a key upshot of this conclusion is that simple scavenging of polythionates via microbial activity cannot account for the observed stimulation of sulfate release in the biotic reactors.

The pH of cultures that were buffered, either by Pipes, shale, or both, remained largely circumneutral over the course of the experiment (Fig. 2A-D). The exception was the shale-free S+Py-B reactors, in which pH decreased to ca. 6 in conjunction with extensive pyrite oxidation (Fig. 2A). The S+Py+Sh-UB reactors, which had an initial pH of 7.8, also exhibited biologically accelerated pyrite oxidation (Fig. 2H). Together these results show that this process can occur over a fairly wide range in the circumneutral pH range. The unbuffered S+Py reactors underwent a precipitous drop in pH over the course of the experiment, and biological enhancement of sulfate generation stopped once the pH reached ca. 4. Concurrent with the decrease in pH were a rapid decrease in ATP (Fig. 2J), decline in the abundance of OTUs of the genus *Thiobacillus* (Fig. 6), and accumulation of polythionates (Fig. 2N). Together these results suggest cellular death as a result of rapid acidification. Net microbial growth (i.e. increase in ATP) coupled to pyrite oxidation was not observed in any of the other inoculated reactor systems. The simplest explanation for this result is that heterotrophic organisms that had colonized the minerals (see Table S3) *in situ* declined in biomass when transferred to organics-free SH-AGW. These results preclude direct assessment of whether or not any chemolithoautotrophic growth took place in the inoculated reactors, although genomic evidence (see section 3.4.2) suggests that such growth could have taken place.

Marked differences were observed in the surface morphology and mineralogy of pyrite from the abiotic vs. biotic shale-free reactors (Fig. 4). The accumulation of goethite on pyrite surfaces under abiotic conditions is consistent with studies of the naturally weathered pyrites at SSHCZO (Gu et al., 2019), where oxidized pyrite grains show a sequential transition from poorly crystalline Fe-oxides to goethite, with goethite more abundant at the outer rim. It is possible that microbially-enhanced oxidation of pyrite resulted in a more rapid oxide

precipitation, preventing the crystallization to goethite at the pyrite surface (Pichler and Veizer, 1999). Additionally, bacterial cells have been shown to stabilize ferrihydrite, allowing the extended persistence of poorly crystalline phases (Kennedy et al., 2004).

In the presence of shale, both the biotic and abiotic oxidation of pyrite were repressed compared to identical conditions with no shale added. It has previously been reported that the formation of a silicate stabilized passivation layer can greatly inhibit pyrite oxidation (Evangelou, 2001). As shale dissolution was observed across all shale amended reactors (demonstrated by an increase in Ca and other cation concentrations; Fig. 2Q-T, Fig. S1), it is likely that Si was released to solution during dissolution, and that the lower aqueous Si concentration in pyrite amended shale reactors (S+Sh+Py) relative to non-pyrite amended shale reactors (S+Sh) (see Fig S1K-L) is reflective of Si sorption. Si is strongly sorptive to Fe-oxyhydroxides at near neutral pH (Swedlund and Webster, 1999), and the lack of goethite crystals in both buffered and unbuffered S+Py+Sh reactors (Fig. 5) can be explained by the incorporation of Si into the Fe-oxyhydroxide, preventing the further crystallization to crystalline phases such as goethite (Deng, 1997). Similar differences in morphologies between pyrite surface layers formed were observed during neutral pH (7.4) leaching with and without added Si in solution (Fan et al., 2017). Fan and colleagues (2017) demonstrated that without Si, pyrite surfaces displayed a needle like structure consistent with goethite; and that when Si was added to solution, Si was associated with an amorphous Fe-oxyhydroxide coating. The amorphous nature of the Si-Fe-oxyhydroxide coating was associated with decreased release of sulfate, a phenomenon attributed to the lower porosity of this layer when compared to layers of discrete goethite crystallites. These observations explain the overall suppression of both biotic and abiotic sulfate release in the presence of shale. When Pipes was not supplied as a buffer, live, inoculated

reactors showed an even further suppression of sulfate release not observed under equivalent abiotic conditions (compare Figs. 2G and H). We speculate that this effect is likely attributable to a physiological effect related to the elevated pH of the unbuffered reactors.

4.2 Metabolic Pathways and Potential Mechanisms for Accelerated Pyrite Oxidation

MAGs obtained from the pyrite enrichment culture were investigated using metagenomics to gain insight into the potential chemolithotrophic pathways involved in pyrite oxidation. Percak-Dennett and colleagues (2017) proposed a sorbed Fe redox cycling model for microbially-mediated pyrite oxidation, whereby microbial Fe(II) oxidation at the pyrite surface accelerates mineral dissolution. In this model, enzymatic Fe(II) oxidation promotes pyrite oxidation through increased rates of sorbed Fe redox cycling coupled to conduction of electrons to the mineral surface (Moses and Herman, 1991; Percak-Dennett et al., 2017). Metagenomic sequence analysis showed that organisms in the Percak-Dennett et al. (2017) cultures contained extracellular electron transport (EET) pathways postulated to be involved in enzymatic Fe(II) oxidation by neutrophilic FeOB (He et al., 2017). In contrast to those cultures, Fe(II) oxidation does not appear to be the dominant mechanism for acceleration of pyrite oxidation in our experiments. Homologs to either the MtoAB or Cyc2 based pathways for aerobic Fe(II) oxidation (see He et al., 2017 for review) were found in 14 MAGs obtained from the metagenomic coassembly, (Fig. 7). However, the relatively low abundance of these MAGs, coupled with the 16S rRNA gene community analysis from days 21 and 77 of the experiment (Fig. 6), suggests that their contribution to pyrite oxidation were marginal. If sorbed Fe redox cycling was the dominant mechanism, one would expect FeOB to be of higher abundance than SOB, the opposite of what we observed. Based on 16S rRNA gene amplicon analysis of enrichment cultures, the most dominant organisms during times of high pyrite oxidation rates were related to the genus

Thiobacillus. Two *Thiobacillus*-related MAGs were obtained from the metagenomic coassembly, neither of which contained the well described MtoABCD (Beckwith et al., 2015; Liu et al., 2012) or Cyc2 (Castelle et al., 2008; McAllister et al., 2019) type pathways for EET (see Fig. 7). Nevertheless, the possibility remains for an alternative Fe(II) oxidation pathway. For example, a porin-periplasmic multicopper oxidase (MCO) of the PcoA and PcoB protein families has been hypothesized to be involved in chemolithotrophic Fe(II) oxidation (He et al., 2017), and homologs to PcoAB are present in the genome of the two *Thiobacillus* MAGs as well as the genome of *T. denitrificans* ATCC 25259. However, genomic analysis of potential nitrate dependent Fe(II) oxidation pathways in *T. denitrificans* ATCC 25259 did not indicate the upregulation of a MCO, and a screen of 20,000 random mutants did not yield a Fe(II) oxidation defective mutant that would suggest a role for MCO (Beller et al., 2013). The PcoAB type MCO of *T. denitrificans* ATCC 25259 is found within a large gene cluster encoding other genes associated with metal resistance, including two heavy metal efflux systems and a Hg^{2+} resistance system (Beller et al., 2006). These results suggest that PcoAB may, in fact, act a conveyor of copper resistance as opposed to a Fe(II) oxidation pathway in *T. denitrificans*. Furthermore, while *T. denitrificans* is purported to oxidize nanocrystalline pyrite coupled to nitrate reduction (Bosch et al., 2012), these results were not replicable with purely crystalline pyrite, and it has been suggested that the observed reduction of nitrate resulted from the chemolithotrophic oxidation of reduced sulfur species as impurities in the specimen pyrite or residual S from the initial inocula (Yan et al., 2019). Together these findings suggest that Fe(II) oxidation at the pyrite surface by *Thiobacillus* was not responsible for microbially-enhanced sulfate release in our experiments.

The presence of the full Sox pathway in putative *Thiobacillus* MAGs is in accordance with the "indirect polythionate intermediate model" proposed by Percak-Dennett et al. (2017). In this model surface associated SOB scavenge polythionate intermediates (e.g. thiosulfate) released from partial abiotic oxidation of pyrite. The supposition then is that consumption of polythionate intermediates increase the overall reaction rate via a Le Chatelier effect. Although SOB have long been recognized to accelerate the oxidation of thiosulfate relative to strictly chemical oxidation (Tuttle and Jannasch, 1976), it is unlikely that Le Chatelier's principle alone can be invoked to explain the enhanced release of sulfate to solution under biotic conditions. This mechanism would assume that the dominant product released from the oxidation of pyrite is polythionates, and that the conversion of polythionates to sulfate is rate limiting. However, as discussed above, both our results and those of Moses and Herman (1991; 1987) show that sulfate that is the primary product of abiotic pyrite oxidation at neutral pH, with the rate of polythionate generation being several-fold lower than sulfate generation. In addition, studies with the moderately acidophilic SOB *Thiomonas intermedia*, which has been shown to oxidize intermediate reduced S compounds formed by abiotic FeS_2 oxidation (rather than FeS_2 directly), demonstrated that rates of pyrite oxidation were not affected by the presence of microbial activity (Arkesteyn, 1980; Schippers et al., 1996). This argument is further supported by thermodynamic calculations which demonstrate that the free energy of the reaction is unaffected by the concentration of $S_2O_3^{2-}$ (Percak-Dennett et al., 2017). Regardless of whether or not polythionates were produced as intermediates in the biotic reactors, or if scavenging of chemically produced polythionates occurred, our data point to the need for an alternative model by which microorganism can accelerate sulfate release from pyrite.

The lack of polythionate accumulation in biotic reactors could in fact point to an altogether different mechanism of pyrite oxidation in biotic reactors relative to simple consumption of polythionate intermediates by SOB. One intriguing possibility is the involvement of a dedicated outer membrane protein that interacts directly with the pyrite surface. Intracellularly, S transfer reactions often involve multiple transfers of persulfide moieties between enzymes containing sulfhydryl (thiol) functional groups (e.g. cysteine). Extracellularly, sulfhydryl containing outer membrane proteins (OMPs) have been proposed to mobilize elemental sulfur in acidiphilic S-oxidizing bacteria of the genus *Acidithiobacillus*. The OMP is postulated to form a persulfide bound between a cysteine residue and extracellular sulfur with the sulfane sulfur then serving as the substrate of the periplasmic sulfur dioxygenase (Rohwerder and Sand, 2003). Similar models have been described in *A. caldus* (Chen et al., 2012; Mangold et al., 2011) and *A. thiooxidans* (Yin et al., 2014). Interestingly, thiol containing OMPs have also been shown to be differentially expressed in phylogenetically distant mesoacidiphilic to extremely acidiphilic sulfur oxidizing microorgansims grown on S^0, including the firmicute *Sulfobacillus thermosulfidooxidans* and the Archeon *Acidianus manzaensis* (Liu et al., 2015). While the above studies are restricted to acidiphilic taxa, a hypothetical OMP in the neutrophilic ε-proteobacterial SOB *Sulfurimonas denitrificans* was recently shown to be enriched in the proteome when the organism was grown on solid phase cyclooctasulfur (S_8) compared to thiosulfate (Gotz et al., 2019). While the function of this protein remains unknown, Gotz and colleagues (2019) identified homologs in other *Campylobacteria* species implicated in the oxidation of elemental sulfur and suggest it may be involved in the activation of S_8.

While no homologs to the hypothetical protein postulated to be involved in S_8 oxidation were found in the *Thiobacillus* MAGs, the possibility remains of an analogous feature that could

mediate the metabolism of extracellular pyrite-S. Although speculative, it is interesting to note the presence of a gene cluster encoding a putative T2SS or T4SS protein secretion systems (see section 3.4.3) downstream of the Sox operon in the most abundant *Thiobacillus* related MAG (Fig. 8). T2SS are widely distributed amongst the *Proteobacteria* and employed for a variety of purposes including virulence, adhesion and nutrient acquisition (Cianciotto, 2005). While most T2SS secreted proteins are soluble, diffusing away from the cell, T2SS is also known to secrete membrane anchored proteins (Rondelet and Condemine, 2013) including the lipoproteins MtrC and OmcA used in respiration of insoluble Fe(III) oxide minerals by *Shewanella oneidensis* (DiChristina et al., 2002; Shi et al., 2008). Rather than for the export of an OM anchored protein, another possible role of the putative secretory system could be the formation of a pilus-like structure that could interact directly with pyrite surfaces. While T2SS pseudopilins are largely confined to the periplasmic space, it has been shown that they are capable of forming full pilus-like structures extending to the cell surface (Durand et al., 2003; Sauvonnet et al., 2000). Two pseudopilin homologs in the *Thiobacillus* MAG are predicted to be extracellular (Fig. 8), in addition to the outer membrane hypothetical protein (OM20) which is predicted to be a psuedopilin based on structural analysis. The putative pseudopilin subunits contain multiple conserved cysteine residues (Fig. 9), which could, in theory, be used to transport extracellular persulfide groups to the periplasm for oxidation via the Sox pathway. It remains possible that the conserved cysteine residues common amongst the putative (pseudo)pilin proteins are of a structural nature, forming C-C disulphide bonds common to true T4SS pilins (Parge et al., 1995). However, Protein Family (Pfam) alignments of T2SS protein G (PF08334) and TSS2 pseudopilin PulG (PF11773) do not contain any conserved cysteine residues, suggesting their role is not likely to be purely structural if they are, in fact, T2SS pseudopilins. Due to the high

degree of similarity between T2SS and T4SS (Peabody et al., 2003) and their overall low similarity to the homologs of these proteins found in the *Thiobacillus* MAGs, it is difficult at this point to infer with certainty which class of secretory systems is constituted by the gene cluster in Fig. 8. Regardless, the fact that the nearest Blastp hits to the above-described putative proteins identified in the *Thiobacillus* related MAG are SOB is thought provoking, raising the question of their potential involvement in extracellular pyrite oxidation via a "direct sulfur oxidation" mechanism.

4.3 Environmental Implications

The enhanced generation of sulfate in presence of a live inoculum under all conditions tested (Fig. 2E-H) confirms the previously described (Percak-Dennett et al., 2017) ability of microorganisms from subsurface pyrite weathering environments to accelerate aerobic oxidation of pyrite *in vitro.* The previous study (Percak-Dennett et al., 2017) was conducted with organisms from unconsolidated Miocene-age lacustrine deposits from the Hanford 300 Area site in eastern Washington (Peretyazhko et al., 2012) where geochemical data suggest that oxidation of pyrite is taking place in the vicinity of redox transition zone ca. 18 m below the ground surface (Lin et al., 2012). Although this system differs fundamentally from the hydrogeochemical environment at Shale Hills (see below), the fact that aerobic chemolithotrophic organisms from both environments are able to accelerate pyrite oxidation suggests that such organisms may be common in pyrite-bearing subsurface environments. This idea is supported by recent preliminary studies which demonstrated the ability of aerobic groundwater microorganisms to accelerate oxidation of native pyrite phases in sandstone aquifer sediments from Wisconsin (Haas et al., 2019).

It is important to consider the physical and geological characteristics of subsurface environments when evaluating what role chemolithotrophs may play in the oxidation of reduced Fe and S minerals in natural systems. To illustrate this idea, consider the subsurface oxidative weathering of Fe(II)-silicate minerals in granitic bedrock (Rio Blanco Quartz Diorite) from the Luquillo Critical Zone Observatory in Puerto Rico. In this system, chemolithotrophic FeOB reside in partially altered, fractured, rocky material termed the "rindlet zone" (Turner et al., 2003), where directly contact with mineral surfaces is feasible. In the outer rindlet zone the weathering of the Fe(II)-silicate mineral hornblende is rapid, becoming completely depleted over a scale of centimeters (Buss et al., 2005; Buss et al., 2008). We recently demonstrated in laboratory experiments that chemolithotrophic FeOB can mediate the oxidation of the Fe(II)-silicate minerals biotite and hornblende in the Rio Blanco Quartz Diorite at substantial rates compared to zero rates of reaction under abiotic conditions (Napieralski et al., 2019). Although translation of the laboratory results to in situ weathering rates is not yet possible, the presence of fractures and the existence of relatively fine-grained granitic clasts within the rindlet zone strongly suggests that microorganisms are likely to play a role in oxidative Fe(II)-silicate weathering. Similar conclusions were reached by Percak-Dennett et al. (2017) regarding the likely participation of chemolithotrophic microorganisms in pyrite oxidation within the redox transition zone at the Hanford 300 Area site.

In contrast to the Hanford 300 Area redox transition and Luquillo rindlet zone environments, oxidation of pyrite in the Rose Hill Shale at the SSHCZO occurs at a depth below where a significant disaggregation of the nanoporous protolith is observed (Brantley et al., 2013). Thus, direct contact of microbial cells with pyrite is without question limited by the nanoporosity of the Rose Hills Shale, with the potential exception of pyrite exposed on fracture surfaces (see

illustration in Fig. 1). In light of this reality, it seems unlikely that a direct contact mechanism (e.g. either the previously proposed sorbed Fe redox cycling mechanism, or the newly proposed direct sulfur oxidation pathway) can be a large contributor to oxidative weathering of pyrite at SSHCZO. In addition, in stark contrast to the total lack of abiotic Fe(II)-silicate oxidation after ca. 2.4 years of abiotic incubation reported by Napieralski and colleagues (2019), our experiments show that significant pyrite oxidation can proceed under long-term abiotic conditions. As evidenced by the careful analytical work of Gu et al. (2019), S is completely depleted during *in situ* pyrite weathering at the grain scale within the nanoporous matrix at SSHCZO. The lack of observable S phases on the oxidized pyrite indicates complete S removal and suggests that diffusion of thiosulfate (or sulfate) is not limiting with regard to *in situ* oxidation. Hence, scavenging of polythionates via the "polythionate intermediate model" is also unlikely to lead to accelerated pyrite oxidation *in situ.* This assertion is in accordance with our experimental findings that thiosulfate consumption by SOB is unlikely to significantly accelerate pyrite oxidation *in vitro* (see section 4.1). It thus seems unlikely that neither FeOB nor SOB can effectively accelerate pyrite oxidation at a large scale in the Rose Hill Shale.

Despite the assertion that pyrite oxidation at SSHCZO must largely proceed abiotically, this work provides new insight into the potential mechanisms by which microorganisms may accelerate pyrite oxidation at circumneutral pH. In circumneutral environments where the geological setting is appropriate to allow for direct microbial colonization of mineral surfaces, it is conceivable that microbially-mediated pyrite oxidation may be an important, perhaps dominant, biogeochemical phenomenon. Studies in a wide range of such pyrite oxidizing environments have noted an abundance of organisms of the genus *Thiobacillus*, suggestive of a common functionality for this ubiquitous taxon. Investigations of black shale weathering have

identified *Thiobacillus* related 16S rRNA gene sequences in an *in situ* incubation experiment (Zhu and Reinfelder, 2012) and in a study investigating black shale weathering profile developed near a roadcut in southwest China (Li et al., 2014). Additionally, it has been reported that pyrite exerts a strong mineralogical control on microbial community structure in subglacial environments (Mitchell et al., 2013) and lithoautotrophic oxidation of sulfide minerals in such environments, including by *Thiobacillus* (Harrold et al., 2015), is postulated to be a driver of subglacial primary productivity and mineral weathering (Boyd et al., 2014; Montross et al., 2013; Skidmore et al., 2005). Rapid exposure of pyrite in recent landslides (Emberson et al., 2016) could also produce a habitat hosting circumneutral pH pyrite oxidation activity. Similarly, microbial circumneutral pyrite oxidation is likely to be of importance in the early stages of AMD generation where mining activity exposes fresh mineral surfaces for microbial colonization prior to the onset of rapid acidification. Investigations of mine tailings have shown that pH is an important driver of microbial community structure (Chen et al., 2013; Chen et al., 2014) and *Thiobacillus* seems to be an important community member in mining waste (Blowes et al., 2003; Korehi et al., 2014; Liu et al., 2014; Schippers et al., 2010).

5 Conclusions

Pyrite oxidizing enrichment cultures established using an inoculum from a natural subsurface pyrite weathering system demonstrated enhanced sulfate generation relative to uninoculated controls under circumneutral pH conditions. Whether artificially buffered with Pipes or naturally buffered by the native shale, rapid acidification of the bulk culture media was prevented despite extensive pyrite oxidation, resulting in long-term circumneutral pH conditions where organisms of the genus *Thiobacillus* dominated enrichment cultures. Metagenomic analysis revealed that the dominant chemolithotrophic pathway in enrichment cultures was reduced S oxidation. The

most abundant chemolithotrophic MAG, a putative *Thiobacillus* species, contained a full reduced S oxidation pathway. Scavenging of polythionate intermediates is insufficient to explain the enhanced generation of sulfate from pyrite in the presence of SOB. We thus propose a new "direct sulfur oxidation" pathway to explain this phenomenon. While we conclude that the sorbed Fe redox model proposed by Percak-Dennett and colleagues (2017) is not likely to the dominant mechanism of accelerated pyrite oxidation in our enrichment cultures, it can by no means be discounted as a potential pathway in all systems. The possibility remains that FeOB are capable of accelerating the circumneutral oxidation of pyrite and that our enrichment in SOB is unique to this study. In the context of subsurface shale weathering, the oxidation of pyrite in the Rose Hill Shale at SSHCZO largely proceeds abiotically, as physical contact between mineral surfaces and living cells, which is almost certainly required for biotic catalysis (either by the sorbed Fe redox cycling or the direct sulfur oxidation pathway), is likely not possible in the nanoporous shale matrix. However, our understanding of microbial chemolithotrophic oxidation of pyrite at circumneutral pH is still in its infancy, and further studies in the types of environments likely to be conducive to the process are needed to gain a fuller understanding of mechanistic underpinnings and biogeochemical significance of this as yet poorly documented phenomenon.

Acknowledgements

We thank the NSF Susquehanna Shale Hills Critical Zone Observatory (SSHCZO) for access to facilities and assistance with field work. This work was supported by the NASA Astrobiology Institute and a University of Wisconsin Microbiome Initiative award to EER.

References

Alneberg, J. et al., 2014. Binning metagenomic contigs by coverage and composition. Nat Methods, 11(11): 1144-6.

Altschul, S.F., Gish, W., Miller, W., Myers, E.W., J., L.D., 1990. Basic Local Alignment Search Tool. Journal of Molecular Biology(215): 403-410.

Amiotte Suchet, P., Probst, J.-L., Ludwig, W., 2003. Worldwide distribution of continental rock lithology: Implications for the atmospheric/soil CO2uptake by continental weathering and alkalinity river transport to the oceans. Global Biogeochemical Cycles, 17(2): n/a-n/a.

Appia-Ayme, C., Guiliani, N., Ratouchniak, J., Bonnefoy, V., 1999. Characterization of an operon encoding two c-type cytochromes an aa3-type cytochrome oxidase, and rusticyanin in Acidithiobcillus ferrooxidans ATCC 33020. Applied and Environmental Microbiology, 65(11): 4781-4787.

Arkesteyn, G.J.M.W., 1980. Pyrite oxidation in acid sulphate soils: The role of miroorganisms. Plant and Soil, 54(1): 119-134.

Aronesty, E., 2013. Comparison of Sequencing Utility Programs. The Open Bioinformatics Journal, 7: 1-8.

Baker, B.J., Banfield, J.F., 2003. Microbial communities in acid mine drainage. FEMS Microbiology Ecology, 44(2): 139-152.

Beckwith, C.R. et al., 2015. Characterization of MtoD from Sideroxydans lithotrophicus: a cytochrome c electron shuttle used in lithoautotrophic growth. Front Microbiol, 6: 332.

Beller, H.R. et al., 2006. The genome sequence of the obligately chemolithoautotrophic, facultatively anaerobic bacterium Thiobacillus denitrificans. J Bacteriol, 188(4): 1473-88.

Beller, H.R. et al., 2013. Genome-enabled studies of anaerobic, nitrate-dependent iron oxidation in the chemolithoautotrophic bacterium Thiobacillus denitrificans. Front Microbiol, 4: 249.

Berner, R.A., 2006. GEOCARBSULF: A combined model for Phanerozoic atmospheric O2 and CO2. Geochimica et Cosmochimica Acta, 70(23): 5653-5664.

Blowes, D.W., Ptacek, C.J., Jambor, J.L., Weisener, C.G., 2003. The Geochemistry of Acid Mine Drainage, Treatise on Geochemistry, pp. 149-204.

Bolton, E.W., Berner, R.A., Petsch, S.T., 2006. The Weathering of Sedimentary Organic Matter as a Control on Atmospheric O2: II. Theoretical Modeling. American Journal of Science, 306(8): 575-615.

Bosch, J., Lee, K.Y., Jordan, G., Kim, K.W., Meckenstock, R.U., 2012. Anaerobic, nitrate-dependent oxidation of pyrite nanoparticles by Thiobacillus denitrificans. Environ Sci Technol, 46(4): 2095-101.

Bosch, J., Meckenstock, R.U., 2012. Rates and potential mechanism of anaerobic nitrate-dependent microbial pyrite oxidation. Biochem Soc Trans, 40(6): 1280-3.

Boyd, E.S., Hamilton, T.L., Havig, J.R., Skidmore, M.L., Shock, E.L., 2014. Chemolithotrophic primary production in a subglacial ecosystem. Appl Environ Microbiol, 80(19): 6146-53.

Brantley, S.L., Holleran, M.E., Jin, L., Bazilevskaya, E., 2013. Probing deep weathering in the Shale Hills Critical Zone Observatory, Pennsylvania (USA): the hypothesis of nested chemical reaction fronts in the subsurface. Earth Surface Processes and Landforms, 38(11): 1280-1298.

Buss, H.L. et al., 2005. The coupling of biological iron cycling and mineral weathering during saprolite formation, Luquillo Mountains, Puerto Rico. Geobiology, 3: 247-260.

Buss, H.L., Sak, P.B., Webb, S.M., Brantley, S.L., 2008. Weathering of the Rio Blanco quartz diorite, Luquillo Mountains, Puerto Rico: Coupling oxidation, dissolution, and fracturing. Geochimica et Cosmochimica Acta, 72(18): 4488-4507.

Caporaso, J.G. et al., 2010a. PyNAST: a flexible tool for aligning sequences to a template alignment. Bioinformatics, 26(2): 266-7.
Caporaso, J.G. et al., 2010b. QIIME allows analysis of high-throughput community sequencing data. Nature Methods, 7(5): 335-336.
Castelle, C. et al., 2008. A new iron-oxidizing/O2-reducing supercomplex spanning both inner and outer membranes, isolated from the extreme acidophile Acidithiobacillus ferrooxidans. J Biol Chem, 283(38): 25803-11.
Chen, L. et al., 2012. Acidithiobacillus caldus sulfur oxidation model based on transcriptome analysis between the wild type and sulfur oxygenase reductase defective mutant. PLoS One, 7(9): e39470.
Chen, L.X. et al., 2013. Shifts in microbial community composition and function in the acidification of a lead/zinc mine tailings. Environ Microbiol, 15(9): 2431-44.
Chen, Y.T. et al., 2014. Biogeochemical processes governing natural pyrite oxidation and release of acid metalliferous drainage. Environ Sci Technol, 48(10): 5537-45.
Cianciotto, N.P., 2005. Type II secretion: a protein secretion system for all seasons. Trends Microbiol, 13(12): 581-8.
Clesceri, L.S., Greenberg, A.E., Eaton, A.D., 1998. Standard methods for the examination of water and wastewater, American Public Health Association. Washington, DC: 4-415.
Cockell, C.S. et al., 2011. Molecular characterization and geological microenvironment of a microbial community inhabiting weathered receding shale cliffs. Microbial Ecology, 61(1): 166-181.
Colmer, A.R., Hinkle, M.E., 1947. The Role of Microorganisms in Acid Mine Drainage: A Preliminary Report. Science, 106(2751): 253-256.
Converse, B.J., McKinley, J.P., Resch, C.T., Roden, E.E., 2015. Microbial mineral colonization across a subsurface redox transition zone. Front Microbiol, 6: 858.
Crooks, G.E., Hon, G., Chandonia, J.M., Brenner, S.E., 2004. WebLogo: A sequence logo generator. Genome Research, 14(6): 1188-1190.
Dahl, C. et al., 2005. Novel genes of the dsr gene cluster and evidence for close interaction of Dsr proteins during sulfur oxidation in the phototrophic sulfur bacterium Allochromatium vinosum. J Bacteriol, 187(4): 1392-404.
Dahl, C., Franz, B., Hensen, D., Kesselheim, A., Zigann, R., 2013. Sulfite oxidation in the purple sulfur bacterium Allochromatium vinosum: identification of SoeABC as a major player and relevance of SoxYZ in the process. Microbiology, 159(Pt 12): 2626-2638.
Deng, Y., 1997. Formation of iron(III) hydroxides from homogeneous solutions. Water Research, 31(6): 1347-1354.
DiChristina, T.J., Moore, C.M., Haller, C.A., 2002. Dissimilatory Fe(III) and Mn(IV) reduction by Shewanella putrefaciens requires ferE, a homolog of the pulE (gspE) type II protein secretion gene. J Bacteriol, 184(1): 142-51.
Durand, E. et al., 2003. Type II protein secretion in Pseudomonas aeruginosa: the pseudopilus is a multifibrillar and adhesive structure. J Bacteriol, 185(9): 2749-58.
Durham, B.W., 1974. Stability of Weak Sodium Thiosulfate Solutions. Analytical Chemistry, 46(14): 2245.
Edgar, R.C., 2004. MUSCLE: Multiple sequence alignment with high accuracy and high throughput. Nucleic Acids Research, 32(5): 1792-1797.
Edgar, R.C., 2010. Search and clustering orders of magnitude faster than BLAST. Bioinformatics, 26(19): 2460-1.

Edwards, K.J., Rogers, D.R., Wirsen, C.O., McCollom, T.M., 2003. Isolation and Characterization of Novel Psychrophilic, Neutrophilic, Fe-Oxidizing, Chemolithoautotrophic - and -Proteobacteria from the Deep Sea. Applied and Environmental Microbiology, 69(5): 2906-2913.

Emberson, R., Hovius, N., Galy, A., Marc, O., 2016. Oxidation of sulfides and rapid weathering in recent landslides. Earth Surface Dynamics, 4(3): 727-742.

Emerson, D. et al., 2013. Comparative genomics of freshwater Fe-oxidizing bacteria: implications for physiology, ecology, and systematics. Front Microbiol, 4: 254.

Emerson, D., Fleming, E.J., McBeth, J.M., 2010. Iron-oxidizing bacteria: an environmental and genomic perspective. Annu Rev Microbiol, 64: 561-83.

Evangelou, V.P., 2001. Pyrite microencapsulation technologies: Principles and potential field application. Ecological Engineering, 17(2-3): 165-178.

Fan, R. et al., 2017. The Formation of Silicate-Stabilized Passivating Layers on Pyrite for Reduced Acid Rock Drainage. Environ Sci Technol, 51(19): 11317-11325.

Friedrich, C.G., Rother, D., Bardischewsky, F., Quentmeier, A., Fischer, J., 2001. Oxidation of reduced inorganic sulfur compounds by bacteria: emergence of a common mechanism? Appl Environ Microbiol, 67(7): 2873-82.

Gotz, F. et al., 2019. Transcriptomic and proteomic insight into the mechanism of cyclooctasulfur- versus thiosulfate-oxidation by the chemolithoautotroph Sulfurimonas denitrificans. Environ Microbiol, 21(1): 244-258.

Gu, X., Heaney, P., Aarão Reis, F.D.A., Wang, K., Brantley, S.L., 2019. Deep abiotic weathering of pyrite affects atmospheric oxygen and riverine fluxes of sulfur. Science, Submitted.

Guindon, S. et al., 2010. New algorithms and methods to estimate maximum-likelihood phylogenies: assessing the performance of PhyML 3.0. Syst Biol, 59(3): 307-21.

Haaijer, S.C.M., Lamers, L.P.M., Smolders, A.J.P., Jetten, M.S.M., Op den Camp, H.J.M., 2007. Iron Sulfide and Pyrite as Potential Electron Donors for Microbial Nitrate Reduction in Freshwater Wetlands. Geomicrobiology Journal, 24(5): 391-401.

Haas, L.D., Roden, E.E., Ginder-Vogel, M., Zambito, J.J., 2019. Microbially-mediated pyrite oxidation at circumneutral pH in sandstones of Trempealeau County, WI. Geological Society of American Annual Meeting. Abstract 104-8.

Harrold, Z.R. et al., 2015. Aerobic and Anaerobic Thiosulfate Oxidation by a Cold-Adapted, Subglacial Chemoautotroph. Appl Environ Microbiol, 82(5): 1486-95.

He, S., Barco, R.A., Emerson, D., Roden, E.E., 2017. Comparative Genomic Analysis of Neutrophilic Iron(II) Oxidizer Genomes for Candidate Genes in Extracellular Electron Transfer. Front Microbiol, 8: 1584.

Hyatt, D. et al., 2010. Prodigal: prokaryotic gene recognition and translation initiation site identification. BMC Bioinformatics, 11: 119.

Jin, L. et al., 2014. The CO 2 consumption potential during gray shale weathering: Insights from the evolution of carbon isotopes in the Susquehanna Shale Hills critical zone observatory. Geochimica et Cosmochimica Acta, 142: 260-280.

Jin, L. et al., 2010. Mineral weathering and elemental transport during hillslope evolution at the Susquehanna/Shale Hills Critical Zone Observatory. Geochimica et Cosmochimica Acta, 74(13): 3669-3691.

Jin, L. et al., 2011. Characterization of deep weathering and nanoporosity development in shale--A neutron study. American Mineralogist, 96(4): 498-512.

Jørgensen, C.J., Jacobsen, O.S., Elberling, B., Aamand, J., 2009. Microbial Oxidation of Pyrite Coupled to Nitrate Reduction in Anoxic Groundwater Sediment. Environmental Science & Technology, 43(13): 4851-4857.

Kang, D.D. et al., 2019. MetaBAT 2: an adaptive binning algorithm for robust and efficient genome reconstruction from metagenome assemblies. PeerJ, 7: e7359.

Kelley, L.A., Mezulis, S., Yates, C.M., Wass, M.N., Sternberg, M.J.E., 2015. The Phyre2 web portal for protein modeling, prediction and analysis. Nature Protocols, 10(6): 845-858.

Kennedy, C.B., Scott, S.D., Ferris, F.G., 2004. Hydrothermal phase stabilization of 2-line ferrihydrite by bacteria. Chemical Geology, 212(3-4): 269-277.

Koch, T., Dahl, C., 2018. A novel bacterial sulfur oxidation pathway provides a new link between the cycles of organic and inorganic sulfur compounds. ISME J, 12(10): 2479-2491.

Korehi, H., Blothe, M., Schippers, A., 2014. Microbial diversity at the moderate acidic stage in three different sulfidic mine tailings dumps generating acid mine drainage. Res Microbiol, 165(9): 713-8.

Le, S.Q., Gascuel, O., 2008. An improved general amino acid replacement matrix. Mol Biol Evol, 25(7): 1307-20.

Li, D., Liu, C.M., Luo, R., Sadakane, K., Lam, T.W., 2015. MEGAHIT: an ultra-fast single-node solution for large and complex metagenomics assembly via succinct de Bruijn graph. Bioinformatics, 31(10): 1674-6.

Li, J. et al., 2014. Bacteria diversity, distribution and insight into their role in S and Fe biogeochemical cycling during black shale weathering. Environ Microbiol, 16(11): 3533-47.

Lin, X. et al., 2012. Distribution of microbial biomass and potential for anaerobic respiration in hanford site 300 area subsurface sediment. Applied and Environmental Microbiology, 78(3): 759-767.

Littke, R., Klussmann, U., Krooss, B., Leythaeuser, D., 1991. Quantification of loss of calcite, pyrite, and organic matter due to weathering of Toarcian black shales and effects on kerogen and bitumen characteristics. Geochimica et Cosmochimica Acta, 55(11): 3369-3378.

Liu, H.C., Xia, J.L., Nie, Z.Y., Zhen, X.J., Zhang, L.J., 2015. Differential expression of extracellular thiol groups of moderately thermophilic Sulfobacillus thermosulfidooxidans and extremely thermophilic Acidianus manzaensis grown on S(0) and Fe (2.). Arch Microbiol, 197(6): 823-31.

Liu, J. et al., 2014. Correlating microbial diversity patterns with geochemistry in an extreme and heterogeneous environment of mine tailings. Appl Environ Microbiol, 80(12): 3677-86.

Liu, J. et al., 2012. Identification and Characterization of MtoA: A Decaheme c-Type Cytochrome of the Neutrophilic Fe(II)-Oxidizing Bacterium Sideroxydans lithotrophicus ES-1. Front Microbiol, 3: 37.

Ma, L. et al., 2013. Regolith production and transport in the Susquehanna Shale Hills Critical Zone Observatory, Part 1: Insights from U-series isotopes. Journal of Geophysical Research: Earth Surface, 118(2): 722-740.

Ma, L., Jin, L., Brantley, S.L., 2011. Geochemical behaviors of different element groups during shale weathering at the Susquehanna/Shale Hills Critical Zone Observatory. Applied Geochemistry, 26: S89-S93.

Mangold, S., Valdes, J., Holmes, D.S., Dopson, M., 2011. Sulfur metabolism in the extreme acidophile acidithiobacillus caldus. Front Microbiol, 2: 17.
McAllister, S.M. et al., 2019. Validating the Cyc2 neutrophilic Fe oxidation pathway using meta-omics of Zetaproteobacteria iron mats at marine hydrothermal vents.
McKibben, M.A., Barnes, H.L., 1986. Oxidation of pyrite in low temperature acidic solutions: Rate laws and surface textures. Geochimica et Cosmochimica Acta, 50(7): 1509-1520.
Mitchell, A.C., Lafrenière, M.J., Skidmore, M.L., Boyd, E.S., 2013. Influence of bedrock mineral composition on microbial diversity in a subglacial environment. Geology, 41(8): 855-858.
Montross, S.N., Skidmore, M., Tranter, M., Kivimäki, A.-L., Parkes, R.J., 2013. A microbial driver of chemical weathering in glaciated systems. Geology, 41(2): 215-218.
Moore, E.R.B. et al., 2006. Nonmedical: Pseudomonas. In: Dworkin, M., Falkow, S., Rosenberg, E., Schleifer, K.-H., Stackebrandt, E. (Eds.), The Prokaryotes: Volume 6: Proteobacteria: Gamma Subclass. Springer New York, New York, NY, pp. 646-703.
Moses, C.O., Herman, J.S., 1991. Pyrite oxidation at circumneutral pH. Geochimica et Cosmochimica Acta, 55(2): 471-482.
Moses, C.O., Kirk Nordstrom, D., Herman, J.S., Mills, A.L., 1987. Aqueous pyrite oxidation by dissolved oxygen and by ferric iron. Geochimica et Cosmochimica Acta, 51(6): 1561-1571.
Napieralski, S.A. et al., 2019. Microbial chemolithotrophy mediates oxidative weathering of granitic bedrock. PNAS, Submitted.
Nicholson, R.V., Gillham, R.W., Reardon, E.J., 1988. Pyrite oxidation in carbonate-buffered solution: 1. Experimental kinetics. Geochimica et Cosmochimica Acta, 52(5): 1077-1085.
Nor, Y.M., Tabatabai, M.A., 1975. Colorimetric Determination of Microgram Quantities of Thiosulfate and Tetrathionate. Analytical Letters, 8(8): 537-547.
Parge, H.E. et al., 1995. Structure of the fibre-forming protein pilin at 2.6 Å resolution. Nature, 378(6552): 32-38.
Parks, D.H., Imelfort, M., Skennerton, C.T., Hugenholtz, P., Tyson, G.W., 2015. CheckM: assessing the quality of microbial genomes recovered from isolates, single cells, and metagenomes. Genome Res, 25(7): 1043-55.
Peabody, C.R. et al., 2003. Type II protein secretion and its relationship to bacterial type IV pili and archaeal flagella. Microbiology, 149(Pt 11): 3051-72.
Percak-Dennett, E. et al., 2017. Microbial acceleration of aerobic pyrite oxidation at circumneutral pH. Geobiology, 15(5): 690-703.
Peretyazhko, T.S. et al., 2012. Pertechnetate (TcO4 -) reduction by reactive ferrous iron forms in naturally anoxic, redox transition zone sediments from the Hanford Site, USA. Geochimica et Cosmochimica Acta, 92: 48-66.
Pichler, T., Veizer, J., 1999. Precipitation of Fe(III) oxyhydroxide deposits from shallow-water hydrothermal fluids in Tutum Bay, Ambitle Island, Papua New Guinea. Chemical Geology, 162(1): 15-31.
Pott, A.S., Dahl, C., 1998. Sirohaem sulfite reductase and other proteins encoded by genes at the dsr locus of Chromatium vinosum are involved in the oxidation of intracellular sulfur. Microbiology, 144(7): 1881-1984.
Quast, C. et al., 2013. The SILVA ribosomal RNA gene database project: improved data processing and web-based tools. Nucleic Acids Res, 41(Database issue): D590-6.

Raiswell, R., Canfield, D.E., 2012. The iron biogeochemical cycle past and present. Geochemical Perspectives, 1(1): 1-232.
Rohwerder, T., Sand, W., 2003. The sulfane sulfur of persulfides is the actual substrate of the sulfur-oxidizing enzymes from Acidithiobacillus and Acidiphilium spp. Microbiology, 149(Pt 7): 1699-710.
Rondelet, A., Condemine, G., 2013. Type II secretion: the substrates that won't go away. Res Microbiol, 164(6): 556-61.
Sauvonnet, N., Vignon, G., Pugsley, A.P., Gounon, P., 2000. Pilus formation and protein secretion by the same machinery in Escherichia coli. EMBO, 19(10): 2221-2228.
Schippers, A. et al., 2010. The biogeochemistry and microbiology of sulfidic mine waste and bioleaching dumps and heaps, and novel Fe(II)-oxidizing bacteria. Hydrometallurgy, 104(3-4): 342-350.
Schippers, A., Von Rège, H., Sand, W., 1996. Impact of microbial diversity and sulfur chemistry on safeguarding sulfudic mine waste. Minerals Engineering, 9(10): 1069-1079.
Seemann, T., 2014. Prokka: rapid prokaryotic genome annotation. Bioinformatics, 30(14): 2068-9.
Shi, L. et al., 2008. Direct involvement of type II secretion system in extracellular translocation of Shewanella oneidensis outer membrane cytochromes MtrC and OmcA. J Bacteriol, 190(15): 5512-6.
Skidmore, M., Anderson, S.P., Sharp, M., Foght, J., Lanoil, B.D., 2005. Comparison of microbial community compositions of two subglacial environments reveals a possible role for microbes in chemical weathering processes. Appl Environ Microbiol, 71(11): 6986-97.
Stookey, L.L., 1970. Ferrozine-Anew spectrophotometric reagent for iron. Analytical Chemistry, 42(7): 778-781.
Sullivan, P.L. et al., 2016a. Oxidative dissolution under the channel leads geomorphological evolution at the Shale Hills catchment. American Journal of Science, 316(10): 981-1026.
Sullivan, P.L. et al., 2016b. CZ-tope at Susquehanna Shale Hills CZO: Synthesizing multiple isotope proxies to elucidate Critical Zone processes across timescales in a temperate forested landscape. Chemical Geology, 445: 103-119.
Swedlund, P.J., Webster, J.G., 1999. Adsorption and polymerisation of silicic acid on ferrihydrite, and its effect on arsenic adsorption. Water Research, 33(16): 3413-3422.
Turner, B.F., Stallard, R.F., Brantley, S.L., 2003. Investigation of in situ weathering of quartz diorite bedrock in the Rio Icacos basin, Luquillo Experimental Forest, Puerto Rico. Chemical Geology, 202(3-4): 313-341.
Tuttle, J.H., Jannasch, H.W., 1976. Microbial utilization of thiosulfate in the deep sea. Limnology and Oceanography, 21(5): 697-701.
Uritskiy, G.V., DiRuggiero, J., Taylor, J., 2018. MetaWRAP-a flexible pipeline for genome-resolved metagenomic data analysis. Microbiome, 6(1): 158.
Vear, A., Curtis, C., 1981. A quantitative evaluation of pyrite weathering. Earth Surface Processes and Landforms, 6(2): 191-198.
Watanabe, T. et al., 2019. Genomes of Neutrophilic Sulfur-Oxidizing Chemolithoautotrophs Representing 9 Proteobacterial Species From 8 Genera. Front Microbiol, 10: 316.
Wirsen, C.O., Jannasch, H.W., Molyneaux, S.J., 1993. Chemosynthetic microbial activity at Mid-Atlantic Ridge hydrothermal vent sites. Journal of Geophysical Research, 98(B6).

Wu, Y.-W., Simmons, B.A., Singer, S.W., 2015. MaxBin 2.0: an automated binning algorithm to recover genomes from multiple metagenomic datasets. Bioinformatics, 32(4): 605-607.
Yan, R. et al., 2019. Effect of Reduced Sulfur Species on Chemolithoautotrophic Pyrite Oxidation with Nitrate. Geomicrobiology Journal, 36(1): 19-29.
Yin, H. et al., 2014. Whole-genome sequencing reveals novel insights into sulfur oxidation in the extremophile Acidithiobacillus thiooxidans. BMC Microbiol, 14: 179.
Yu, C.S., Chen, Y.C., Lu, C.H., Hwang, J.K., 2006. Prediction of protein subcellular localization. Proteins, 64(3): 643-51.
Zhou, J., Bruns, M.A., Tiedje, J.M., 1996. DNA recovery from soils of diverse composition. Applied and Environmental Microbiology, 62(2): 316-322.
Zhu, W., Reinfelder, J.R., 2012. The Microbial Community of a Black Shale Pyrite Biofilm and its Implications for Pyrite Weathering. Geomicrobiology Journal, 29(2): 186-193.

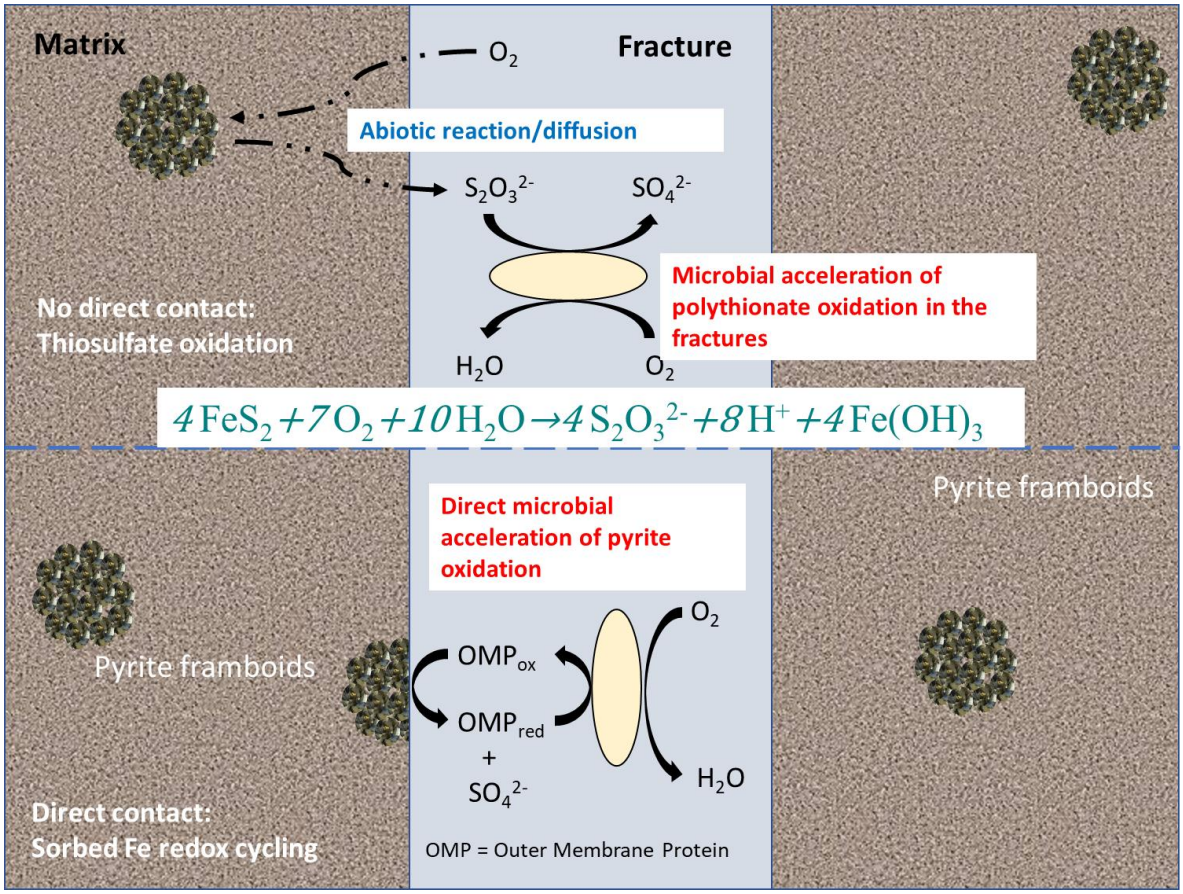

Figure 1: Proposed models for microbially-mediated circumneutral pyrite oxidation in the Shale matrix and fracture network at SSHZO. The indirect polythionate intermediate model (top) allows for microbial colonization of fracture spaces and consumption of abiotically generated polythionates diffusing through the matrix to the fractures. The direct oxidation model (bottom) requires cell-mineral contact and is thus restricted to the matrix-fracture interface.

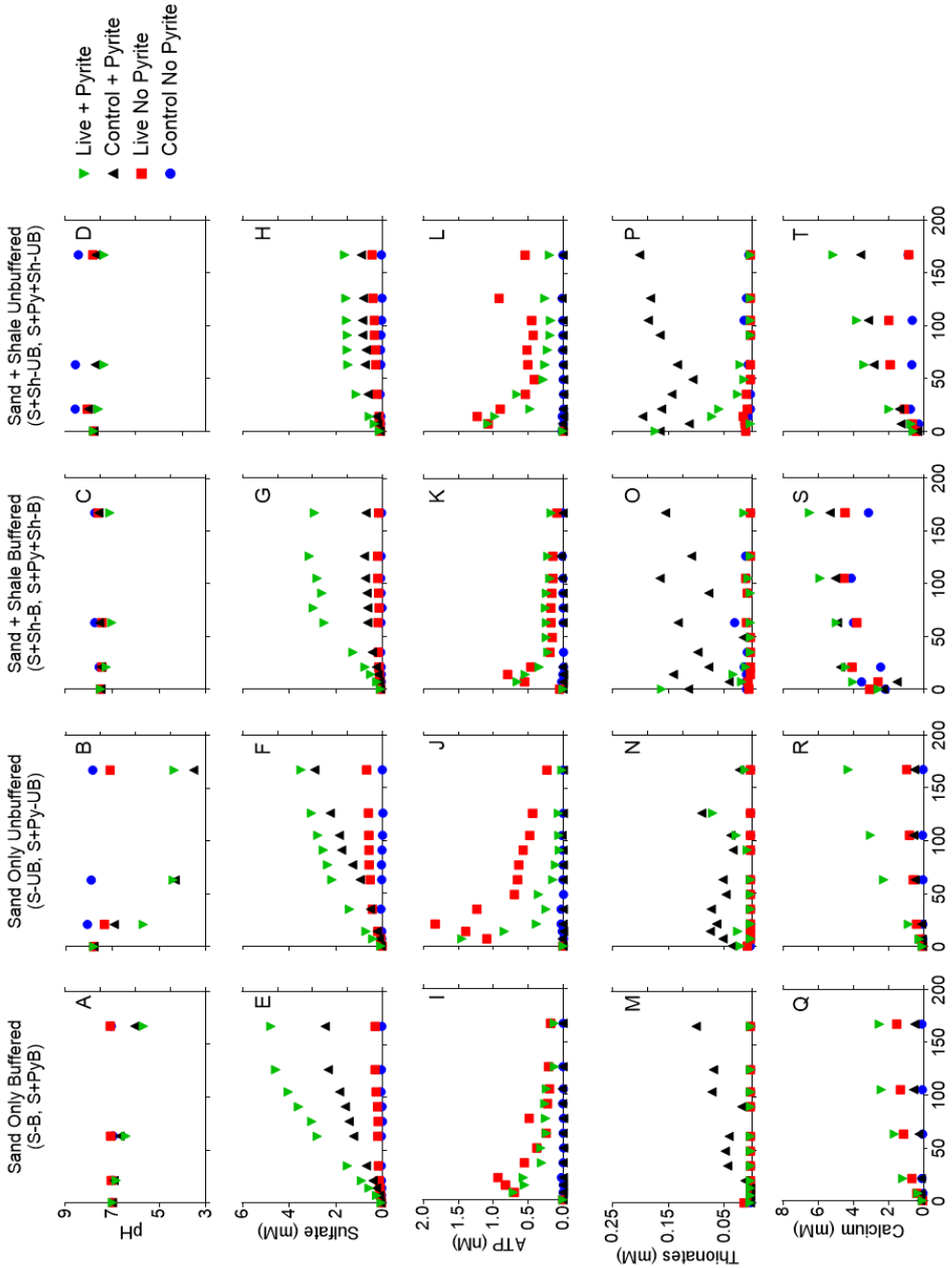

Figure 2: Average pH (A-D), sulfate concentration (E-H), ATP content (I-L), total polythionate (M-P), and calcium concentration (Q-T) in duplicate reactors for each experimental condition.

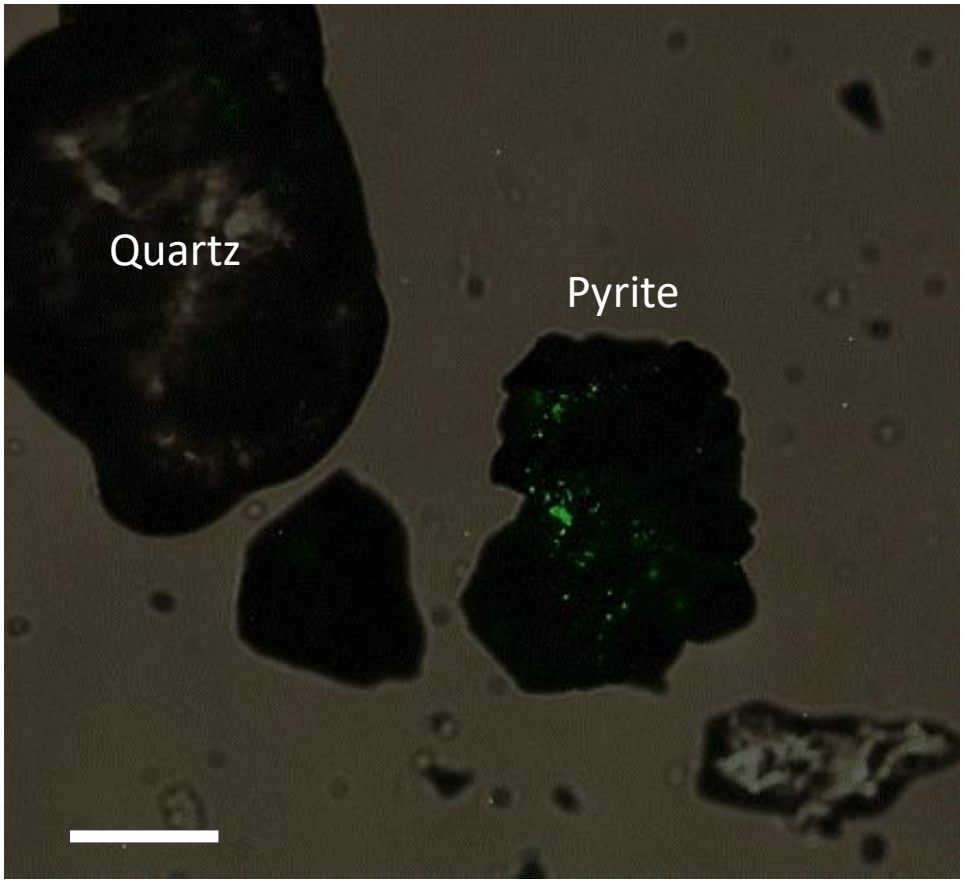

Figure 3: Composite (epifluorescence and light) image of SYTO stained microbially colonized pyrite grains after 77 days of incubation. Cells are preferentially adhered to pyrite surfaces rather than quartz grains or in background medium. Scale bar equals 20 µm.

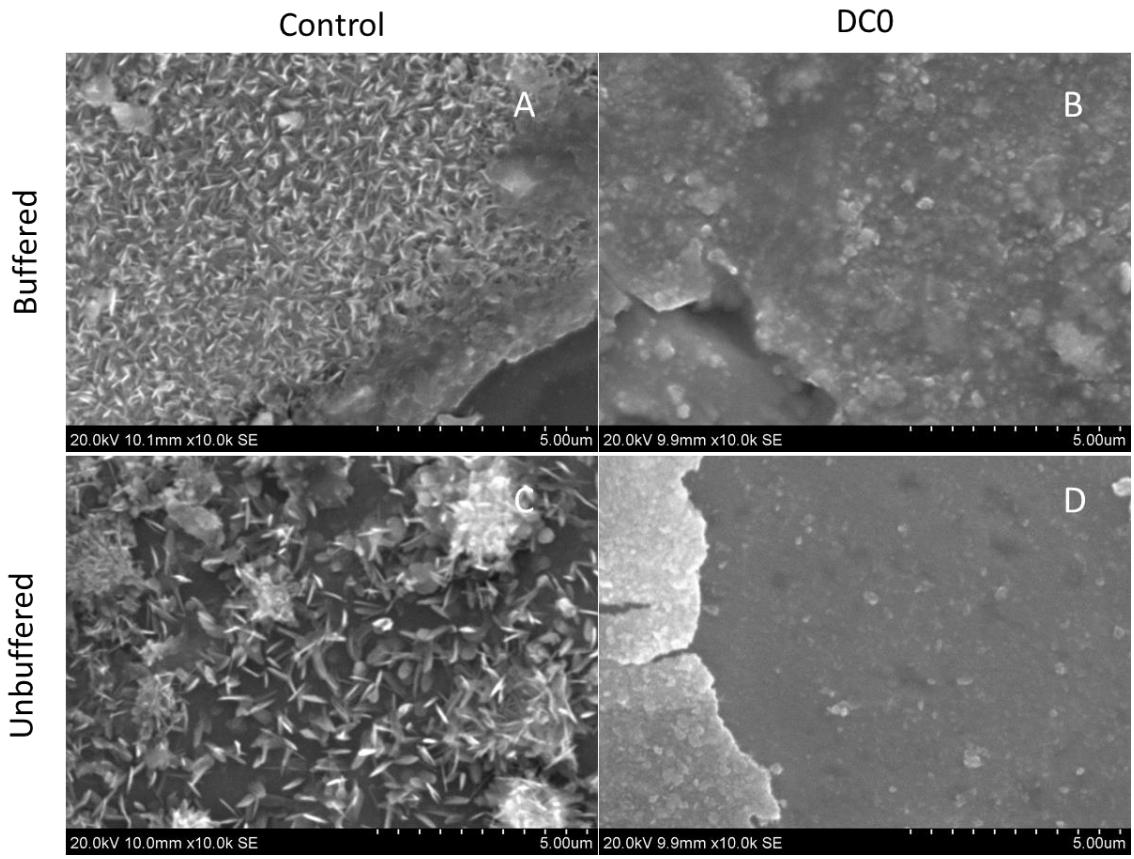

Figure 4: SEM images of pyrite grains from S+Py reactors after abiotic incubation (A and C) and incubation with a live inoculum (B and D) for buffered (A and B) and unbuffered (C and D) reactors. Note the presence of discrete Fe oxide nanocrystals in the abiotic systems which were much less abundance in the live cultures.

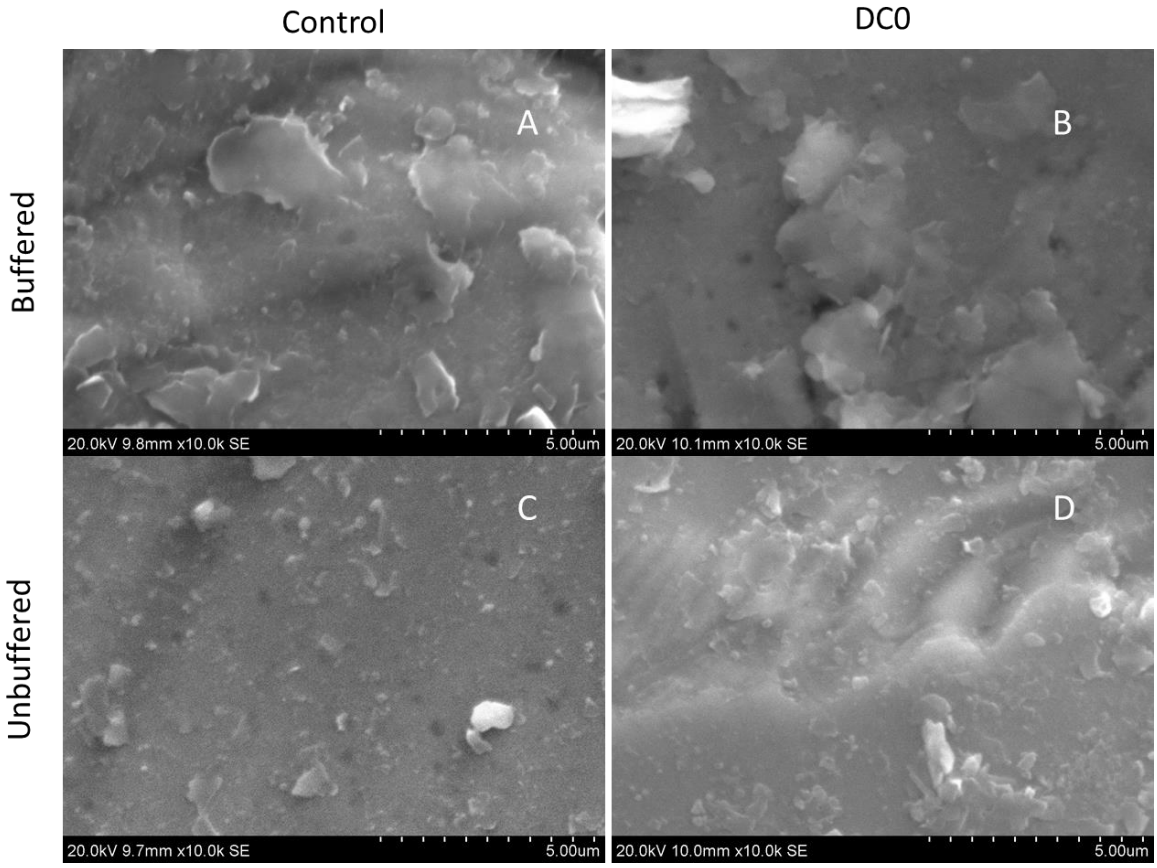

Figure 5: Figure 4: SEM images of pyrite grains from S+Py+Sh reactors after abiotic incubation (A and C) and incubation with a live inocula (B and D) for buffered (A and B) and unbuffered reactors. Note the difference in surface morphology and lack of crystalline phases in the abiotic control relative to S+Py reactors.

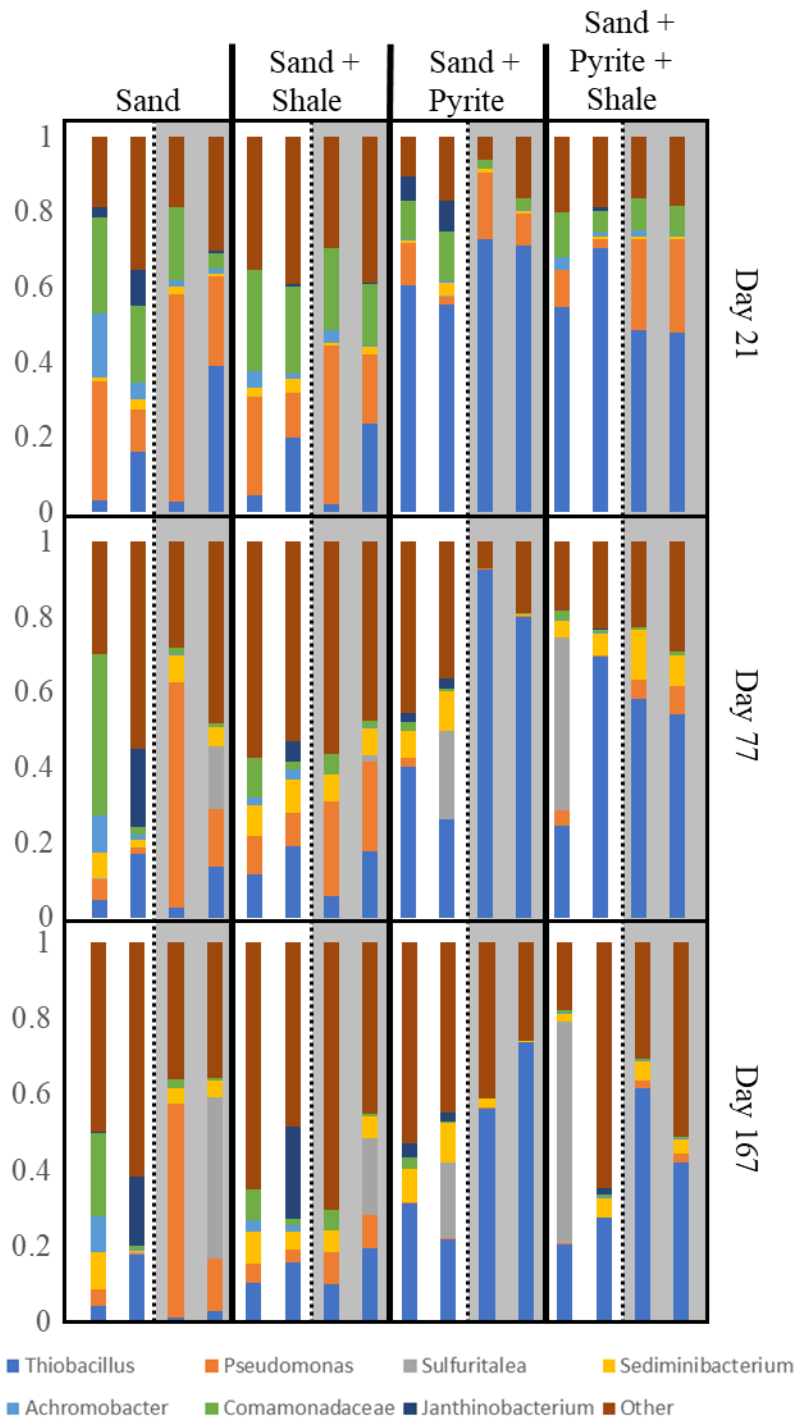

Figure 6: 16S rRNA gene amplicon sequencing results showing the relative abundance of the dominant genera for each sample after 21 (top), 77 (middle) and 167 (bottom) days of incubation for each reactor. Buffered and unbuffered reactors are delimited by a dashed line for each mineral treatment, with buffered reactors shaded in grey.

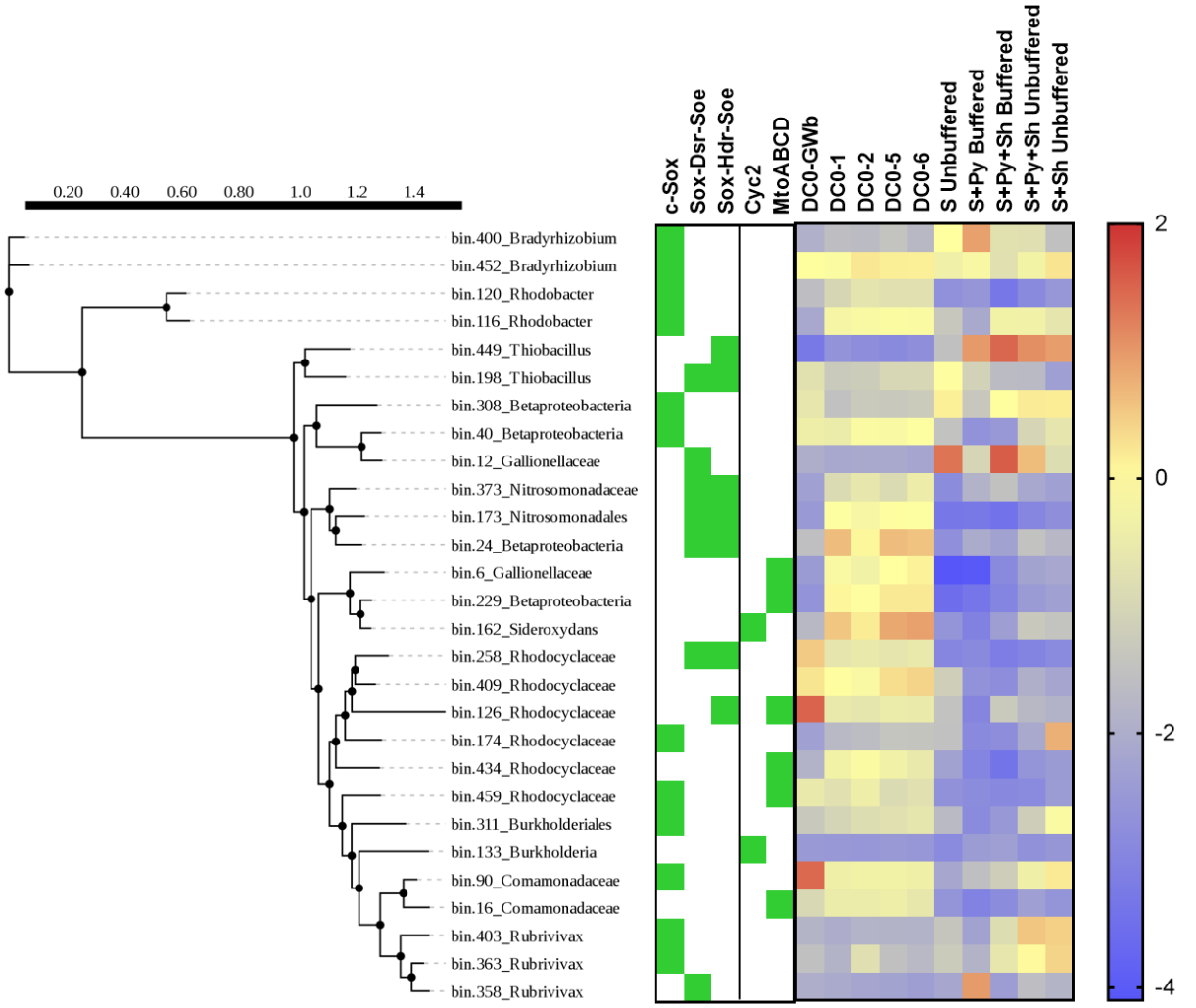

Figure 7: Heat map indicating the putative taxonomy and abundance (log genomes per million reads) of chemolithoautotrophic MAGs obtained from the metagenomic coassembly across all samples in the coassembly (Groundwater; DC0-GwB, *in situ* mineral deployments; DC01-6 and enrichment cultures for which metagenomic library preparation was successful). The presence of each lithotrophic pathway for either S oxidation (c-Sox, Sox-Dsr-Soe and Sox-Hdr-Soe) or Fe oxidation (Cyc2 and MtoABCD) in each MAG is indicated by a green square. For clarity only MAGs containing either an Fe or S oxidation pathway as well as a full CO_2 fixation pathway are shown.

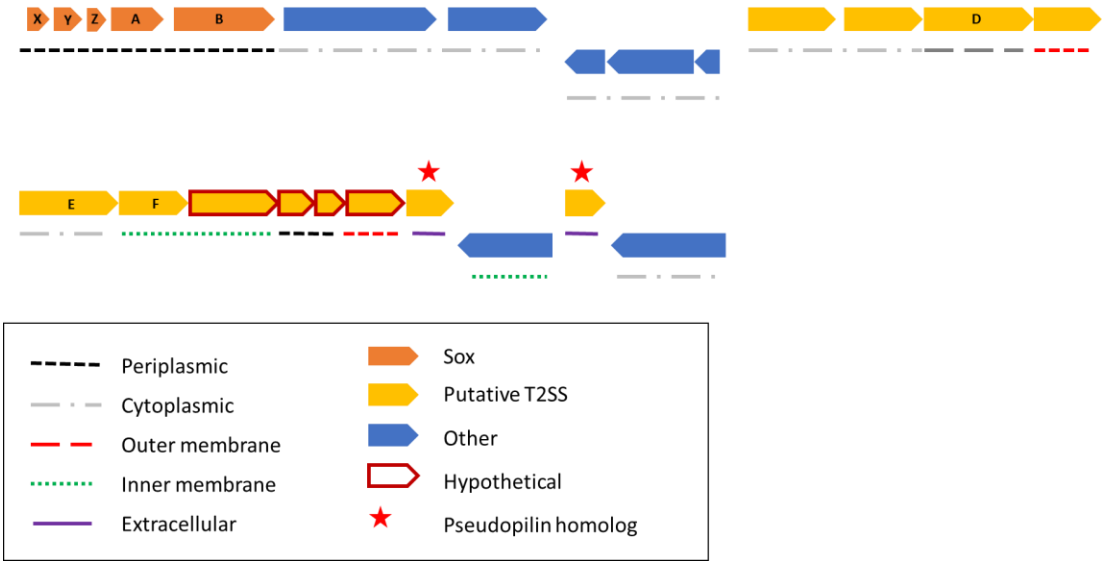

Figure 8: Gene map of the Sox gene cluster (orange) from MAG 449, a putative *Thiobacillus* strain illustrating the genomic relationship to a putative T2SS system (Gsp, yellow). Predicted subcellular locations are provided. Hypothetical proteins and putative psuedopilin homologs are indicated.

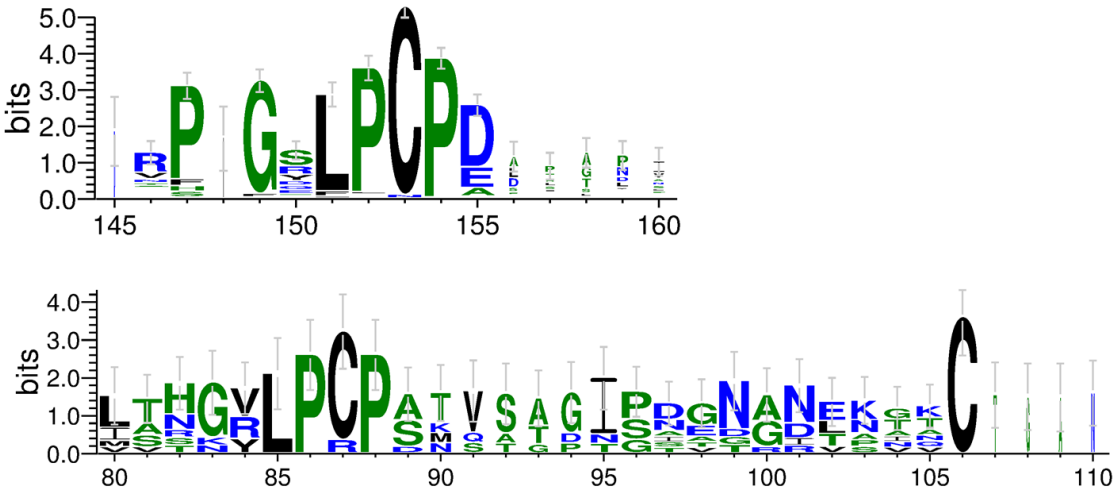

Figure 9: Alignment showing conserved motifs of the hypothetical sulfhydryl-containing outer membrane protein (top) and the adjacent pseudopilin (bottom) (see Figure 8) and homologs identified by Blastp (top) showing conserved regions, including cysteine residues.

Table 1: Sulfate releases rate over the first 35 days of incubation

	35-day sulfate release (mM day^{-1})†	R^2	Rate fold increase	Initial sulfate (mM)*	Final sulfate (mM)*	Total sulfate released (mM)*	Total release fold change
Sand Only Buffered							
Live + Py	0.042 ± 0.001	0.9934	2.328	0.085 ± 0.0005	4.794 ± 1.523	4.709 ± 1.522	1.988
Control + Py	0.018 ± 0.0001	0.9798		0.098 ± 0.009	2.466 ± 0.128	2.369 ± 0.119	
Sand Only Unbuffered							
Live + Py	0.034 ± 0.041	0.9907	2.624	0.086 ± 0.004	3.502 ± 0.688	3.416 ± 0.692	1.203
Control +Py	0.013 ± 0.001	0.9877		0.084 ± 0.022	2.923 ± 1.012	2.839 ± 0.990	
Sand +Shale Buffered							
Live + Py	0.034 ± 0.001	0.9916	3.431	0.110 ± 0.013	2.929 ± 0.583	2.819 ± 0.596	4.657
Control +Py	0.001 ± 0.001	0.9481		0.117 ± 0.002	0.722 ± 0.156	0.605 ± 0.154	
Sand +Shale Unbuffered							
Live + Py	0.028 ± 0.001	0.9965	1.897	0.158 ± 0.054	1.630 ± 0.192	1.475 ± 0.138	1.853
Control +Py	0.015 ± 0.004	0.6793		0.125 ± 0.027	0.921 ± 0.810	0.796 ± 0.783	

†From linear regression of sulfate concentrations over 35 days for individual reactors and error of the slope
*Average ± range of duplicate reactors

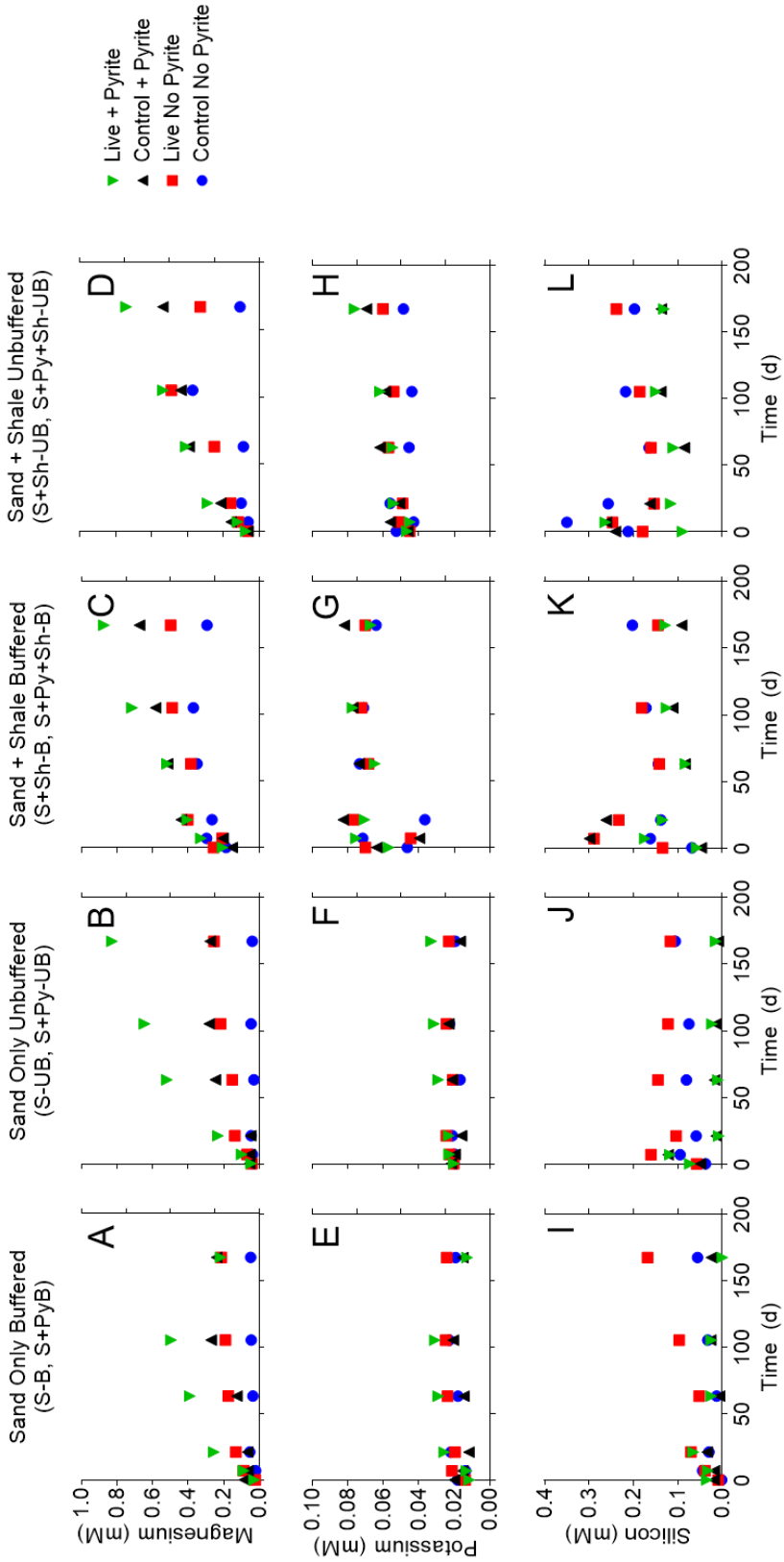

Figure S1: Average magnesium (A-D), potassium (E-H) and silicon (I-L) concentrations in duplicate reactors for each experimental condition.

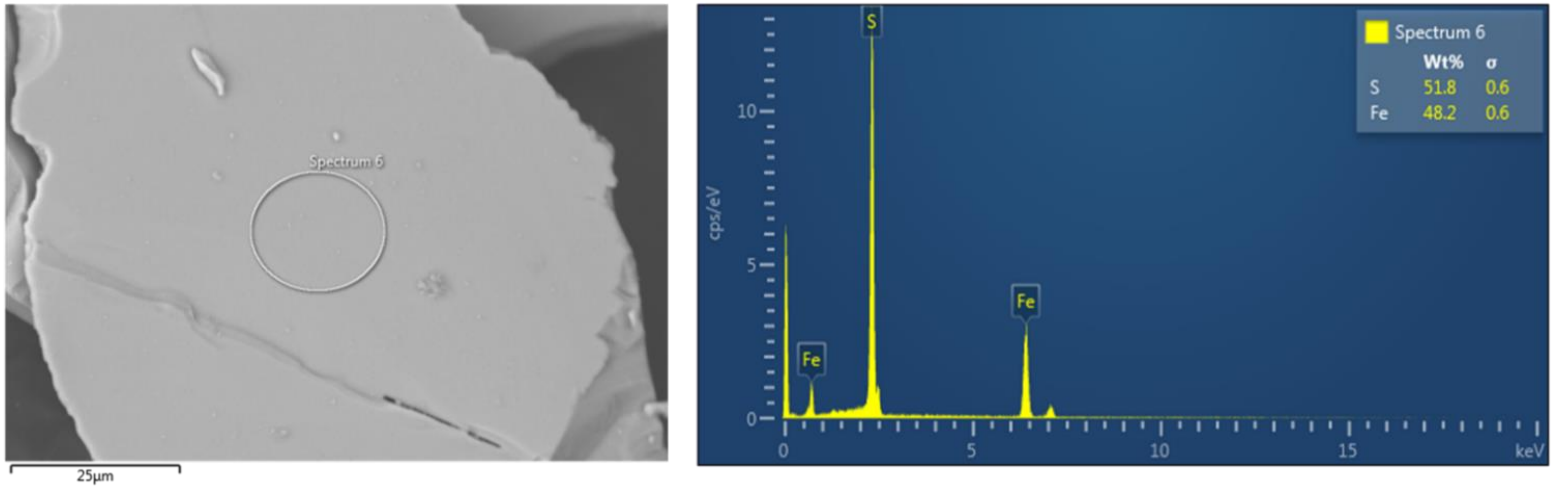

Figure S2: SEM image of a representative initial time zero pyrite surface after cleaning via sonication and dilute HNO_3 and corresponding EDS spectra.

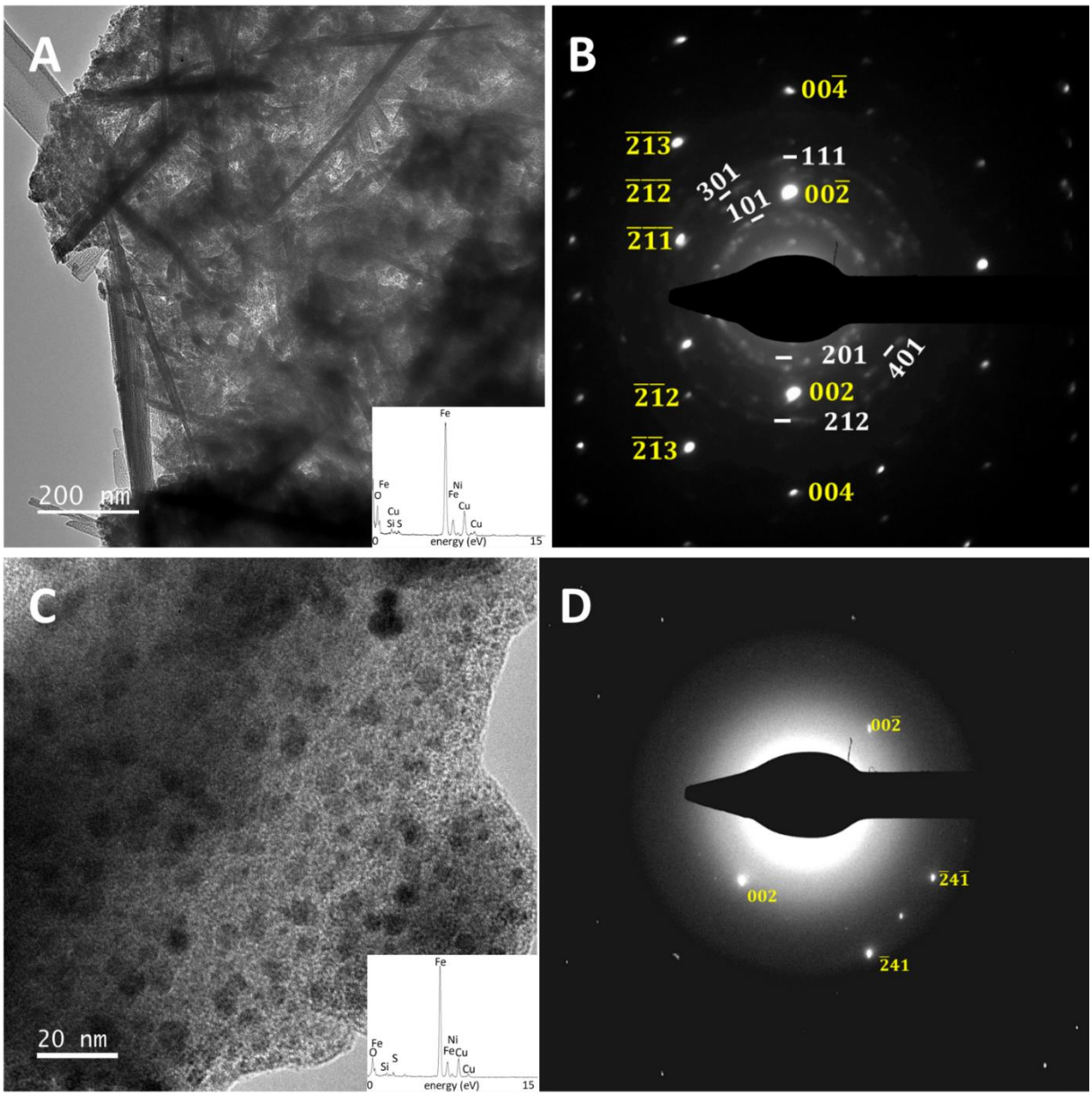

Figure S3: Bight-field TEM images (A and C) and selected-area diffraction (SAED) patterns (B and D) of pyrite surface after 167 days of abiotic incubation (top) and incubation with a live inoculum over the same time frame (bottom) in S+Py-B reactors. A and C have X-ray EDS spectra inserted at lower right corner for goethite and amorphous Fe-oxihydroxide or 2-line ferrihydrite, respectively. In SAED patterns, diffraction spots labeled in yellow are from pyrite and white dotted rings are from the surface goethite. After abiotic incubation, pyrite surfaces were coated with needle-like crystalline goethite while incubation with a live inoculum resulted in 2-line ferrihydrite.

Table S1. Groundwater geochemistry in well DC0 at SSHCZO.

Parameter	Value	Units	Date(es)	Reference
Temperature	18.2	°C	24 Aug 2017	This study
pH	7.4		24 Aug 2017	This study
Conductivity	136	μS/cm	24 Aug 2017	This study
Eh (SHE)	-181	mV	24 Aug 2017	This study
Dissolved O_2	0.035	mM	24 Aug 2017	This study
Ca	0.384	mM	24 Aug 2017	This study
K	0.079	mM	24 Aug 2017	This study
Mg	0.327	mM	24 Aug 2017	This study
Na	0.079	mM	24 Aug 2017	This study
Si	0.018	mM	24 Aug 2017	This study
Fe	0.029	mM	24 Aug 2017	This study
Mn	0.0012	mM	24 Aug 2017	This study
Alkalinity	0.734	mM	2013-2014 (n=9)	Sullivan et al. (2016)
Cl^-	0.096	mM	2013-2014 (n=9)	Sullivan et al. (2016)
SO_4^{2-}	0.008	mM	2013-2014 (n=9)	Sullivan et al. (2016)
NO_3^-	0.003	mM	2013-2014 (n=9)	Sullivan et al. (2016)

Table S2: Most abundant bacterial genera (or higher classification if unresolvable) in DC0 groundwater based 16S rRNA amplicon gene sequencing

Phylum	Class	Order	Family	Genus	DC0.GWa	Rank Abundance	DC0.GWb	Rank Abundance
Proteobacteria	Betaproteobacteria	Methylophilales	Methylophilaceae		0.1321	1	0.0835	2
Proteobacteria	Gammaproteobacteria	Methylococcales	Crenotrichaceae	Crenothrix	0.0860	2	0.0441	8
Proteobacteria	Alphaproteobacteria	Caulobacterales	Caulobacteraceae		0.0539	3	0.0261	15
Firmicutes	Clostridia	Clostridiales	[Acidaminobacteraceae]	Acidaminobacter	0.0507	4	0.1055	1
Proteobacteria	Betaproteobacteria	Rhodocyclales	Rhodocyclaceae		0.0473	5	0.0509	4
Proteobacteria	Alphaproteobacteria	Rhodospirillales	Rhodospirillaceae		0.0458	6	0.0385	10
Proteobacteria	Betaproteobacteria	Burkholderiales	Comamonadaceae		0.0424	7	0.0395	9
Proteobacteria	Alphaproteobacteria	Rhodobacterales	Rhodobacteraceae	Rhodobacter	0.0356	8	0.0309	14
Bacteroidetes	[Saprospirae]	[Saprospirales]	Chitinophagaceae	Sediminibacterium	0.0331	9	0.0448	7
Proteobacteria	Deltaproteobacteria	Desulfuromonadales	Geobacteraceae	Geobacter	0.0319	10	0.0469	6
Proteobacteria	Betaproteobacteria	Burkholderiales	Comamonadaceae	Other	0.0305	11	0.0351	11
Bacteroidetes	Bacteroidia	Bacteroidales			0.0301	12	0.0315	13
Firmicutes	Clostridia	Clostridiales	Veillonellaceae	Pelosinus	0.0282	13	0.0610	3
Firmicutes	Clostridia	Clostridiales	Clostridiaceae	Clostridium	0.0253	14	0.0252	16
Spirochaetes	Spirochaetes	Spirochaetales	Spirochaetaceae	Treponema	0.0199	15	0.0474	5
Proteobacteria	Gammaproteobacteria	Enterobacteriales	Enterobacteriaceae		0.0175	16	0.0345	12
Actinobacteria	Actinobacteria	Actinomycetales	ACK-M1		0.0135	17	0.0163	19
Proteobacteria	Betaproteobacteria	Rhodocyclales	Rhodocyclaceae	Dechloromonas	0.0131	18	0.0026	38
Bacteroidetes	Bacteroidia	Bacteroidales	BA008		0.0129	19	0.0068	27
Proteobacteria	Alphaproteobacteria	Rhizobiales	Bradyrhizobiaceae		0.0128	20	0.0037	33
Proteobacteria	Deltaproteobacteria	Desulfovibrionales	Desulfovibrionaceae	Desulfovibrio	0.0096	21	0.0158	20
Firmicutes	Clostridia	Clostridiales	[Acidaminobacteraceae]	Fusibacter	0.0090	22	0.0198	18
Chlorobi	Ignavibacteria	Ignavibacteriales	[Melioribacteraceae]		0.0079	23	0.0216	17
OD1	ZB2				0.0078	24	0.0139	21
Proteobacteria	Gammaproteobacteria	Pseudomonadales	Pseudomonadaceae	Pseudomonas	0.0067	25	0.0004	89
Proteobacteria	Betaproteobacteria				0.0066	26	0.0023	42
Other	Other	Other	Other	Other	0.0065	27	0.0072	25
Proteobacteria	Betaproteobacteria	Rhodocyclales	Rhodocyclaceae	Sulfuritalea	0.0054	28	0.0044	32
Proteobacteria	Betaproteobacteria	Burkholderiales	Oxalobacteraceae	Janthinobacterium	0.0053	29	0.0018	46
Proteobacteria	Deltaproteobacteria	Myxococcales			0.0051	30	0.0027	37

Table S3: Most abundant bacterial genera (or higher classification if unresolvable) in DC0 *in situ* mineral deployments based 16S rRNA amplicon gene sequencing.

Phylum	Class	Order	Family	Genus	DC0.1	Rank Abundance	DC0.2	Rank Abundance	DC0.5	Rank Abundance	DC0.6	Rank Abundance
Proteobacteria	Deltaproteobacteria	Desulfuromonadales	Geobacteraceae	Geobacter	0.1200	1	0.1245	1	0.1250	1	0.1035	1
Nitrospirae	Nitrospira	Nitrospirales	[Thermodesulfovibrionaceae]	LCP-6	0.0620	2	0.0278	6	0.0587	3	0.0464	3
Firmicutes	Clostridia	Clostridiales	[Acidaminobacteraceae]	Fusibacter	0.0474	3	0.0760	3	0.0225	7	0.0476	2
Firmicutes	Clostridia	Clostridiales	Clostridiaceae	Clostridium	0.0298	4	0.0955	2	0.0887	2	0.0200	11
Nitrospirae	Nitrospira	Nitrospirales	[Thermodesulfovibrionaceae]	GOUTA19	0.0267	5	0.0108	16	0.0196	8	0.0229	8
Proteobacteria	Betaproteobacteria	Burkholderiales	Comamonadaceae		0.0259	6	0.0187	10	0.0332	4	0.0323	6
Nitrospirae	Nitrospira	Nitrospirales	[Thermodesulfovibrionaceae]		0.0204	7	0.0328	4	0.0173	10	0.0100	23
Proteobacteria	Betaproteobacteria	SBla14			0.0195	8	0.0076	29	0.0234	6	0.0346	5
Proteobacteria	Betaproteobacteria	Methylophilales			0.0177	9	0.0075	30	0.0182	9	0.0157	15
GN04	GN15				0.0170	10	0.0061	37	0.0100	23	0.0147	17
Acidobacteria	Holophagae	Holophagales	Holophagaceae		0.0161	11	0.0229	7	0.0126	15	0.0384	4
OP8	OP8_1	SHA-124			0.0155	12	0.0053	42	0.0124	17	0.0165	13
Chlorobi	Ignavibacteria	Ignavibacteriales	[Melioribacteraceae]		0.0152	13	0.0196	9	0.0090	24	0.0145	18
Proteobacteria	Deltaproteobacteria	Syntrophobacterales	Syntrophaceae		0.0145	14	0.0094	23	0.0139	14	0.0142	20
Proteobacteria	Deltaproteobacteria	Desulfovibrionales	Desulfovibrionaceae	Desulfovibrio	0.0142	15	0.0078	28	0.0113	20	0.0205	10
Nitrospirae	Nitrospira	Nitrospirales	FW		0.0139	16	0.0061	36	0.0104	22	0.0149	16
Spirochaetes	[Leptospirae]	[Leptospirales]	Sediment-4	SJA-88	0.0135	17	0.0057	39	0.0149	11	0.0078	33
Proteobacteria	Deltaproteobacteria	Desulfobacterales	Desulfobulbaceae	Desulfobulbus	0.0129	18	0.0138	13	0.0147	12	0.0214	9
Firmicutes	Clostridia	Clostridiales	Veillonellaceae		0.0128	19	0.0160	11	0.0079	29	0.0122	21
Proteobacteria	Betaproteobacteria	Rhodocyclales	Rhodocyclaceae		0.0127	20	0.0090	24	0.0142	13	0.0263	7
Proteobacteria	Betaproteobacteria	Gallionellales	Gallionellaceae	Gallionella	0.0118	21	0.0067	33	0.0105	21	0.0187	12
Proteobacteria	Alphaproteobacteria	Rhizobiales	Methylocystaceae	Methylosinus	0.0105	22	0.0066	34	0.0124	16	0.0116	22
Proteobacteria	Alphaproteobacteria	Rhizobiales	Bradyrhizobiaceae		0.0104	23	0.0130	14	0.0119	18	0.0099	24
Other	Other	Other	Other	Other	0.0100	24	0.0101	19	0.0075	31	0.0094	25
Chloroflexi	Ellin6529				0.0100	25	0.0042	55	0.0087	25	0.0084	29
Proteobacteria	Betaproteobacteria	Rhodocyclales	Rhodocyclaceae	Dechloromonas	0.0096	26	0.0097	20	0.0040	48	0.0161	14
Proteobacteria	Gammaproteobacteria	Methylococcales	Crenotrichaceae	Crenothrix	0.0091	27	0.0104	18	0.0083	26	0.0076	34
Proteobacteria	Alphaproteobacteria	Sphingomonadales	Sphingomonadaceae	Sphingomonas	0.0091	28	0.0055	40	0.0035	58	0.0050	44
Bacteroidetes	Bacteroidia	Bacteroidales			0.0088	29	0.0121	15	0.0056	40	0.0144	19
Proteobacteria	Alphaproteobacteria	Caulobacterales	Caulobacteraceae		0.0086	30	0.0088	26	0.0080	28	0.0093	26

Table S4: Abundance (log genomes per million reads) and putative taxonomy of the top 30 most abundant MAGs from *in situ* microcosms

Phylum	Class	Order	Family	Genus	DC0.1	Rank Abundance	DC0.2	Rank Abundance	DC0.5	Rank Abundance	DC0.6	Rank Abundance
Proteobacteria	Deltaproteobacteria	Desulfuromonadales	Geobacteraceae	Geobacter	0.1200	1	0.1245	1	0.1250	1	0.1035	1
Nitrospirae	Nitrospira	Nitrospirales	[Thermodesulfovibrionaceae]	LCP-6	0.0620	2	0.0278	6	0.0587	3	0.0464	3
Firmicutes	Clostridia	Clostridiales	[Acidaminobacteraceae]	Fusibacter	0.0474	3	0.0760	3	0.0225	7	0.0476	2
Firmicutes	Clostridia	Clostridiales	Clostridiaceae	Clostridium	0.0298	4	0.0955	2	0.0887	2	0.0200	11
Nitrospirae	Nitrospira	Nitrospirales	[Thermodesulfovibrionaceae]	GOUTA19	0.0267	5	0.0108	16	0.0196	8	0.0229	8
Proteobacteria	Betaproteobacteria	Burkholderiales	Comamonadaceae		0.0259	6	0.0187	10	0.0332	4	0.0323	6
Nitrospirae	Nitrospira	Nitrospirales	[Thermodesulfovibrionaceae]		0.0204	7	0.0328	4	0.0173	10	0.0100	23
Proteobacteria	Betaproteobacteria	SBla14			0.0195	8	0.0076	29	0.0234	6	0.0346	5
Proteobacteria	Betaproteobacteria	Methylophilales			0.0177	9	0.0075	30	0.0182	9	0.0157	15
GN04	GN15				0.0170	10	0.0061	37	0.0100	23	0.0147	17
Acidobacteria	Holophagae	Holophagales	Holophagaceae		0.0161	11	0.0229	7	0.0126	15	0.0384	4
OP8	OP8_1	SHA-124			0.0155	12	0.0053	42	0.0124	17	0.0165	13
Chlorobi	Ignavibacteria	Ignavibacteriales	[Melioribacteraceae]		0.0152	13	0.0196	9	0.0090	24	0.0145	18
Proteobacteria	Deltaproteobacteria	Syntrophobacterales	Syntrophaceae		0.0145	14	0.0094	23	0.0139	14	0.0142	20
Proteobacteria	Deltaproteobacteria	Desulfovibrionales	Desulfovibrionaceae	Desulfovibrio	0.0142	15	0.0078	28	0.0113	20	0.0205	10
Nitrospirae	Nitrospira	Nitrospirales	FW		0.0139	16	0.0061	36	0.0104	22	0.0149	16
Spirochaetes	[Leptospirae]	[Leptospirales]	Sediment-4	SJA-88	0.0135	17	0.0057	39	0.0149	11	0.0078	33
Proteobacteria	Deltaproteobacteria	Desulfobacterales	Desulfobulbaceae	Desulfobulbus	0.0129	18	0.0138	13	0.0147	12	0.0214	9
Firmicutes	Clostridia	Clostridiales	Veillonellaceae		0.0128	19	0.0160	11	0.0079	29	0.0122	21
Proteobacteria	Betaproteobacteria	Rhodocyclales	Rhodocyclaceae		0.0127	20	0.0090	24	0.0142	13	0.0263	7
Proteobacteria	Betaproteobacteria	Gallionellales	Gallionellaceae	Gallionella	0.0118	21	0.0067	33	0.0105	21	0.0187	12
Proteobacteria	Alphaproteobacteria	Rhizobiales	Methylocystaceae	Methylosinus	0.0105	22	0.0066	34	0.0124	16	0.0116	22
Proteobacteria	Alphaproteobacteria	Rhizobiales	Bradyrhizobiaceae		0.0104	23	0.0130	14	0.0119	18	0.0099	24
Other	Other	Other	Other	Other	0.0100	24	0.0101	19	0.0075	31	0.0094	25
Chloroflexi	Ellin6529				0.0100	25	0.0042	55	0.0087	25	0.0084	29
Proteobacteria	Betaproteobacteria	Rhodocyclales	Rhodocyclaceae	Dechloromonas	0.0096	26	0.0097	20	0.0040	48	0.0161	14
Proteobacteria	Gammaproteobacteria	Methylococcales	Crenotrichaceae	Crenothrix	0.0091	27	0.0104	18	0.0083	26	0.0076	34
Proteobacteria	Alphaproteobacteria	Sphingomonadales	Sphingomonadaceae	Sphingomonas	0.0091	28	0.0055	40	0.0035	58	0.0050	44
Bacteroidetes	Bacteroidia	Bacteroidales			0.0088	29	0.0121	15	0.0056	40	0.0144	19
Proteobacteria	Alphaproteobacteria	Caulobacterales	Caulobacteraceae		0.0086	30	0.0088	26	0.0080	28	0.0093	26

Table S5: Blastp hits to the hypothetical outer membrane protein (OM20) from the *Thiobacillus* strain used in the alignment to identify conserved domains (see figure 9)

Target NCBI accession number	% Identity	Alignment length	evalue	bit score	%positives
WP_124704254.1	73.502	317	1.92E-147	427	83.28
OYY47200.1	53.182	220	4.33E-66	222	67.27
WP_027457713.1	40.952	315	3.52E-58	199	57.14
WP_027457713.1	40.952	315	3.52E-58	199	57.14
KAB2928174.1	39.721	287	2.14E-50	179	58.19
AAZ48141.1	41.489	282	1.35E-47	172	58.16
KPK07657.1	40.664	241	3.44E-43	166	56.43
WP_059420635.1	38.415	328	1.00E-38	150	50.3
OGA66848.1	41.564	243	1.12E-38	154	53.91
SBT07738.1	39.844	256	8.17E-37	144	55.86
OGV73905.1	37.572	346	1.28E-36	144	48.55
HBA90777.1	38.095	294	1.66E-35	142	51.02
OGA70656.1	37.179	234	4.19E-35	144	56.84
HCV13277.1	35.831	307	4.50E-35	139	47.88
EXI65891.1	35.831	307	5.43E-35	139	47.88
WP_109014866.1	36.533	323	3.17E-33	135	49.23
TLD46298.1	35.048	311	5.02E-33	134	48.23
TLD46298.1	35.048	311	5.02E-33	134	48.23
PIX76149.1	40.789	228	1.51E-32	134	55.26
OGA07483.1	39.474	228	1.56E-32	134	55.7
OJW51632.1	36.577	298	2.66E-32	132	49.33
OIP10414.1	40.789	228	2.87E-32	134	55.26
WP_009206639.1	34.627	335	3.51E-32	133	45.97
OGT30091.1	36.364	231	4.30E-32	137	54.98
TMH47248.1	37.443	219	9.11E-32	135	54.34
OGS90635.1	38.095	252	1.12E-31	131	55.16
TSA49167.1	34.713	314	1.50E-31	131	50.64
HCA27896.1	39.738	229	1.79E-31	134	58.08
KFB66439.1	35.959	292	7.29E-31	128	51.37
TMH90698.1	40.306	196	7.30E-31	132	55.61
OGA31856.1	39.344	244	1.86E-30	131	53.69
RPJ47870.1	38.683	243	7.67E-30	127	51.03
WP_124948748.1	36.842	247	1.25E-29	125	54.25
OGS81224.1	34.818	247	1.46E-29	127	51.82
EXI65219.1	35.913	323	2.13E-29	124	47.99
WP_138677328.1	35.714	294	2.48E-29	124	51.02
TMQ78494.1	35.154	293	2.50E-29	125	50.51
KFB78475.1	35.354	297	4.43E-29	124	49.16
KXS33488.1	39.035	228	8.17E-29	126	53.51
OGS99736.1	39.382	259	4.87E-28	123	51.74
TMH29402.1	39.796	196	5.96E-28	118	52.04
PZP62728.1	39.526	253	5.15E-27	121	53.75
PZP62728.1	30.464	151	8.3	40.4	46.36
SBT08220.1	35.385	325	1.42E-26	117	48.62
OGA29479.1	38.776	245	2.49E-26	119	53.88
OFZ95027.1	38.776	245	2.64E-26	119	53.88

OGA70520.1	38.776	245	2.69E-26	119	53.88
WP_147798944.1	39.526	253	7.97E-26	118	53.75
WP_147798944.1	30.464	151	8.7	40.4	45.7
WP_087447985.1	31.627	332	1.56E-25	114	46.99
TNC96997.1	31.449	283	2.03E-25	116	49.82
OGB99399.1	39.091	220	2.59E-25	115	49.09
OGS93970.1	32.927	246	2.62E-25	115	51.22
EXI81860.1	35.017	297	6.21E-25	112	47.47
PPC93348.1	34.177	237	6.54E-25	114	51.48
KPK15849.1	38.356	219	8.99E-25	114	52.97
TMH99633.1	33.613	238	1.83E-24	110	50.42
OGS74972.1	32.645	242	5.99E-24	112	52.07
MPZ47615.1	40	210	6.12E-24	110	49.05
TAK41967.1	37.089	213	6.86E-24	112	51.64
WP_132970794.1	33.065	248	2.28E-23	109	47.58
TAH46322.1	35.47	234	2.46E-23	109	51.28
OFZ65775.1	33.333	291	3.16E-23	110	46.74
TXT29090.1	32.83	265	4.11E-23	110	47.17
OFZ66657.1	33.992	253	5.25E-23	108	52.96
WP_132920971.1	31.132	318	5.72E-23	108	43.71
OGT14318.1	30.061	326	5.84E-23	109	44.79
TCV80075.1	31.132	318	1.11E-22	108	43.71
RPI46686.1	28.247	308	2.21E-22	107	45.78
TMH60946.1	40.212	189	8.44E-22	106	55.03
RME34772.1	37.607	234	1.42E-21	105	51.71
OHC81517.1	36.364	231	1.55E-21	105	51.95
TSA15772.1	34.4	250	3.56E-21	105	49.2
WP_072428345.1	32.661	248	3.97E-21	103	50
OFZ87631.1	37.395	238	4.09E-21	104	55.04
OGS99320.1	33.333	258	5.19E-21	103	49.61
TXT27004.1	30.769	273	5.49E-21	103	48.72
HAJ71988.1	30.315	254	1.01E-20	101	50
OYY06174.1	38.496	226	1.75E-20	100	52.65
PKO94673.1	37.395	238	2.13E-20	103	51.68
HAF00572.1	30.315	254	2.34E-20	101	50
OAI50344.1	31.481	270	2.40E-20	102	47.41
TLS18815.1	33.2	250	2.99E-20	102	50
OGA50514.1	34.513	226	3.19E-20	102	50
RKZ44291.1	31.557	244	3.64E-20	102	50
WP_014236484.1	33.2	250	4.96E-20	102	50
WP_152090542.1	33.2	250	7.29E-20	101	50
TAJ91442.1	32.609	230	8.09E-20	101	50.87
HCC53608.1	31.6	250	8.35E-20	101	48.8
OGA08024.1	32.389	247	9.92E-20	100	51.01
WP_091197656.1	32.963	270	1.14E-19	99.8	47.78
WP_028455227.1	28.814	295	1.91E-19	99	44.41
WP_121242663.1	35.918	245	2.17E-19	100	49.8
WP_130460154.1	33.6	250	2.87E-19	99.8	50.4
WP_109039567.1	29.795	292	5.37E-19	99	42.81
TMH83391.1	34.764	233	5.41E-19	98.6	46.35
SFZ76001.1	35.455	220	5.49E-19	98.6	49.55

WP_095524992.1	33.498	203	7.01E-19	97.1	48.28
EKD99148.1	35.021	237	7.37E-19	98.6	50.63
WP_095530115.1	33.498	203	1.16E-18	96.3	48.28
WP_130106331.1	30.075	266	3.68E-18	95.9	45.49
PCI82427.1	28.939	311	7.84E-18	93.2	44.69

Table S6: Blastp hits to the hypothetical extracellular protein adjacent to OM20 from the *Thiobacillus* strain used in the alignment to identify conserved domains (see Fig. 9)

Target NCBI accession number	% Identity	Alignment length	evalue	bit score	%positives
WP_124704253.1	73.705	251	4.73E-129	375	83.67
GBL45435.1	74.731	186	1.40E-95	287	84.95
WP_147070006.1	57.851	242	3.23E-84	261	72.73
WP_147070006.1	57.851	242	3.23E-84	261	72.73
AKU24756.1	44.398	241	5.09E-60	199	61.83
WP_050408182.1	44.398	241	5.14E-60	199	61.83
TDI81398.1	46.281	242	3.40E-59	197	64.46
WP_117010235.1	44.223	251	3.84E-59	196	62.95
WP_093557759.1	44.49	245	9.69E-59	196	60.41
WP_020706449.1	44.444	252	1.08E-58	195	63.49
HAT31414.1	44.583	240	2.50E-58	194	62.5
WP_107872471.1	45.417	240	2.58E-58	194	62.92
WP_070361541.1	45.418	251	3.84E-58	194	62.15
TCQ47998.1	45.643	241	8.01E-58	193	63.49
WP_132136935.1	45.643	241	9.50E-58	193	63.49
WP_116990984.1	44.048	252	1.13E-57	193	62.3
WP_057154682.1	45.417	240	3.40E-57	192	62.08
MQA23704.1	43.6	250	4.77E-57	191	61.6
WP_076571039.1	45.02	251	9.38E-57	191	61.35
WP_008447822.1	44.622	251	2.33E-56	189	61.35
WP_065309137.1	44.355	248	2.84E-56	189	60.08
WP_035819700.1	44.4	250	3.50E-56	189	62
WP_106758036.1	43.902	246	3.55E-56	189	60.98
WP_099417734.1	45.417	240	3.89E-56	189	59.17
WP_092799983.1	45.833	240	4.06E-56	189	61.25
WP_034755300.1	45.161	248	4.30E-56	189	60.89
WP_141169841.1	43.548	248	4.88E-56	189	60.48
WP_072453272.1	45.161	248	7.24E-56	188	60.89
WP_099377539.1	45.161	248	7.40E-56	188	61.29
WP_099403081.1	45.643	241	7.56E-56	188	63.07
WP_135208752.1	44.167	240	8.56E-56	188	61.25
WP_058049959.1	43.902	246	9.19E-56	188	61.79
WP_071323173.1	45.228	241	1.15E-55	188	61.83
WP_124946866.1	44.939	247	1.21E-55	187	64.78
WP_099376148.1	45	240	1.46E-55	187	61.67
WP_145879739.1	42.449	245	1.67E-55	187	60
WP_128142804.1	43.2	250	1.76E-55	187	60.8
WP_152259652.1	44.223	251	1.87E-55	187	60.56
WP_139089609.1	43.2	250	2.14E-55	187	60.8
WP_100427572.1	45.565	248	2.18E-55	187	60.48
WP_099411444.1	45.643	241	3.10E-55	187	61.83
WP_152283525.1	43.825	251	4.36E-55	186	60.96
WP_142303431.1	46	250	4.61E-55	186	60.4
WP_102123041.1	46.473	241	4.66E-55	186	61.83
WP_101481758.1	45.417	240	7.42E-55	186	62.08
WP_152254571.1	44.444	243	9.63E-55	186	61.73

WP_086148553.1	44.583	240	1.05E-54	185	61.25
WP_102299577.1	44.583	240	1.10E-54	185	61.25
WP_121669847.1	45.228	241	1.27E-54	185	61.83
WP_094445096.1	45.041	242	1.31E-54	185	59.92
WP_094445096.1	45.041	242	1.31E-54	185	59.92
WP_093388731.1	44.939	247	1.33E-54	185	59.11
WP_070222891.1	45.122	246	1.53E-54	185	60.57
WP_056391934.1	43.75	240	1.79E-54	184	61.67
WP_070304932.1	43.6	250	1.87E-54	184	60.4
TFH07555.1	42.975	242	2.32E-54	185	63.22
WP_070291216.1	45	240	2.51E-54	184	61.67
WP_152241616.1	43.333	240	2.66E-54	184	60
WP_092605497.1	44.628	242	5.73E-54	183	61.16
WP_051780580.1	41.909	241	5.92E-54	183	63.07
WP_017875233.1	42.52	254	6.79E-54	183	59.84
CDG82736.1	41.909	241	8.02E-54	183	63.07
TDI74009.1	43.933	239	8.03E-54	183	62.34
WP_057265073.1	42.149	242	8.25E-54	183	60.74
WP_137312592.1	40.964	249	1.11E-53	182	59.44
WP_086140994.1	43.902	246	1.15E-53	182	59.76
WP_090442122.1	41.322	242	1.39E-53	182	60.33
WP_130314345.1	41.322	242	2.14E-53	182	61.16
WP_070281979.1	44.262	244	2.15E-53	182	61.07
WP_099393986.1	44.262	244	2.79E-53	182	61.07
WP_055926632.1	41.736	242	4.06E-53	181	61.98
WP_070256776.1	44.262	244	4.26E-53	181	61.07
WP_034781084.1	43.852	244	4.79E-53	181	61.07
WP_077405867.1	43.478	253	7.36E-53	181	59.68
WP_054267795.1	41.7	247	9.72E-53	180	58.7
WP_099667511.1	43.21	243	2.59E-52	179	61.32
WP_099879746.1	41.7	247	7.45E-52	178	59.11
WP_099879746.1	41.7	247	7.45E-52	178	59.11
WP_056154771.1	42.629	251	7.51E-52	178	58.17
WP_090185174.1	40.562	249	1.09E-51	177	57.03
OFZ69886.1	42.966	263	1.87E-51	178	59.32
WP_028102466.1	42.083	240	3.69E-51	176	61.25
WP_145647222.1	41.25	240	1.61E-50	175	60.42
WP_090319726.1	41.833	251	1.88E-50	174	56.57
WP_092270027.1	41.079	241	1.95E-50	174	58.51
WP_110847589.1	41.079	241	2.17E-50	174	58.51
WP_130189784.1	40.417	240	3.35E-50	174	58.75
WP_126073445.1	41.909	241	3.80E-50	174	57.68
WP_047551922.1	42.5	240	4.03E-50	173	60
WP_056148409.1	40.8	250	4.41E-50	173	58
WP_019920702.1	40.161	249	9.30E-50	172	57.83
HCA27895.1	45	240	1.41E-49	172	62.08
MPQ57525.1	40	250	2.41E-49	171	58
WP_116533185.1	40.856	257	3.15E-49	174	57.98
WP_072787408.1	40.249	241	6.09E-49	171	58.51
WP_070251853.1	40.496	242	1.92E-48	169	59.09
PPC93347.1	42.623	244	2.86E-48	169	61.48

WP_147951821.1	39.516	248	2.76E-47	166	60.48
WP_112937212.1	39.516	248	2.88E-47	166	60.48
HAF00571.1	43.568	241	4.10E-47	165	59.75

Table S7: Total sulfate release and polythionate accumulation in abiotic reactors, and their respective ratio

	Initial sulfate (mM)	Final sulfate (mM)	Total sulfate released (mM)	Initial polythionates (mM)	Final polythionates (mM)	Total polythionate accumulation (mM)	Sulfate: polythionate accumulation
Sand Only Buffered							
Control + Py	0.098	2.466	2.369	0.0041	0.1007	0.097	24.524
Sand Only Unbuffered							
Control +Py	0.084	2.251*	2.167	0.0363	0.0713*	0.035	61.914
Sand +Shale Buffered							
Control +Py	0.117	0.722	0.605	0.1147	0.1553	0.041	14.901
Sand +Shale Unbuffered							
Control +Py	0.125	0.921	0.796	0.1651	0.2015	0.036	21.868

*Day 126 value used for calculation as the final polythionate concentration was below initial value

Chapter 3

The weathering microbiome of an outcropping granodiorite

Stephanie A. Napieralski[1*] and Eric E. Roden[1]

[1]Department of Geoscience, University of Wisconsin-Madison, Madison WI 53706

[*]Corresponding author email: snapieralski@wisc.edu

Running Title: The Weathering Microbiome

In preparation for submission to Applied and Environmental Microbiology

Abstract

Microorganisms have long been recognized for their capacity to catalyze the weathering of silicate minerals. While the vast majority of studies on terrestrial silicate weathering focus on heterotrophically based mechanism of mineral weathering for nutrient acquisition, it has been recently demonstrated that lithotrophic iron oxidizing bacteria (FeOB) are capable of coupling the oxidation of silicate mineral Fe(II) to metabolic energy generation and cellular growth. However, in natural systems complex microbial consortia can exist and interact to influence biogeochemical cycles. Here we combine microbiological and metagenomic analyses to investigate the potential interactions amongst metabolically diverse microorganisms in the near surface weathering of an outcrop of the Rio Blanco Quartz Diorite (DIO) in the Luquillo Mountains of Puerto Rico. Laboratory based lithotrophic incubations utilizing ground DIO as metabolic energy source of lithotrophic iron oxidizing bacteria (FeOB) further confirmed our previous study on the ability of FeOB to grow via the oxidation of silicate-bound Fe(II). Dramatically accelerated rates of Fe(II)-oxidation were associated with an enrichment for microorganisms with the genetic capacity for extracellular electron transfer (EET). After a period of lithotrophic oxidation and supplementation with glucose, microbially oxidized DIO displayed an enhanced susceptibility to the weathering activity of heterotrophic microorganisms compared to unoxidized mineral suspensions. We conclude that chemolithotrophic and heterotrophic microorganism can coexist and contribute to the overall weathering of the bedrock outcrop.

Importance

We utilized an outcrop of the Rio Blanco Quartz Diorite to investigate the potential for *in situ* interactions between chemolithotrophically and heterotrophically driven modes of biogeochemical weathering. A previous study on the subsurface microbial weathering of the Rio Blanco Quartz Diorite recently demonstrated that chemolithotrophic Fe(II)-oxidizing bacteria (FeOB) can utilized mineral-derived Fe(II) as a source of metabolic energy. The associated redox driven mineralogical changes rendered the Fe(II)-minerals more susceptible to proton promoted dissolution via dilute acid. Here we demonstrate that prior Fe(II) oxidation by FeOB also increases the efficiency at which heterotrophic microorganisms can solubilize cations from Fe(II)-silicates. We conclude that chemolithotrophic FeOB and heterotrophic microorganisms can coexist and outline potential *in situ* metabolic interactions that are likely contribute to the weathering of bedrock in the presence of organic carbon inputs.

Introduction

The weathering of Earth's continental crust involves a complex set of physical, geochemical and biological reactions. As microorganisms are ubiquitous in soils and sedimentary environments, often preferentially associated with mineral surfaces (Hazen et al., 1991) they have vast potential to enhance mineral weathering thus impacting the cycling of bioessential elements between the lithosphere and the biosphere. Microbiological impacts on the weathering processes, from the aid in physical disaggregation by mechanical forcing to enhanced chemical dissolution has long been recognized and is extensively described (Banfield et al., 1999; Uroz et al., 2009). Well established mechanisms of microbially enhanced mineral dissolution revolve around heterotrophic metabolisms, where microorganisms solubilize mineral components to meet their nutritional needs for conveyance of a growth benefit (Bennett et al., 2001) and provide valuable

ecosystem services for higher biota (Calvaruso et al., 2006; Lambers et al., 2009). Acidolysis and chelation by organic acids (Drever and Stillings, 1997; Uroz et al., 2009) as well as siderophores (Buss et al., 2007; Kalinowski et al., 2000; Liermann et al., 2000) have been extensively invoked when relating microbial activity to mineral weathering.

Redox active elements, such as Fe, are often a major component of igneous rocks. If Fe constituents a considerable component of the mineral structure, redox reactions can occur prior to bulk dissolution if the kinetics of electron transfer are faster than structural disintegration (White, 1990). The oxidation of Fe(II) is in fact often rate limiting in terms of Fe(II) mineral weathering (Hering and Stumm, 1990). Fe(II) silicates in fresh rock, in disequilibrium with Earth's oxidizing surficial environment, represent a vast supply of electrons to potentially fuel microbial metabolism and growth. Chemolithotrophic Fe(II)-oxidizing bacteria (FeOB) are known to occupy distinct environmental niches where opposing gradients of ferrous iron [Fe(II)] and oxidants (e.g. O_2) intersect, such as freshwater iron seeps and hydrothermal vents (Emerson et al., 2010). By analogy, the interface between reduced igneous rock and the oxidizing atmosphere represents such a gradient, albeit a very sharp, solid phase one, that theoretically can provide energy to fuel biomass production (Buss et al., 2005; Jakosky and Shock, 1998; Shock, 2009). While studies have suggested that FeOB are capable of direct utilization of the structural Fe(II) in silicate minerals (Popa et al., 2012; Shelobolina et al., 2012b) and glasses (Bailey et al., 2009; Henri et al., 2015), only recently has the ability of FeOB to utilize crystalline silicate-bound Fe(II) for metabolic energy generation and subsequent growth been demonstrated (Napieralski et al., 2019). By combining microbiological and metagenomic based approaches, we demonstrated that FeOB can dramatically accelerate the oxidation of silicate mineral bound Fe(II) via extracellular electron transfer (EET) coupled to cellular growth, and that the

subsequent oxidative weathering of the minerals biotite and hornblende by within granitic rocks resulted in subtle changes to the surface structure that rendered the mineral more susceptible to proton promoted dissolution via dilute acid. While not explicitly demonstrated, the redox driven mineralogical transformations associated with FeOB activity should also affect the efficiency at which heterotrophic microorganisms are able to solubilize cations for nutritional purposes.

It is important to consider the entire suite of biogeochemical reactions that may be mediated by complex microbial communities in natural systems. Our previous work specifically investigated the role of chemolithotrophic FeOB in the subsurface (ca. 8 m) weathering of the Rio Blanco Quartz Diorite (Napieralski et al., 2019), well below the rooting zone where organic carbon content is minimal. In contrast, the near surface, where inputs from plant derived organic matter are substantial, a more complex interplay between heterotrophically and lithotrophically mediated processes may be involved in the weathering of Fe(II)-silicates. In order to address this potential interplay, samples were collected for enrichment culturing and metagenomic analysis from near-surface outcrop of the rapidly weathering Rio Blanco Quartz Diorite of the Luquillo Mountains, Puerto Rico (Buss et al., 2008) (Figure 1). After establishment, Fe(II)-silicate oxidizing enrichment cultures were amended with additional carbon to assess the degree to which prior lithotrophic activity might enhance the cation solubilizing ability of heterotrophic microorganisms.

Materials and Methods

Field sampling

In June of 2017, samples were collected from a road cut exposure of the Rio Blanco Quartz Diorite (abbreviated hereafter as “DIO”) previously described by Buss and colleagues (2008)

(See Figure 1). Rindlets nearest the weathering corestone were carefully excavated using a rock hammer and spatula, previously sterilized by ethanol soaking and flame, and placed into sterile Whirlpack bags. Samples were then placed in coolers and shipped overnight to The University of Wisconsin-Madison where portions were promptly placed at -80°C and 4°C for DNA extraction and enrichment culturing, respectively.

Chemolithotrophic enrichment culturing

Chemolithotrophic Fe(II)-oxidizing cultures were established as previously described with DIO and Fe(II)-free quartz sand (QTZ) (Napieralski et al., 2019). Briefly, 5.0 g of ground and sieved (<45 µM) DIO or quartz sand (Acros Chemicals 140-381 µm) were added to 50 mL of Luquillo artificial ground water (L-AGW), autoclaved anoxically, and aerated with sterile air. 5 v/v% CO_2 was added to the headspace and the appropriate bottles were inoculated with ca. 1.0 g of material from the DIO outcrop that had been aseptically fragmented. No mineral amendment controls were also prepared by adding ca. 1.0 g of inocula to 50 mL of L-AGW without additional minerals (NoMin). Samples were taken immediately following inoculation and at 41, 82, 105,130,182,252,334 and 615 days for analyses as described below.

Heterotrophic incubations

After 615 days of initial chemolithotrophic incubation, 5.0 mL of DIO from one replicate (to ensure consistency of substrate) of both live inoculated and abiotic control reactors was removed and the solids separated via centrifugation. The aqueous phase was discarded, and the solids were resuspended in 40 mL of fresh L-AGW. The resultant slurry was equally divided among 2 fresh, sterilized bottles to generate duplicate reactors of DIO-Ox+Gluc-Inoc and DIO-Cont+Gluc-Inoc reactors. Reactors were reseeded with ca. 0.1 g of DIO outcrop material and 1.0

mM filter sterilized glucose was added to each. As an abiotic control, 5.0 mL of the second replicate of the abiotic control from the chemolithotrophic incubations was similarly prepared in fresh L-AGW with glucose but was left uninoculated (DIO-Cont+Gluc-Sterile). Samples were taken at T_0, and after 1,3,14,28 and 60 days of incubation for the analyses described below.

Analytical methods

ATP: ATP content of enrichment cultures was determined via luminescence using BacTiter-Glo^{TM} (Promega, Madison WI) as previously described (Napieralski et al., 2019). **Solid-phase Fe(II):** The ratio of Fe(II) to total Fe released by 0.5 M HCl extraction was determined on the solid phase of 1.0 mL of total enrichment culture subsamples. The solids were separated via centrifugation and extracted for 24 hours in 5 mL of 0.5 M HCl on an orbital shaker. Fe(II) of each extract was determined by the standard Ferrozine assay (Stookey, 1970) and the measurement was repeated after the addition of hydroxylamine-HCl for determination of Fe(total). **Cations:** The aqueous phase from duplicate reactors was pooled, diluted 1:5 in 5 mM HNO_3 and filtered through a 0.22 µm filter. Major cation concentrations (Ca, K, Mg, Na) were determined using inductively coupled plasma optical emission spectroscopy (ICP-OES).

DNA extraction, metagenomic sequencing and assembly

DNA was extracted from duplicate outcrop (Gb-OC) and 182 day enrichment culture material (DIO-Inoc QTZ-Inoc and NoMin-Inoc) utilizing previously described (Napieralski et al., 2019) adaptations to the SDS-based DNA extraction method of Zhou and colleagues (Zhou et al., 1996). DNA was submitted to the University of Wisconsin-Madison Biotechnology Sequencing Center for shotgun metagenomic library preparation and 2x250 sequencing on the Illumina HiSeq 2500 rapid platform. Raw reads were quality filtered using the default parameters Trim-

Galore. Concatenated reads from all samples were assembled using IDBA-UD (Peng et al., 2012) utilizing the high-performance computing cluster at the Center for High Throughput Computing at University of Wisconsin-Madison.

Metagenomic analysis

Metagenome assembled genomes (MAGs) were obtained from the metagenomic coassembly using the Bin Refinement module of metaWRAP (Uritskiy et al., 2018) with initial bin sets generated using MetaBat2 (Kang et al., 2019) and Concoct (Alneberg et al., 2014). Quality, completion and initial taxonomy of refined MAGs were assessed using CheckM (Parks et al., 2015). Final consensus taxonomy of MAGs was determined using the Classify Bins module of metaWRAP and extraction of essential single-copy genes as described by He et al. (2016) for each MAG. The relative abundance of each MAG (genomes per million reads) across all samples in the coassembly was determined using the Bin Quantification module of metaWRAP. Open reading frames (ORFs) were predicted and annotated using Prokka (Seemann, 2014). Subcellular location of putative proteins was predicted using Cello (Yu et al., 2006). Putative extracellular electron transfer (EET) pathways for iron oxidation were identified as previously described (He et al., 2017) using BLASTP and HMMsearch for homologs to the Cyc2-type system of *Acidithiobacillus ferrooxidans* (Castelle et al., 2008) and MtoAB of *Sideroxydans lithotrophicus* ES-1 (Liu et al., 2012). Putative siderophore biosynthesis pathways were identified using HMMsearch for the PFAMs associated with non-ribosomal peptide synthesis (NRPS) condensation and adenylation domains as well as the conserved IucAC domains of NPRS-independent synthesis (NIS) (Hopkinson and Barbeau, 2012). Selected MAGs were investigated for the presence of carbohydrate active enzymes using the dbCAN webserver (Yin et al., 2012).

Results

Initial chemolithotrophic incubation

Over the course of the 615-day chemolithotrophic incubation, Fe(II)/Fe(total) declined from an average of 0.857 to 0.664 in the live DIO reactors; no systematic change in Fe(II)/Fe(total) was observed in sterile, abiotic controls (Figure 2A). The ATP content of all inoculated reactors decline precipitously from initial values of ca. 1.3 nM over the first 130 days of incubation (Figure 2B). In DIO cultures, ATP content stabilized at an average of ca. 0.6 nM for the duration of the experiment, whereas ATP continued to decline to ca. 0.13 and 0.15 nM in QTZ and NoMin (inoculum only) cultures, respectively. No net change in background ATP (abiotic control) was observed.

The release of major rock forming cations (Ca, Mg, K and Na) was detected in all DIO amended reactors (Figure 3). Both Ca and Na concentrations showed a modest increase in net release in inoculated reactors relative to sterile abiotic controls (Figure 3A,B). Final Ca concentrations reached 0.124 and 0.160 mM in control and live inoculated reactors, respectively corresponding to increases in concentration of 0.050 and 0.091 mM Ca over the course of the experiment. Final Na concentrations increased to 0.288 and 0.326 mM in the control and live reactors, respectively. Thus, 0.041 and 0.037 mM more Ca and Na, respectively, was released in the presence of a live inoculum relative to sterile controls. Ca and Na release was also detected in the inoculum only NoMin reactors, indicating release from DIO in the inoculum. No difference in Mg concentration between control and live reactors was observed, nor was there any release of Mg in NoMin reactors (Figure 3C). K release was also not detected in NoMin reactors, and in contrast to Ca and Na, overall release of K was higher in abiotic reactors relative to live

inoculated (Figure 3D), with 0.06 mM more K released in abiotic reactors over the course of the experiment.

Heterotrophic incubation

Addition of glucose to stimulate heterotrophic metabolism after imposed chemolithotrophic conditions resulted in immediate cell growth, with ATP increasing to 6-7 nM in live reactors after 1 day (Fig. 4B). After initial growth, ATP content of the reactors declined over the remaining 60 days to an average final concentration of ca. 1.1 nM. Small changes were observed in Fe(II)/Fe(tot) for both glucose amended reactor sets, declining from an average of 0.664 to 0.633 in live cultures containing microbially oxidized DIO from the previous chemolithotrophic enrichment culture (DIO-Ox+Gluc-Inoc), and from an average of 0.829 to 0.794 in live cultures containing unoxidized DIO from previous abiotic controls (DIO-Cont+Gluc-Inoc) (Figure 4A). No oxidation was observed in the glucose-amended abiotic control (DIO-Cont+Gluc-Sterile) containing DIO from previous abiotic controls.

The release of all cations was stimulated in live cultures containing both previously oxidized and unoxidized DIO relative to unoxidized abiotic controls (Figure 5). Average final concentrations and total release of Ca and Mg were slightly higher (ca. 0.04 mM) in live cultures containing previously oxidized DIO compared to unoxidized (Figure 5A,C). The opposite trend was observed in K release, with final K concentrations being an average of 0.040 mM higher in DIO-Cont+Gluc-Inoc reactors (Figure 5D). Final average Na concentrations overlapped within the error of the replicates, though an average of 0.022 mM more Na was released in DIO-Cont+Gluc-Inoc vs. DIO-Ox+Gluc-Inoc reactors (Figure 5B).

Metagenomic analysis

A total of 84 MAGs (>70% complete, <10% redundant) were obtained from the metagenomic coassembly. Of the 84 MAGs, 12 contained homologs to EET pathways putatively involved in Fe(II) oxidation, with 9 MAGs containing Cyc2 homologs, 3 containing MtoAB, and one containing both. Of these putative FeOB, 5 also contained RuBisCO (Figure 6). In reactors amended with DIO, putative chemolithotrophic FeOB are enriched relative to the *in situ* samples and diorite free (NoMin and QTZ) reactors (Figure 6). The most abundant MAG in each replicate of the diorite oxidizing cultures was a putative chemolithoautotrophic γ-proteobacteria, most closely affiliated with the family *Acidiferrobacteraceae*. However, each replicate was dominated by a different *Acidiferrobacteracea*e MAG. While the most abundant MAG in DIO-OC-A contained homologs to both Cyc2 and MtoAB, the dominant MAG in DIO-OC-B contained only Cyc2. Putative siderophore biosynthesis pathways were identified in 9 MAGs (Figure 6). Compared to the diorite oxidizing enrichment cultures, MAGs containing putative siderophore biosynthesis pathways are overall more abundant *in situ.*

The 2 most abundant MAGs in both *in situ* libraries is a Sphignobacteriaceae, putatively of the genus *Mucilaginibacter* (Figure 6). In addition to containing a putative NRPS-type siderophore biosynthesis pathway, the *Mucilaginibacter* MAGs are enriched in carbohydrate active enzymes, particularly glycosyltransferases and glycoside hydrolases. Also abundant are β-proteobacteria, with 4 of the top 10 most abundant MAGs in both *in situ* metagenomes belonging to the β-proteobacteria, 3 of which to the order Burkholderiales. In addition, 2 of the top 10 MAGs contain putative EET pathways but did not contain RuBisCO or other carbon fixation pathway, an MtoAB in a β-proteobacteria and Cyc2 in a Nitrospiraceae.

Discussion

Initial chemolithotrophic incubations

The results of this study confirm the previously reported (Napieralski et al., 2019) ability of chemolithotrophic microorganisms from the Rio Blanco quartz diorite weathering environment to catalyze oxidation of Fe(II)-silicate phase in fresh rock (Figures 2A and 4A). In contrast to our previous findings, biologically enhanced release of Ca and Na was observed during initial chemolithotrophic incubation under all experimental conditions, including during incubation of endogenous DIO in the inoculum. Our 2019 study on the potential role of FeOB in DIO weathering utilized inocula from the subsurface rindlet-saprolite interface, well below the rooting zone where organic carbon content is very low (Buss et al., 2005). As such, transfer of labile organics and actively metabolizing heterotrophic cells upon inoculation of enrichment cultures was likely to have been limited. The present study is thus fundamentally different in that the initial inoculum was obtained from a surficially exposed outcrop with visible roots and vegetation (see Figure 1), and organic matter was undoubtably transferred into the enrichment cultures upon inoculation. While it is well established that in the presence of organic carbon amendments microorganisms can enhance the release of major rock forming cations (Frey et al., 2010; Wu et al., 2008), similar results have also been noted in a study of granitic gneisses and diorites incubated with only natural sediment and glacial waters without carbon or other nutrient amendment (Montross et al., 2013). These results indicate that even small amounts of naturally derived organic carbon are capable of supporting microbially enhanced mineral dissolution.

Due to the input of carbon and active heterotrophic biomass in the inoculum, we are presently unable to directly link oxidation of the DIO to FeOB growth. ATP concentrations

declined over time in all inoculated (Figure 2), which suggests that microbial growth coupled to Fe(II) oxidation was insufficient to compensate for the decline in heterotrophic biomass initially present in the inoculum. These results are consistent with a recent study utilizing microbially colonized shale for the establishment of chemolithotrophic pyrite-oxidizing enrichment cultures (Napieralski et al., 2020). Nevertheless, the rate and extent of the decline in ATP concentration was lower in reactors amended with DIO compared to those without added DIO (QTZ and NoMin; see Figure 2), suggestive of ATP generation linked to chemolithotrophic metabolism. The final "steady-state" ATP concentration of ca. 0.6 nM observed here is comparable to that reported by Napieralski and colleagues (2019) in the previous study on the chemolithotrophic oxidation of the DIO, where growth yield calculations were consistent with previously reported for yields for FeOB in opposing gradient media (Sobolev and Roden, 2004). Thus, the accelerated oxidation of mineral-associated Fe(II) (Figure 2) and presence and enrichment of multiple MAGs containing Fe(II)-oxidizing EET systems (Figure 6) is consistent with the growth of chemolithotrophic FeOB in the present study.

Putative chemolithotrophic pathways

In both replicates of the diorite oxidizing enrichment cultures, the most abundant MAG belongs to the family *Acidiferrobacteraceae* (Figure 6) and contains a Cyc2 homolog. The family *Acidiferrobacteraceae* is currently described as harboring acidiphilic Fe and S oxidizers (Issotta et al., 2018), as well as neutrophilic S oxidizers (Kojima et al., 2015; Kojima et al., 2016). Members of the genus *Acidiferrobacter* encompassing the acidophilic FeOB have been shown to contain homologs to Cyc2 as well as rusticyanin (Issotta et al., 2018), an acid-stable copper protein utilized by *Acidithiobacillus ferrooxidans* for electron transfer during Cyc2 dependent Fe(II)oxidation (Castelle et al., 2008), but not present in neutrophilic FeOB genomes

(Barco et al., 2015; He et al., 2017; McAllister et al., 2019). Rusticyanin homologs were not identified in any of the *Acidiferrobacteraceae* MAGs obtained in this study. While there are currently no described neutrophilic FeOB within the *Acidiferrobacteraceae*, Meier and colleagues (2019) identified 16S rRNA gene sequences related to *Acidiferrobacteraceae* as being potentially involved in soil formation at a site selected to be free of influence of sulfides and where the pH was circumneutral. As our knowledge of the diversity of metabolic capacity of FeOB is rapidly expanding with the increase of environmental metagenomic data, the possibility remains that there are previously unrecognized neutrophilic FeOB within the family *Acidiferrobacteraceae.*

The taxonomy of the putative FeOB MAGs obtained in this study largely varied from the MAGs obtained from the subsurface weathering cultures, which included β-proteobacteria of the genus *Cupriavidus* and order Burkholderiales (Napieralski et al., 2019). A notable exception is the presence of a highly abundant *Xanthomonadaceae* MAG closely related to the non-autotrophic soil bacterium *Dyella japonica* A8 (Chen and Chan, 2012) which we previously identified as containing a homolog to Cyc2. Interestingly, Uroz and colleagues (2009) noted the ability of a *Dyella* sp. to solubilize biotite and other *Dyella* sp. have been isolated or identified from weathering environments (Uroz et al., 2011; Zhao et al., 2013), though no genomes are available to assess whether they contain Cyc2 homologs. In addition to the *Xanthomonadaceae* MAG, 4 additional MAGs identified in this study containing putative EET pathways lacked RuBisCO. While alternative carbon fixation pathways exist, they tend to be phylogenetically restricted, with the vast majority of α, β and γ-proteobacteria utilizing the Calvin Cycle (Hugler and Sievert, 2011). Two of the MAGs containing EET but not RuBisCO belong to organisms of the phylum *Nitrospirae,* which are known to use the reductive tricarboxylic acid cycle (rTCA)

for carbon assimilation. Although the rTCA cycle shares many of the same genes as the TCA cycle, the unique enzyme 2-oxoglutarate synthase can be used to distinguish the two pathways (Hugler and Sievert, 2011). As this gene was not present in either *Nitrospirae* MAG, it seems likely that they cannot grow autotrophically. The differences in the taxonomy of the putative chemolithotrophic FeOB identified in this study compared to the study on subsurface weathering of the DIO suggests that the ability to utilize mineral-bound Fe(II) for metabolic energy generation may not be a unique feature of any given FeOB. Rather, it may be a trait shared amongst FeOB as supported by previous studies where phylogenetically diverse bacteria, putatively FeOB, were isolated on Fe(II)-phyllosilicate minerals (Benzine et al., 2013; Shelobolina et al., 2012a).

Effect of prior oxidation on mineral weatherability

In line with previous observations on heterotrophically based weathering (Bennett et al., 2001; Wu et al., 2008), the addition of organic carbon stimulated the release of major cations relative to sterile controls (Figure 5). In addition, with the exception of Na (Fig. 5B), prior microbial DIO oxidation had a small but detectable influence on subsequent heterotrophically-mediated cation release. In the DIO, Na resides primarily in the mineral plagioclase (Na-Ca feldspar), which is unresponsive to Fe(II) oxidation due to the lack of Fe in the crystal structure. Thus, plagioclase would not be expected to be subject to crystallographic defects associated with charge imbalance generated by the oxidation of structural Fe (Napieralski et al., 2019; Shelobolina et al., 2012b). A modest increase in the amount of Ca released was observed in DIO-Ox+Gluc-Inoc vs. DIO-Cont+Gluc-Inoc reactors (Figure 4A), although this difference was not outside of the error (range) of duplicate reactors. Plagioclase constitutes ca. 56.4 wt % of the DIO compared to the ca 6.3% of hornblende (White et al., 1998), the two mineral phases in which Ca is concentrated.

Thus, the input of Ca from the redox-responsive hornblende is likely to be low compared to that from plagioclase. An enhanced release of Mg was also observed from previously oxidized diorites (Figure 5C). Mg is primarily sourced from the redox active minerals hornblende and biotite, which can account for enhanced release from the oxidized DIO. Biotite is also the major source of K in the DIO. Similar to our previous observations (Napieralski et al., 2019), we observed that K release is repressed when biotite has been oxidized (Figure 5D). This surprising effect is best attributed to the assertation by Gilkes and colleagues (1973a; 1973b) that oxidation of Fe(II) in biotite changes the orientation of biotite hydroxyl groups, creating a more stable environment for the interlayer cation. However, this is not to say that K cannot become depleted from biotite via microbial activity, as K concentrations are clearly higher in DIO-Ox+Gluc-Inoc and DIO-Cont+Gluc-Inoc than in the abiotic, unoxidized control (DIO-Cont+Gluc-Sterile) (Figure 5D). As biotite found in soils is often at already least partially oxidized/altered (Wilson, 2004), this observation is not at odds with the dogma that microbial activity in the rhizosphere plays an important role in soil fertility by increasing K availability. Put more plainly, the biologically enhanced release of K from partially oxidized biotite is greater than the abiotic release of K in fresh, unoxidized biotite, despite the fact that the prior oxidation of biotite repressed the release of K overall in chemolithotrophic experiments. All together this work is consistent with our previous observation that ferromagnesian minerals which have undergone modest surface oxidation are more susceptible acidolysis by mineral acids, and the supposition that FeOB activity may enhance the weatherability of ferromagnesian minerals (Napieralski et al., 2019).

Potential metabolic interactions *in situ*

We have used microbiological and metagenomic analyses to inform the potential metabolic interactions between community members involved in the surficial weathering of the DIO. It is clear from the *in situ* metagenomes (GbOC-A and GbOC-B) that degradation of complex organics is an important metabolic pathway. Multiple MAGs, including putative *Mucilaginibacter* are enriched in carbohydrate active enzymes. *Mucilaginibacter* sp. have been reported to degrade complex organics such as cellulose and hemicellulose and play an important role in degradation of plant biomass in forest soils (López-Mondéjar et al., 2016). While not directly related to weathering, the enzymatic degradation of complex organic carbon to oligosaccharides facilitates the release of plant-derived carbon to the soil solution (Guggenberger et al., 1994). Once depolymerized, plant derived organic carbon would then be available to other regolith heterotrophs, including multiple β-proteobacteria also abundant in the *in situ* libraries. β-proteobacteria, particularly the *Burkholderiales*, have been shown to be abundant in weathering systems, and while genomic markers of their ability to enhance mineral weathering are lacking, they have been previously reported to correlate with mineral dissolution *in vitro* (Lepleux et al., 2012). With the exception of a single *Cupriavidus* MAG, no siderophore biosynthesis pathways were associated with *Burkholderiales* MAGs. This suggests that their ability to enhance mineral dissolution may rely on mechanisms other than chelation by siderophores, such as organic acid production.

While it might be tempting to think that the availability of carbon would limit chemolithotrophic metabolisms, the data presented herein do not necessarily support that assumption. In the early stages of chemolithotrophic incubation, ATP declined across all experimental conditions (Figure 2A), suggesting an overall decline in microbial biomass. However, ATP in DIO free reactors (NoMin and QTZ) remains elevated above the abiotic

control for the duration of the experiment, indicating actively metabolizing cells, likely oxidizing residual carbon. Assuming a relatively equal input of carbon occurred during inoculation of each reactor, sufficient carbon would similarly be available in diorite amended reactors. As Fe(II)/Fe(tot) declines over the entire course of the experiment (Figure 2A), it therefore does not seem likely that chemolithotrophs was inhibited by the presence of residual carbon and heterotrophic activity. This is further supported by slight decline in Fe(II)/Fe(tot) in glucose amended DIO reactors (Figure 4A). It thus seems possible that the putative chemolithotrophs detected in the metagenomic coassembly can co-exist and metabolize Fe(II) *in situ,* with the oxidative weathering activity of FeOB contributing to the ability of heterotrophic microorganisms to further weather ferromagnesian minerals via other mechanisms, including acidolysis and chelation by siderophores. As siderophores are highly specific to Fe(III), with a low affinity for Fe(II), (Neilands, 1995), the implication is that their mechanism of action in enhanced Fe(II) mineral dissolution must almost certainly require prior oxidation, either chemically or abiotically, to obtain a suitable substrate. Thus, the oxidation of mineral bound Fe(II) by FeOB may act to increase Fe(III) availability for cellular uptake via siderophores.

Environmental implications and future perspectives

We have identified the potential involvement FeOB in silicate mineral weathering in both a subsurface (Napieralski et al., 2019) and surficial quartz diorite weathering environment and have also identified a potential marker for microbial oxidative weathering in Cyc2. In both the present study and our previous work on subsurface weathering, MAGs containing Cyc2 homologs are abundant in Fe(II)-oxidizing enrichment cultures, and the functionality of Cyc2 as an Fe(II) oxidase in neutrophilic FeOB has recently been validated (McAllister et al., 2019). While most studies on *in situ* weathering rely on 16S rRNA gene-based surveys (Liermann et al.,

2014; Wild et al., 2019), taxonomic information alone is often not enough to make metabolic inferences, and the role of non-canonical FeOB is likely be under recognized. Although metagenomic investigations are helping to unravel microbial pathways and biogeochemical implications in a variety of geological habitats (Anantharaman et al., 2016a; Anantharaman et al., 2016b; Colman et al., 2019; Fortney et al., 2018), the terrestrial "weathering microbiome" remains largely unexplored, with the genetic mechanism for biogeochemical weathering only beginning to be revealed (Uroz et al., 2013).

References

Alneberg, J. et al., 2014. Binning metagenomic contigs by coverage and composition. Nat Methods, 11(11): 1144-6.

Anantharaman, K., Breier, J.A., Dick, G.J., 2016a. Metagenomic resolution of microbial functions in deep-sea hydrothermal plumes across the Eastern Lau Spreading Center. ISME J, 10(1): 225-39.

Anantharaman, K. et al., 2016b. Thousands of microbial genomes shed light on interconnected biogeochemical processes in an aquifer system. Nat Commun, 7: 13219.

Bailey, B., Templeton, A., Staudigel, H., Tebo, B.M., 2009. Utilization of Substrate Components during Basaltic Glass Colonization by Pseudomonas and Shewanella Isolates. Geomicrobiology Journal, 26(8): 648-656.

Banfield, J.F., Barker, W.W., Welch, S.A., Taunton, A., 1999. Biological impact on mineral dissolution: application of the lichen model to understanding mineral weathering in the rhizosphere. Proc Natl Acad Sci U S A, 96(7): 3404-3411.

Barco, R.A. et al., 2015. New Insight into Microbial Iron Oxidation as Revealed by the Proteomic Profile of an Obligate Iron-Oxidizing Chemolithoautotroph. Appl Environ Microbiol, 81(17): 5927-37.

Bennett, P.C., Rogers, J.R., Choi, W.J., Hiebert, F.K., 2001. Silicates, silicate weathering, and microbial ecology. Geomicrobiology Journal, 18(1): 3-19.

Benzine, J. et al., 2013. Fe-phyllosilicate redox cycling organisms from a redox transition zone in Hanford 300 Area sediments. Front Microbiol, 4: 388.

Buss, H.L. et al., 2005. The coupling of biological iron cycling and mineral weathering during saprolite formation, Luquillo Mountains, Puerto Rico. Geobiology, 3: 247-260.

Buss, H.L., Lüttge, A., Brantley, S.L., 2007. Etch pit formation on iron silicate surfaces during siderophore-promoted dissolution. Chem Geol, 240(3-4): 326-342.

Buss, H.L., Sak, P.B., Webb, S.M., Brantley, S.L., 2008. Weathering of the Rio Blanco quartz diorite, Luquillo Mountains, Puerto Rico: Coupling oxidation, dissolution, and fracturing. Geochimica et Cosmochimica Acta, 72(18): 4488-4507.

Calvaruso, C., Turpault, M.P., Frey-Klett, P., 2006. Root-associated bacteria contribute to mineral weathering and to mineral nutrition in trees: a budgeting analysis. Appl Environ Microbiol, 72(2): 1258-66.

Castelle, C. et al., 2008. A new iron-oxidizing/O2-reducing supercomplex spanning both inner and outer membranes, isolated from the extreme acidophile Acidithiobacillus ferrooxidans. J Biol Chem, 283(38): 25803-11.

Chen, J.W., Chan, K.G., 2012. Genome sequence of Dyella japonica strain A8, a quorum-quenching bacterium that degrades N-acylhomoserine lactones, isolated from Malaysian tropical soil. J Bacteriol, 194(22): 6331.

Colman, D.R., Lindsay, M.R., Boyd, E.S., 2019. Mixing of meteoric and geothermal fluids supports hyperdiverse chemosynthetic hydrothermal communities. Nat Commun, 10(1): 681.

Drever, J.I., Stillings, L.L., 1997. The role of organic acids in mineral weathering. Colloids and Surfaces A: Physicochemical and Engineering Aspects, 120(1-3): 167-181.

Emerson, D., Fleming, E.J., McBeth, J.M., 2010. Iron-oxidizing bacteria: an environmental and genomic perspective. Annu Rev Microbiol, 64: 561-83.

Fortney, N.W., He, S., Converse, B.J., Boyd, E.S., Roden, E.E., 2018. Investigating the Composition and Metabolic Potential of Microbial Communities in Chocolate Pots Hot Springs. Front Microbiol, 9: 2075.

Frey, B. et al., 2010. Weathering-associated bacteria from the Damma glacier forefield: physiological capabilities and impact on granite dissolution. Appl Environ Microbiol, 76(14): 4788-96.

Gilkes, R.J., Young, R.C., Quirk, J.P., 1973a. Artificial weathering of oxidized biotite: I. potassium removal by sodium chloride and sodium tetraphenylboron solutions. Soil Sci Soc Am J, 37(1): 25-28.

Gilkes, R.J., Young, R.C., Quirk, J.P., 1973b. Artificial weathering of oxidized biotite: II. rates of dissolution in 0.1, 0.01, 0.001M HCl. Soil Sci Soc Am J, 37(1): 29-33.

Guggenberger, G., Zech, W., Schulten, H.R., 1994. Formation and mobilization pathways of dissolved organic matter: evidence from chemical structural studies of organic matter fractions in acid forest floor solutions. Organic Geochemistry, 21(1): 51-66.

Hazen, T.C., Jiménez, L., López de Victoria, G., Fliermans, C.B., 1991. Comparison of bacteria from deep subsurface sediment and adjacent groundwater. Microbial Ecology, 22(1): 293-304.

He, S., Barco, R.A., Emerson, D., Roden, E.E., 2017. Comparative Genomic Analysis of Neutrophilic Iron(II) Oxidizer Genomes for Candidate Genes in Extracellular Electron Transfer. Front Microbiol, 8: 1584.

He, S., Tominski, C., Kappler, A., Behrens, S., Roden, E.E., 2016. Metagenomic Analyses of the Autotrophic Fe(II)-Oxidizing, Nitrate-Reducing Enrichment Culture KS. Appl Environ Microbiol, 82(9): 2656-2668.

Henri, P.A. et al., 2015. Structural Iron (II) of Basaltic Glass as an Energy Source for Zetaproteobacteria in an Abyssal Plain Environment, Off the Mid Atlantic Ridge. Front Microbiol, 6: 1518.

Hering, J.G., Stumm, W., 1990. Oxidative and reductive dissolution of minerals. Reviews in Mineralogy and Geochemistry, 23(1): 427-465.

Hopkinson, B.M., Barbeau, K.A., 2012. Iron transporters in marine prokaryotic genomes and metagenomes. Environ Microbiol, 14(1): 114-28.

Hugler, M., Sievert, S.M., 2011. Beyond the Calvin cycle: autotrophic carbon fixation in the ocean. Ann Rev Mar Sci, 3: 261-89.

Issotta, F. et al., 2018. Insights into the biology of acidophilic members of the Acidiferrobacteraceae family derived from comparative genomic analyses. Res Microbiol, 169(10): 608-617.

Jakosky, B.M., Shock, E.L., 1998. The biological potential of Mars, the early Earth, and Europa. Journal of Geophysical Research: Planets, 103(E8): 19359-19364.

Kalinowski, B.E., Liermann, L.J., Brantley, S.L., Barnes, A., Pantano, C.G., 2000. X-ray photoelectron evidence for bacteria-enhanced dissolution of hornblende. Geochimica et Cosmochimica Acta, 64(8): 1331-1343.

Kang, D.D. et al., 2019. MetaBAT 2: an adaptive binning algorithm for robust and efficient genome reconstruction from metagenome assemblies. PeerJ, 7: e7359.

Kojima, H., Shinohara, A., Fukui, M., 2015. Sulfurifustis variabilis gen. nov., sp. nov., a sulfur oxidizer isolated from a lake, and proposal of Acidiferrobacteraceae fam. nov. and Acidiferrobacterales ord. nov. International Journal of Systematic and Evolutionary Microbiology, 65(10): 3709-3713.

Kojima, H., Watanabe, T., Fukui, M., 2016. Sulfuricaulis limicola gen. Nov., sp. nov., a sulphur oxidizer isolated from a lake. International Journal of Systematic and Evolutionary Microbiology, 66(1): 266-270.

Lambers, H., Mougel, C., Jaillard, B., Hinsinger, P., 2009. Plant-microbe-soil interactions in the rhizosphere: An evolutionary perspective. Plant and Soil, 321(1-2): 83-115.

Lepleux, C., Turpault, M.P., Oger, P., Frey-Klett, P., Uroz, S., 2012. Correlation of the abundance of betaproteobacteria on mineral surfaces with mineral weathering in forest soils. Appl Environ Microbiol, 78(19): 7114-9.

Liermann, L.J., Albert, I., Buss, H.L., Minyard, M., Brantley, S.L., 2014. Relating Microbial Community Structure and Geochemistry in Deep Regolith Developed on Volcaniclastic Rock in the Luquillo Mountains, Puerto Rico. Geomicrobiology Journal, 32(6): 494-510.

Liermann, L.J., Kalinowski, B.E., Brantley, S.L., Ferry, J.G., 2000. Role of bacterial siderophores in dissolution of hornblende. Geochimica et Cosmochimica Acta, 64(4): 587-602.

Liu, J. et al., 2012. Identification and Characterization of MtoA: A Decaheme c-Type Cytochrome of the Neutrophilic Fe(II)-Oxidizing Bacterium Sideroxydans lithotrophicus ES-1. Front Microbiol, 3: 37.

López-Mondéjar, R., Zühlke, D., Becher, D., Riedel, K., Baldrian, P., 2016. Cellulose and hemicellulose decomposition by forest soil bacteria proceeds by the action of structurally variable enzymatic systems. Scientific Reports, 6.

McAllister, S.M. et al., 2019. Validating the Cyc2 neutrophilic Fe oxidation pathway using meta-omics of Zetaproteobacteria iron mats at marine hydrothermal vents.

Meier, L.A. et al., 2019. Pedogenic and microbial interrelation in initial soils under semiarid climate on James Ross Island, Antarctic Peninsula region. Biogeosciences, 16(12): 2481-2499.

Montross, S.N., Skidmore, M., Tranter, M., Kivimäki, A.-L., Parkes, R.J., 2013. A microbial driver of chemical weathering in glaciated systems. Geology, 41(2): 215-218.

Napieralski, S.A. et al., 2019. Microbial chemolithotrophy mediates oxidative weathering of granitic bedrock. PNAS, Submitted.

Napieralski, S.A. et al., 2020. Microbial chemolithotrophic oxidation of pyrite in a subsurface shale weathering environment: geologic considerations and potential mechanisms. In Prep.

Neilands, J.B., 1995. Siderophores: structure and function of microbial iron transport compounds. Journal of Biological Chemistry, 270(45): 26723-26726.

Parks, D.H., Imelfort, M., Skennerton, C.T., Hugenholtz, P., Tyson, G.W., 2015. CheckM: assessing the quality of microbial genomes recovered from isolates, single cells, and metagenomes. Genome Res, 25(7): 1043-55.

Peng, Y., Leung, H.C., Yiu, S.M., Chin, F.Y., 2012. IDBA-UD: a de novo assembler for single-cell and metagenomic sequencing data with highly uneven depth. Bioinformatics, 28(11): 1420-8.

Popa, R., Smith, A.R., Popa, R., Boone, J., Fisk, M., 2012. Olivine-respiring bacteria isolated from the rock-ice interface in a lava-tube cave, a Mars analog environment. Astrobiology, 12(1): 9-18.

Seemann, T., 2014. Prokka: rapid prokaryotic genome annotation. Bioinformatics, 30(14): 2068-9.

Shelobolina, E. et al., 2012a. Isolation of phyllosilicate-iron redox cycling microorganisms from an illite-smectite rich hydromorphic soil. Front Microbiol, 3: 134.

Shelobolina, E. et al., 2012b. Microbial lithotrophic oxidation of structural Fe(II) in biotite. Appl Environ Microbiol, 78(16): 5746-52.

Shock, E.L., 2009. Minerals as energy sources for microorganisms. Economic Geology, 104(8): 1235-1248.

Sobolev, D., Roden, E., 2004. Characterization of a neutrophilic, chemolithoautotrophic Fe(II)-oxidizing β-Proteobacterium from freshwater wetland sediments. Geomicrobiology Journal, 21(1): 1-10.

Stookey, L.L., 1970. Ferrozine-A new spectrophotometric reagent for iron. Analytical Chemistry, 42(7): 778-781.

Uritskiy, G.V., DiRuggiero, J., Taylor, J., 2018. MetaWRAP-a flexible pipeline for genome-resolved metagenomic data analysis. Microbiome, 6(1): 158.

Uroz, S., Calvaruso, C., Turpault, M.P., Frey-Klett, P., 2009. Mineral weathering by bacteria: ecology, actors and mechanisms. Trends Microbiol, 17(8): 378-87.

Uroz, S. et al., 2013. Functional assays and metagenomic analyses reveals differences between the microbial communities inhabiting the soil horizons of a Norway spruce plantation. PLoS One, 8(2): e55929.

Uroz, S., Turpault, M.P., Van Scholl, L., Palin, B., Frey-Klett, P., 2011. Long term impact of mineral amendment on the distribution of the mineral weathering associated bacterial communities from the beech Scleroderma citrinum ectomycorrhizosphere. Soil Biology and Biochemistry, 43(11): 2275-2282.

White, A.F., 1990. Heterogeneous electrochemical reactions associated with oxidation of ferrous oxide and silicate surfaces. Reviews in Mineralogy and Geochemistry, 23(1): 467-509.

White, A.F. et al., 1998. Chemical weathering in a tropical watershed, Luquillo Mountains, Puerto Rico: I. Long-term versus short-term weathering fluxes. Geochimica et Cosmochimica Acta, 62(2): 209-226.

Wild, B. et al., 2019. In-situ dissolution rates of silicate minerals and associated bacterial communities in the critical zone (Strengbach catchment, France). Geochimica et Cosmochimica Acta, 249: 95-120.

Wilson, M.J., 2004. Weathering of the primary rock-forming minerals: processes, products and rates. Clay Minerals, 39: 233-266.

Wu, L., Jacobson, A.D., Hausner, M., 2008. Characterization of elemental release during microbe–granite interactions at T=28°C. Geochimica et Cosmochimica Acta, 72(4): 1076-1095.

Yin, Y. et al., 2012. DbCAN: A web resource for automated carbohydrate-active enzyme annotation. Nucleic Acids Research, 40(W1): W445-W451.

Yu, C.S., Chen, Y.C., Lu, C.H., Hwang, J.K., 2006. Prediction of protein subcellular localization. Proteins, 64(3): 643-51.

Zhao, F. et al., 2013. Dyella jiangningensis sp. nov., a gamma-proteobacterium isolated from the surface of potassium-bearing rock. Int J Syst Evol Microbiol, 63(Pt 9): 3154-7.

Zhou, J., Bruns, M.A., Tiedje, J.M., 1996. DNA recovery from soils of diverse composition. Applied and Environmental Microbiology, 62(2): 316-322.

Figure 1: Outcrop scale photo of a weathering corestone of Rio Blanco Quartz Diorite exposed by road cutting (A). The corestone exhibits spheroidal weathering, with partially altered “rindlets” surrounding the unaltered rock (B). Material for this study was collected near the rindlet-corestone interface (C). Pocket knife for scale (ca. 9 cm).

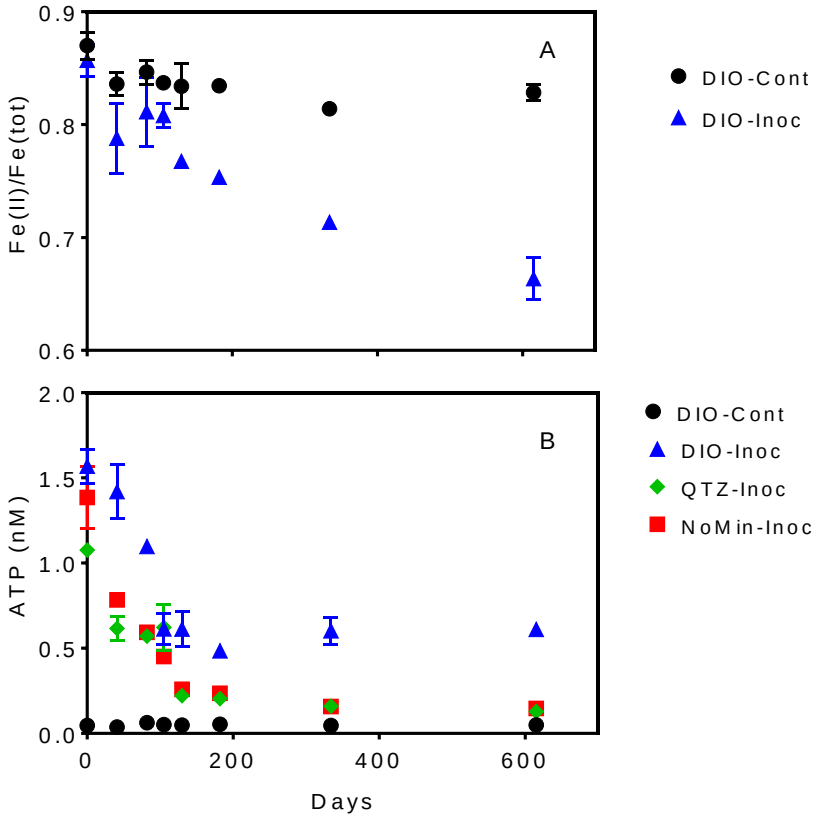

Figure 2: Fe(II)/Fe(tot) of dilute HCl extractable Fe in abiotic uninoculated (DIO-Cont) and live inoculated (DIO-Inoc) diorite enrichment cultures (A). ATP content (nM) of control DIO and inoculated DIO, quartz (QTZ), and inocula only (NoMin) cultures. Data point and error bars denote the mean and range of duplicate reactors.

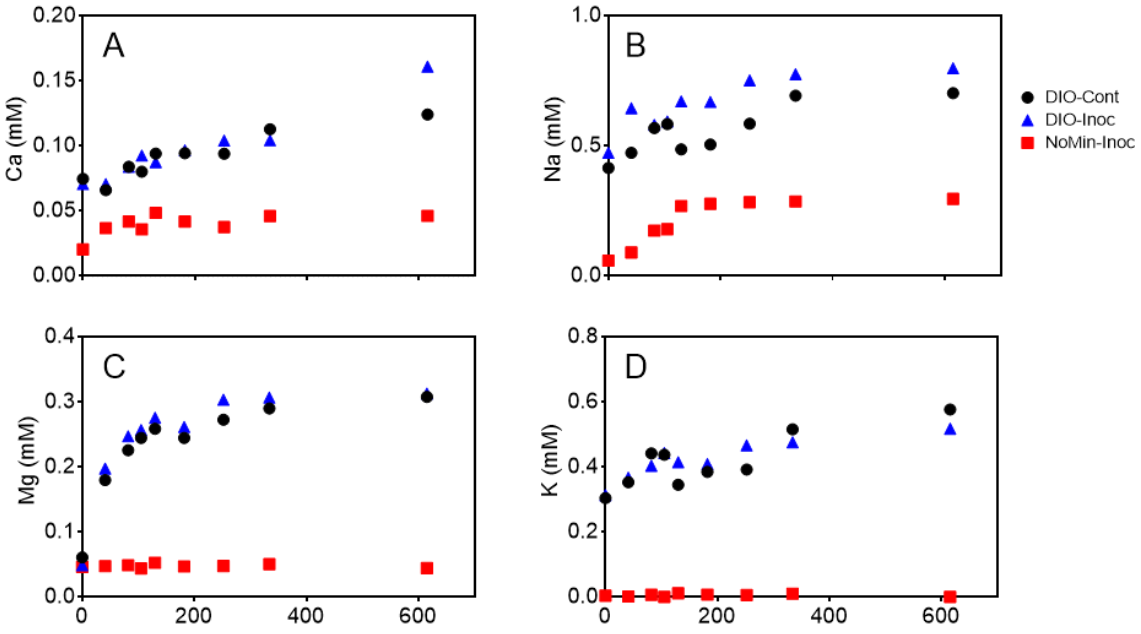

Figure 3: Ca (A), Na (B), Mg (C) and K (D) concentrations (mM) in pooled duplicate control (DIO-Cont), live inoculated (DIO-Inoc), and inocula only (NoMin-Inoc) reactors.

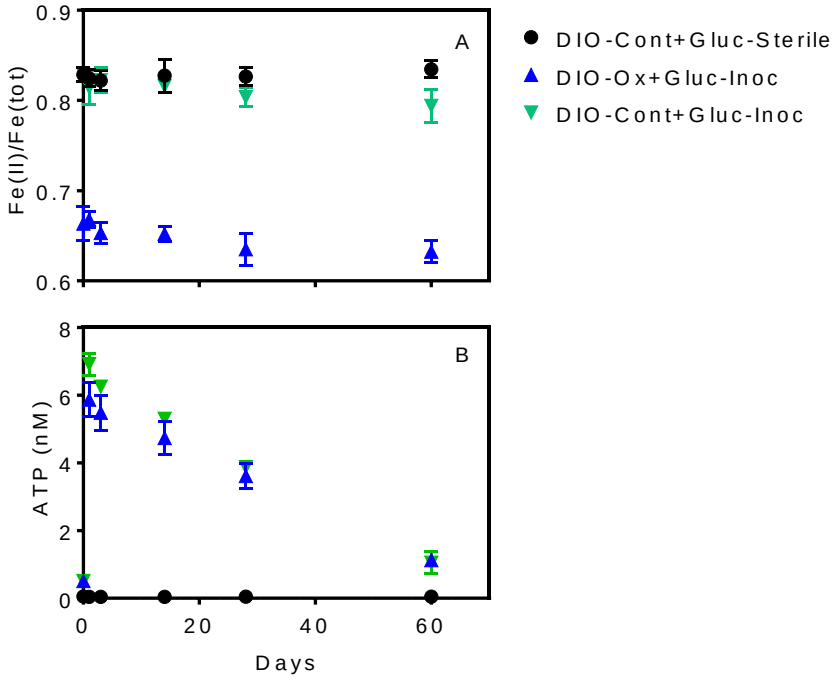

Figure 4: Fe(II)/Fe(tot) (A) and ATP content (B) after supplementation with 1.0 mM glucose in live cultures containing microbially oxidized DIO from the previous chemolithotrophic enrichment culture (DIO-Ox-Gluc-Inoc), live cultures containing unoxidized DIO from previous abiotic controls (DIO-Cont-Gluc-Inoc), or sterile controls containing unoxidized DIO from previous abiotic controls (DIO-Cont+Gluc-Sterile).

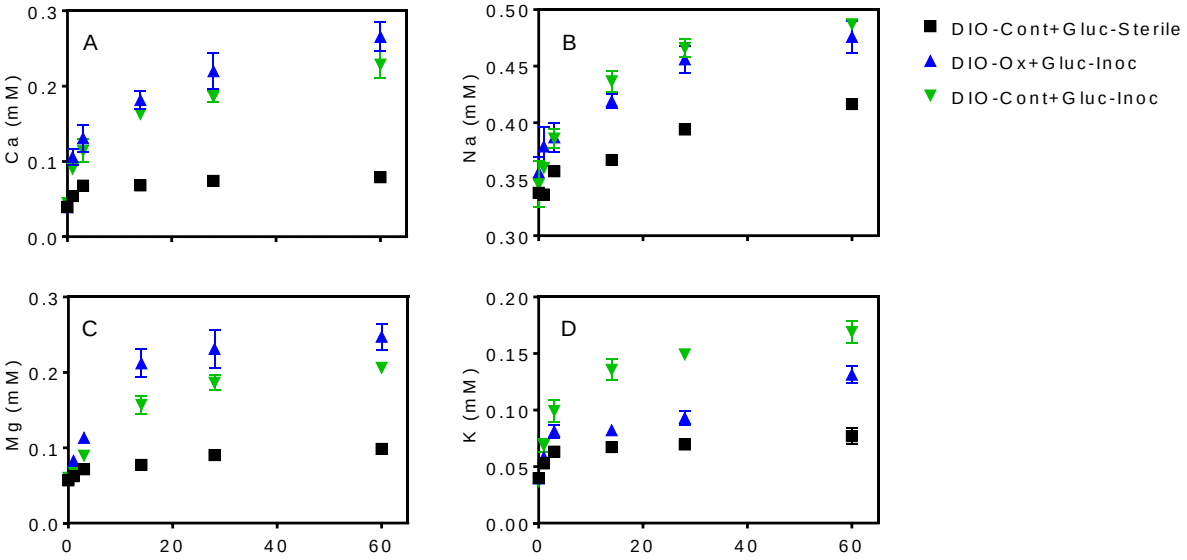

Figure 5: Ca (A), Na (B) Mg (C) and Na (D) concentrations after supplementation with 1.0 mM glucose in live cultures containing microbially oxidized DIO from the previous chemolithotrophic enrichment culture (DIO-Ox-Gluc-Inoc), live cultures containing unoxidized DIO from previous abiotic controls (DIO-Cont-Gluc-Inoc), or sterile controls containing unoxidized DIO from previous abiotic controls (DIO-Cont+Gluc-Sterile).

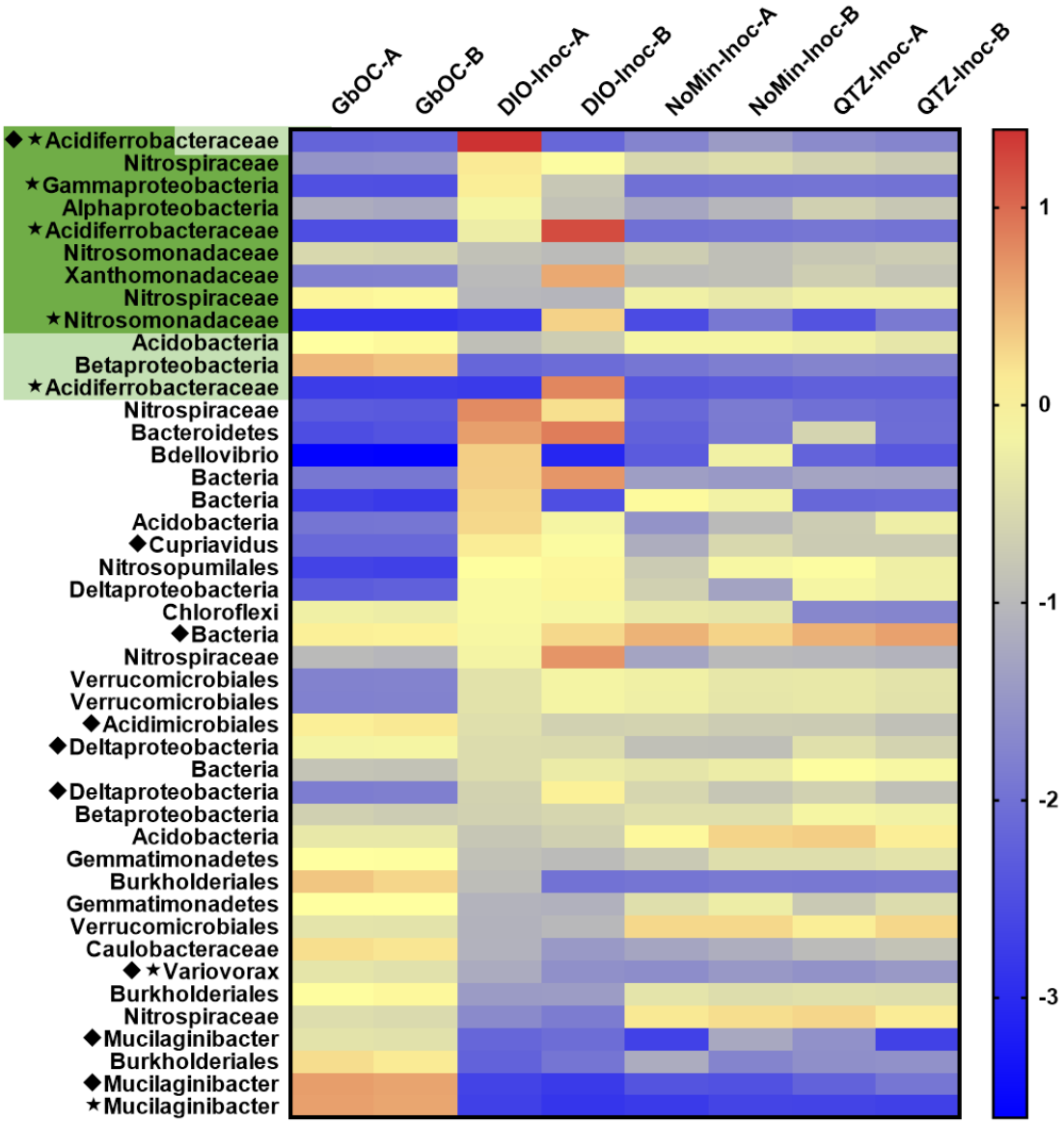

Figure 6: Heat map of the abundance (log genomes per million reads) of selected MAGs (the 10 most abundant MAGs in each sample and all MAGs with EET and siderophore biosynthesis pathways) across all samples in the metagenomic coassembly including duplicate *in situ* outcrop (GbOC) and duplicate inocula only (NoMin-Inoc), quartz (QTZ-Inoc) and diorite (DIO-Inoc) enrichment cultures. Putative FeOB are highlighted, with the presence of Cyc2 homologs in dark green and MtoAB in light green. The presence of RuBisCO is indicated by a star and siderophore biosynthesis by a diamond.

Concluding remarks and future perspectives

In my investigations into the role of chemolithotrophic Fe(II)-oxidizing bacteria (FeOB) on the oxidative weathering of the Fe(II)-silicate minerals biotite and hornblende, described Chapter 1 and its sequel Chapter 3, I demonstrated that mineral bound Fe(II) is a suitable substrate for FeOB metabolism and growth. Growth yield estimates derived from the change in the solid phase Fe(II) and ATP content of diorite oxidizing enrichment cultures are consistent with those previously reported for FeOB. In addition, organisms that genomes encode EET pathways known to be involved in the oxidation of Fe were enriched in the presence of Fe(II) minerals. It was further demonstrated that subtle redox driven mineralogical changes associated with FeOB activity rendered Fe(II)-bearing minerals more susceptible to further weathering, both abiotically by dilute acid and biotically via heterotrophic activity. I conclude that FeOB can, even in the presence of organic carbon, exist and metabolize at the rindlet-saprolite interface in both subsurface and surficial environments. It is important to point out that while FeOB are capable of oxidizing mineral-bound Fe(II), their role in the overall oxidative weathering of the Rio Blanco Quartz Diorite is constrained by abiotic/geologic factors. As fresh crystalline igneous rock such as the Rio Blanco Quartz Diorite is impermeable to objects the size of typical bacteria, in order for microbial colonization of mineral phases to occur, sufficient porosity must be generated, e.g. through a combination of abiotic oxidation facilitated by the diffusion of oxygen (as highlighted in Chapter 1) together with tectonic forces that strain and crack the rocks *in situ*. Hence, while FeOB almost certainly mediate Fe(II)-silicate oxidation, they do not drive the overall weathering process on a geological time scale.

Chapter 2 further highlights the need to consider geological constraints when thinking about the role microorganisms play in *in situ* oxidative weathering. While I conclusively

demonstrate that microorganisms from a subsurface pyrite weathering front can accelerate the circumneutral pH oxidation of pyrite *in vitro*, their ability to act *in situ* is almost certainly limited by access to mineral surfaces due to porosity constraints. Candidly, at the conception of the experiments described in Chapter 2, such limitations were not at the forefront of my mind, nor to as far as I know that of anyone else who was involved in the experiments, all of whom seemed eager to see what role microbes might have. It was not until after the experiments were over and I was wrestling with the data that I came to the somewhat disheartening realization that microbes probably don't mediate pyrite oxidation in situ, a conclusion reached in tandem with the Brantley group at Penn State who were also working (from a geological/geochemical perspective) on pyrite oxidation at SSHCZO. Regardless, Chapter 2 contributes to the scant body of knowledge on the microbial oxidation of pyrite at circumneutral pH and proposes a new mechanism by which the phenomenon might take place.

As with all science, this work raises at least as many questions as it answers. I would however, like to outline a roadmap of work that I envision as being necessary to further unravel how chemolithotrophic microorganisms interact with, and extract energy from insoluble Fe(II)-bearing mineral phases in the Earth's crust.

While Chapter 1 and Chapter 3 demonstrate *in vitro* interactions between chemolithotrophic and heterotrophic taxa under controlled experimental conditions, the fact remains that I have not proven that such reactions proceed *in situ*. Until recently, the genetic basis for Fe(II) oxidation in neutrophilic FeOB was almost completely unknown, despite FeOB being recognized since the mid-1800s. Thus, the tools to fully investigate their environmental distribution have been limited to inference of function from taxonomic relationships to FeOB for which the ability to oxidize Fe(II) has been experimentally verified (e.g. *Sideroxydans*

lithotrophicus ES-1 and *Gallionella capsiferriformans* ES-2). My work, combined with other recent work from Clara Chan's group at the University of Delaware, has identified the outer membrane protein Cyc2 as a potential genetic indicator of Fe(II)-oxidizing capacity that can be employed to identify FeOB in (meta)genomic datasets. As this genetic pathway is relatively newly characterized, automated genomic annotation software, servers, and databases (e.g. IMG, KEGG, Prokka, PFAM etc.) fail to identify and functionally annotate Cyc2 homologs. Hence, unless you know what you are looking for you will not find it by happenstance, or even if you know you want to find it. It is thus likely that FeOB activity may be an overlooked phenomenon, specifically in mineral weathering environments. To this end, I envision a reanalysis of publicly available (meta)genomic datasets to identify Cyc2 in the (meta)genomes of organisms implicated in oxidative mineral weathering. While (meta)genomics is a valuable tool for discerning potential metabolic function, DNA sequencing can only be used to infer what an organism is capable of doing. To further link the oxidation of Fe(II) via Cyc2 to *in situ* oxidative weathering, however, it will be necessary to employ additional omics-based techniques in new, appropriately designed studies. Specifically, (meta)transcriptomics and (meta)proteomic studies will be required to confirm the activity of Cyc2 *in situ* in Fe(II)-silicate weathering environments.

In Chapter 2, I propose a novel pathway for the interaction of sulfur oxidizing bacteria, putatively of the genus *Thiobacillus*, with extracellular pyrite. While supported by geochemical, metagenomic and bioinformatic analyses, at present the existence of the proposed underlying mechanism remains highly speculative. It is obvious, therefore, that much more work beyond the scope of this Ph.D. dissertation is needed to assess whether such a pathway actually exists. The most obvious way to address this issue would be to obtain pure culture isolates of organisms capable of accelerating the circumneutral oxidation of pyrite. While preliminary attempts to

isolate organisms from my Shale Hills enrichment cultures were unsuccessful, I envision a dedicated isolation campaign as ultimately being able to succeed. Such a campaign might target a variety of circumneutral pH pyrite-oxidizing environments, from shale weathering such as SSHCZO to redox transition zones in unconsolidated sediment. Once obtained, genomic sequencing should be employed asses the metabolic potential of the isolates. Pure culture pyrite oxidizing studies could then be employed, in which transcriptomic and proteomic analyses are used to shed light on the expression of genes related to the oxidation of pyrite. Ideally, similar to the proposal of Cyc2 as a marker for Fe(II)-silicate oxidation, a genetic marker for pyrite oxidation could eventually be applied to *in situ* environmental systems, where metagenomic based approaches, coupled with geochemistry, can continue to increase our limited understanding of circumneutral pH pyrite oxidation.

If you made it this far, congratulations and I sincerely hope that my musings have, if not inspired you, at least not bored you to pieces. Thank you for reading.